Ultracool Benchmark Companions to Gaia Stars

Author
Lord Dover

Supervised by
Professor David Pinfield & Dr. Federico Marocco

Centre for Astrophysics Research
School of Physics, Astronomy & Maths
University of Hertfordshire

Submitted to the University of Hertfordshire in partial fulfilment of the requirements of the degree of Master of Science by Research.

February 2019

Abstract

Ultracool dwarfs are stellar and sub-stellar objects with spectral types of M7 or later and effective temperatures below 2700K. Over 1300 have been discovered to date, both as free-floating objects and companions to more massive stars. It is difficult to constrain the physical properties of an ultracool dwarf, as they have low luminosities and are generally not found as close companions. Models for the evolution, composition and atmospheres of ultracool dwarfs depend on having examples with independently measured physical properties; these are known as 'benchmark' ultracool dwarfs. To independently determine a physical property, the ultracool dwarf must be associated with a star. This thesis describes a search for ultracool companions that may be suitable benchmarks using various optical and infrared surveys in combination with the Gaia TGAS and DR2 catalogues. This search utilises existing methods in novel ways to identify and select candidates, with a particular focus on identifying rare or unusual objects that may have features for which there is currently no benchmark. This thesis presents 32 candidate companions that are recommended for follow-up observations, plus a further 227 candidates that require further analysis in future work.

Acknowledgements

First and foremost I would like to thank my principal supervisor Professor David Pinfield along with my secondary supervisor Dr. Federico Marocco for their continued support throughout this fascinating project. This research was supported by Matthew Rickard, who reduced Fourstar images and gave general advice, and Dr. Ben Burningham who assisted with SQL queries for data retrieval. I would also like to thank Adam Erskine-Jones, who contributed to the visual inspection process as part of a four-week Nuffield Research Placement with the Centre for Astrophysics Research.

I would like to thank my family and friends for their unwavering encouragement and support over the past two years, especially my extremely patient and understanding partner Alisha Raj. Furthermore, I would like to extend my gratitude to my fellow students Mubela Mutale, Noah Chanka, Julie Djordjevic, Jonathan Westcott and Tabassum Tanvir for always being available for advice and support. I would also like to thank everyone I have worked with on the department's outreach team during my time as a research student with a special mention for Dr. Samantha Rolfe, David Campbell, Dr. Jim Collett, Dr. Mark Gallaway and Professor Sean Ryan.

This research would not have been possible without a generous tuition fee scholarship from Dr. Brian May, whose endless enthusiasm for both science and music continues to inspire me.

Contents

List of Figures

List of Tables

List of Abbreviations

2MASS - 2-Micron All-Sky Survey

AO - Adaptive Optics

BD - Brown dwarf

DR*x* - Data release x

CDS - Centre de Données astronomiques de Strasbourg

CGB - Confirmable Gaia benchmark

CMD - Colour-magnitude diagram

DECaLS - The Dark Energy Camera Legacy Survey

ESA - European Space Agency

IMF - Initial Mass Function

ING - Isaac Newton Group of Telescopes

IR - Infrared

IRAF - Image Reduction and Analysis Facility

LAS - (UKIDSS) Large Area Survey

Pan-STARRS - Panoramic Survey Telescope and Rapid Response System

NIR - Near-infrared

QSO - Quasi-stellar object

SDSS - Sloan Digital Sky Survey

SNR - Signal-to-noise ratio

TGAS - Tycho-Gaia Astrometric Survey

UCD - Ultracool dwarf

UKIDSS - UKIRT Infrared Deep Sky Survey

UKIRT - UK Infrared Telescope

VISTA - Visible and Infrared Survey Telescope for Astronomy

VHS - VISTA Hemisphere Survey

VLG - Very low gravity

WFCAM - UKIRT Wide Field Camera

WISE - Wide-field Infrared Survey Explorer

1 Introduction

Ultracool dwarfs (hereafter referred to as UCDs) are objects found at the end of the main sequence with spectral types of M7 or later, extending beyond the original Morgan-Keenan system into the L, T and Y spectral types. UCDs have effective temperatures below 2700K [1] and can come in the form of brown dwarfs or low-mass stars.

Brown dwarfs and low-mass stars can be free-floating objects or members of multiple systems. This thesis describes a project to find ultracool companions to stars observed by the Gaia spacecraft that could have their properties constrained well enough to be considered 'benchmark' UCDs. The benefit of looking for companion UCDs is that the properties of the primary can be used to constrain the companion whilst precise parallax measurements from Gaia will allow for good absolute magnitude estimates for the star's companion.

The term 'ultracool' was first used by Kirkpatrick [2] to describe late M dwarfs that lie on the stellar/sub-stellar boundary and exhibit properties of both stars and brown dwarfs. The little radiation UCDs do emit is at NIR/IR wavelengths, making them extremely faint at optical wavelengths. UCDs are thought to be very common, however they are difficult to detect at distances greater than a few hundred parsecs. Despite making up 15% of the solar neighbourhood [3], none are visible to the naked eye on Earth.

Originally known as failed stars or black dwarfs, brown dwarfs are objects that are not massive enough to fuse hydrogen in their cores and are thus not massive enough to be stars. First hypothesised by Kumar [4] and named by Tarter [5], the first indisputable detection of a brown dwarf was not made until 1995 with the 'joint first' discoveries of Gliese 229B [6] and Teide 1 [7].

The hydrogen-burning limit[1] of $\sim 0.077 M_{\odot}$, which is approximately $80 M_{Jup}$ [8], is the boundary that separates stars and brown dwarfs. While they are unable to fuse hydrogen, brown dwarfs can fuse deuterium and sometimes lithium. The ability to fuse deuterium is a second defining characteristic for brown dwarfs as there is also an associated minimum mass of $13 M_{Jup}$ [9]. Below this mass limit, objects are considered to be sub-brown dwarfs or giant planets.

Defining brown dwarfs by mass has been criticised, with some arguing that sub-stellar objects should instead be defined by their formation processes. The most massive known planet [10] is above the deuterium burning limit, leading to confusion regarding the current definition. Chabrier et al. (2014) [11] argues that any free-floating object below the hydrogen-burning limit should be classified as a brown dwarf regardless of its ability to fuse deuterium, while companion brown dwarfs should still have the $13 M_{Jup}$ lower limit. While this theory allows free-floating objects that formed via gravitational collapse to be classified as brown

[1] for solar composition; the limit depends on metallicity

dwarfs, it does not account for objects ejected from proto-planetary systems or captured bodies. For the purposes of this thesis, the IAU $13 - 80M_{Jup}$ range will be used but it should be acknowledged that the difference between giant planets and low-mass brown dwarfs is subject to debate.

Ultracool stars are more simply defined, as they only need to be above the $80M_{Jup}$ hydrogen-burning limit but also below 2700K. While there is no strict upper mass limit, the mass-temperature relationship implies that stars more massive than $\sim 120M_{Jup}$ would be above the 2700K limit. This is, of course, dependent on the composition of the dwarf.

1.0.1 Thesis outline

The first chapter of this thesis provides an overview of UCDs in the context of this project. The relevant observational properties are described for each spectral type to demonstrate the features that can be used to select UCDs and differentiate between them. The formation and evolution of UCDs is then discussed to show the current understanding of UCDs and what can be inferred from observations. Examples of unusual UCDs are then given, demonstrating how they can be identified and why they are important. Finally, the benchmark population is discussed in the context of Gaia, highlighting the significant opportunities presented by the mission.

Chapter two describes the process of identifying candidate companions, starting with a bulk selection from large surveys. The photo-typing method used to classify candidates is then explained, and demonstrated on a test sample, before targets are matched to primaries. A series of decontamination cuts are then described and discussed. The final section of the chapter describes the common proper motion tests used to verify companionship.

The third chapter of this thesis covers an observing run on which this project was allocated a short amount of time. After establishing a list of observable candidates, targets are fully decontaminated and prioritised. A final list of targets, including those not observed, is provided along with an analysis of the data obtained.

Chapter four presents the results of this project's search for ultracool benchmark companions with TGAS and discusses notable candidates. An initial candidate list with Gaia DR2 primaries is also presented and discussed.

The final chapter of this thesis reviews the method developed in this project and the results it produced. Recommendations are given for future applications of this method and future work is discussed.

1.1 Observational properties

1.1.1 M dwarfs

M dwarfs are the most common stars in the universe, however most of these are red dwarfs that are too warm to be UCDs. Both ultracool stars and brown dwarfs can be found within the M classification, but the majority of M dwarf UCDs are stellar and only the youngest, hottest brown dwarfs are classified as M dwarfs.

The infrared photometric profiles for late M dwarfs in figure (1) show some reddening for later M dwarfs, however infrared photometry alone is not enough to separate red dwarfs and UCDs with confidence. Optical colours, on the other hand, have a relatively steep profile with significant reddening that flattens at the M/L boundary in figure (2). As M dwarfs are bright enough for good optical photometry out to several hundred parsecs, i-z observations are very useful for separating red dwarfs and UCDs.

Kirkpatrick et al. (1991) [12] established spectral standards for M dwarfs and published full NIR sequences, which can be seen in figure (3). Early to mid-M dwarfs have obvious TiO absorption lines that become more prominent for later M dwarfs with cooler, more opaque atmospheres. Ultracool subclasses are best characterised by VO absorption lines centred at 7445Å[1] that become stronger for dwarfs with cooler, more opaque atmospheres. Ca II and Fe I lines seen in early/mid-M dwarfs disappear as VO and TiO become prominent.

A useful tool to differentiate low-mass stars and brown dwarfs is the lithium test. Stars older than 100Myr will have burned all of their lithium so it should not appear in their spectra[2] [13]. Young and hot brown dwarfs more massive than $65M_{Jup}$ can burn their lithium, so the absence of lithium does not necessarily rule out a source being a brown dwarf. The lithium test is useful for all spectral types beyond M, but its relevance begins with the hottest brown dwarfs that are found in the late-M region. For a population with a known age, such as the Pleiades open cluster, the lithium test is an excellent diagnostic tool.

Ultracool M dwarf temperatures go down to approximately 2300K and are the brightest UCDs with luminosities within the range $0.0005 > \frac{L}{L_\odot} > 0.00015$ [14]. For stellar UCDs, masses decrease for later types, with the largest UCDs having masses of $\sim 0.1M_\odot$. Both stellar and sub-stellar UCD radii do not vary significantly with mass, remaining approximately Jupiter-sized regardless of mass or spectral type.

1.1.2 L dwarfs

With the discovery of dwarfs cooler than M9.5 that have spectra differing from M dwarfs, the relatively new spectral type L was introduced by Kirkpatrick et al.

[2]Some stars do have lithium in their atmospheres, but they are too luminous to be mistaken for UCDs.

(1999) [15]. The majority of known brown dwarfs are L dwarfs, however low-mass stars are also included in the L dwarf population.

Inherently fainter than M dwarfs, L dwarfs have absolute magnitudes ranging from J=11.5 to J=14 [15] and are approximately one magnitude fainter in H. Brown dwarfs more distant than $\sim 500pc$ are not bright enough for current infrared surveys and close companions are often hidden in noise from their primaries. L dwarfs span a range of ∼2300K to ∼1400K at L8, beyond which the L/T transition appears (discussed shortly).

At L dwarf temperatures, dust condensates form to create clouds. When molecules condense into dust grains, their spectral features are significantly weakened; this is the characteristic feature of L dwarfs.

As shown in figure (4), the most noticeable L dwarf feature is the absence of strong TiO and VO lines, which are replaced as the prominent species by the metallic hydrides CrH (8611Å, 9969Å) and FeH (8692Å, 9896Å) [15]. Additionally, strong atomic lines of alkali metals - labelled in figure (4) - serve as useful L dwarf indicators.

As figures (1) and (2) show, early L dwarfs have very similar broad-band colours to late M dwarfs. There is a gradual reddening in both infrared and optical wavelengths for the L0 - L7 subtypes, beyond which the L/T transition is reached. L/T transition objects are easily spotted in *Y-J*, *J-H* and *H-K* where the colour begins to turn over from red to blue. Optically, there is a sharp reddening through the L/T transition period.

Beyond ∼L8 there is a sharp NIR colour inversion across the temperature range of 1400K to 1200K known as the L/T transition. As the atmosphere cools further, silicate dust disperses while methane and water absorption features strengthen to make the atmosphere significantly bluer. Prominent features in L/T transition objects are CH_4 absorption at 1.65μm and 2.2μm and the *JHK* bands becoming bluer due to H_2O absorption.

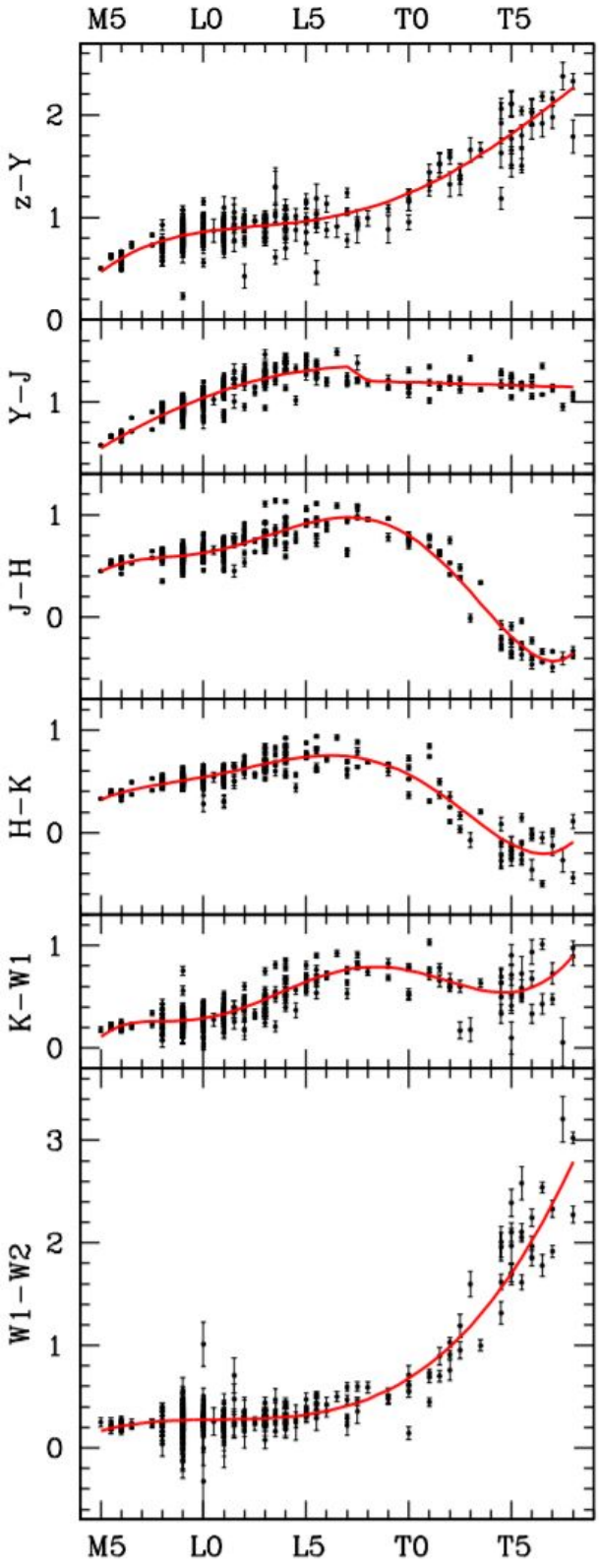

Figure 1: Infrared colours for M5-T9 dwarfs, taken from Skrzypek (2015) [16].

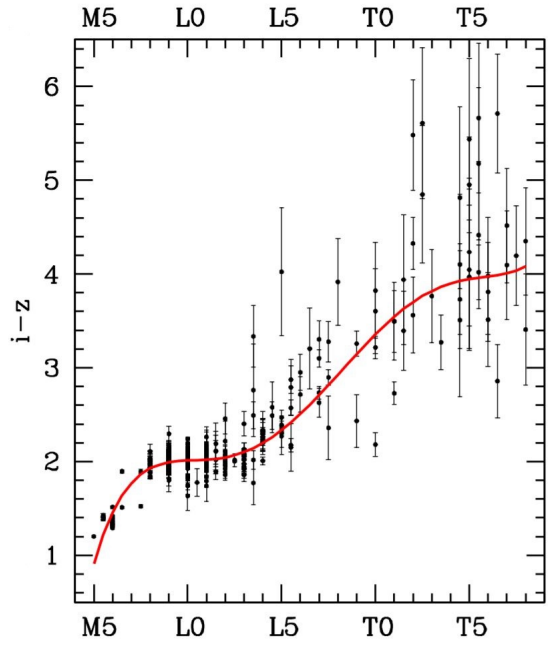

Figure 2: i-z for M5-T9 dwarfs, taken from Skrzypek (2015) [16].

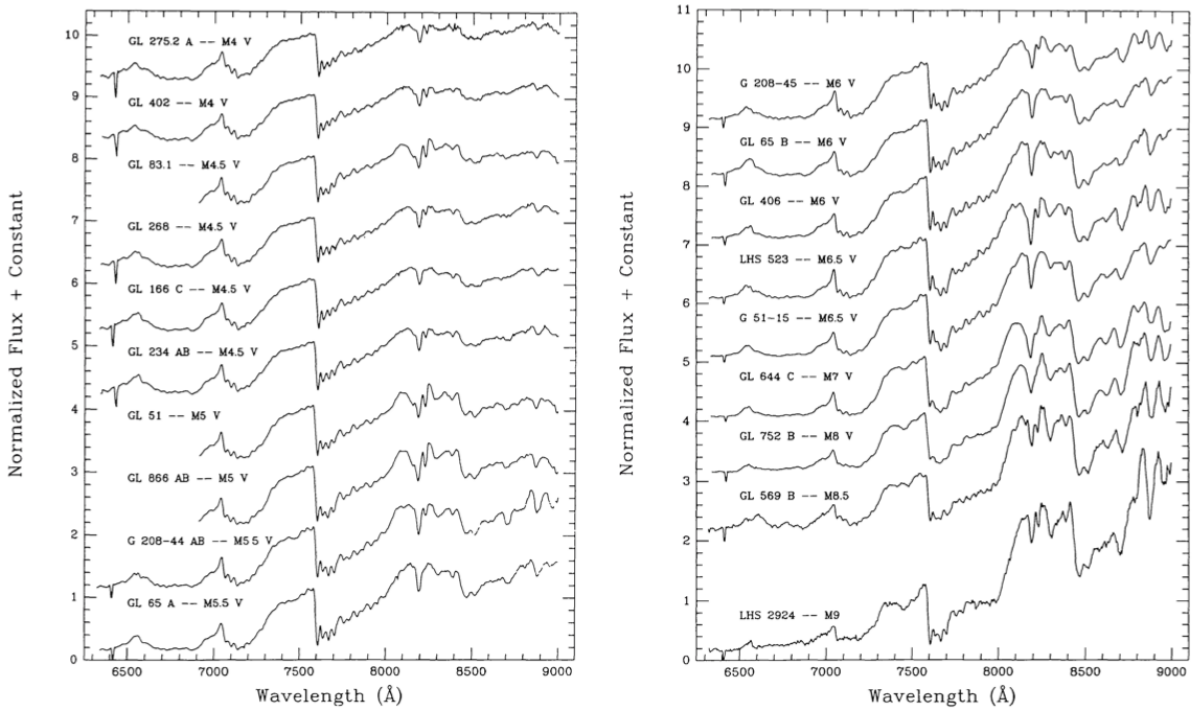

Figure 3: NIR spectral sequence for late/mid M dwarfs, taken from Kirkpatrick et al. (1991) [12].

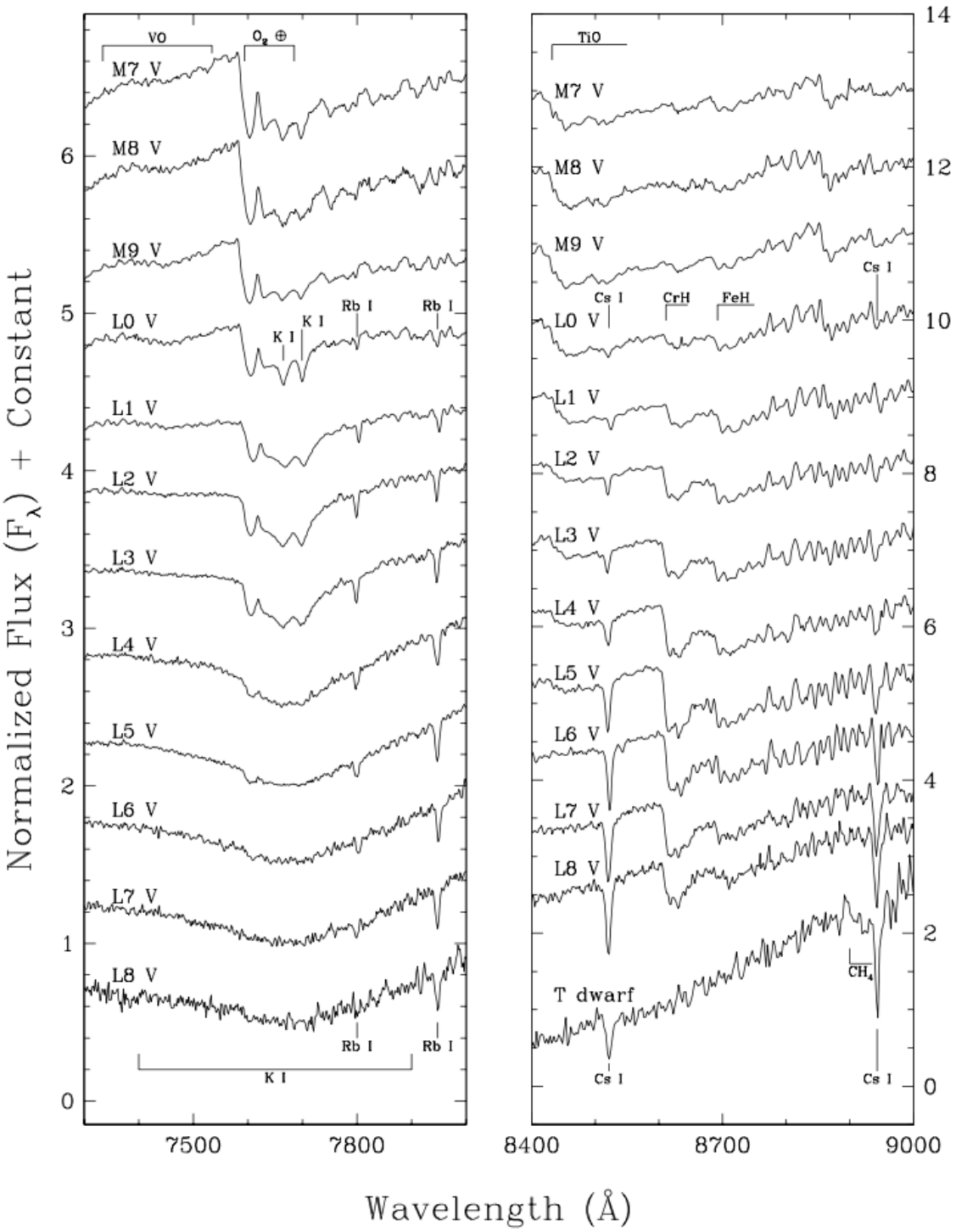

Figure 4: Optical spectral sequence for M7-L8 dwarfs, taken from Kirkpatrick et al. (1999) [15].

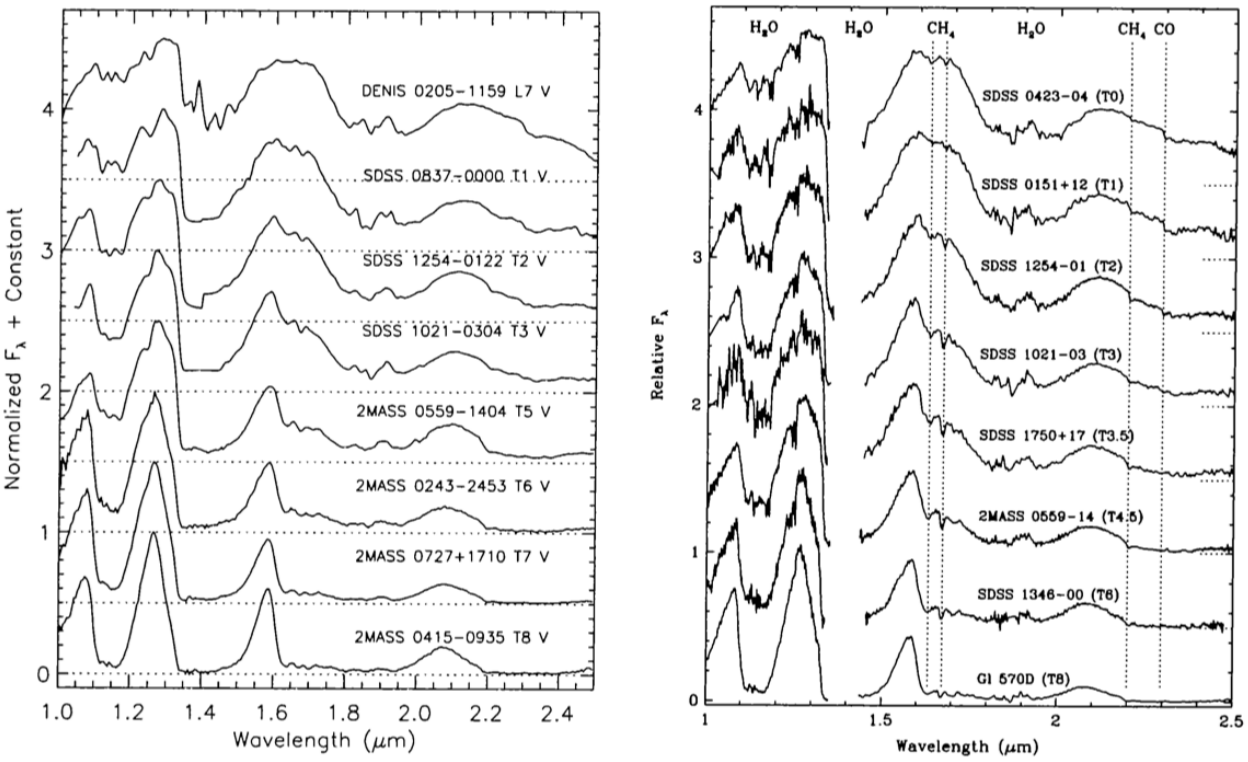

Figure 5: NIR spectral sequence for T dwarfs, taken from Burgasser (2003) [17].

1.1.3 T dwarfs

One of the first known brown dwarfs, Gliese 229B, exhibits strong methane absorption bands that resembled features seen in gas giants. The spectral type T, which is exclusively populated by brown dwarfs, was defined to describe these objects with subtypes up to T8.

As shown in figures (1) and (2), T dwarfs appear quite differently to M and L dwarfs photometrically. They are significantly redder in optical colours, however they become more blue in the NIR through later types.

The T dwarf spectral sequence, shown in figure (5), shows the aforementioned methane absorption bands in the 1-2.5 μm region. The metallic hydride features that define L dwarfs are absent in T dwarf spectra, whilst Na and K lines broaden and H_2O bands deepened in later types. The four peaks clearly visible on the left-hand side of figure (5) are characteristic of T dwarfs, becoming more prominent for later types as the methane and water absorption bands deepen to separate them more clearly. T dwarfs are further characterised by the absence of silicate clouds in the observable photosphere.

1.1.4 Y dwarfs

Y dwarfs are the newest addition to the extended MK sequence and represent the coolest known brown dwarfs, bordering giant planets. The existence of brown dwarfs cooler than T8 was expected by models [18], however as their effective temperatures are below 600K they are very difficult to detect. Only a handful have been discovered to date - approximately 20 - so there is not yet a full spectral sequence for Y dwarfs. The majority of known Y dwarfs were discovered by the WISE survey, which operates in the mid-infrared where Y dwarfs are brightest. The coolest known brown dwarf is cooler than the human body at 250K [19], although this object is likely below the $13M_J$ limit and is only considered to be a brown dwarf based upon its suspected formation process. Depending on the definition used, many Y dwarfs may be free-floating planets or sub-brown dwarfs.

Known Y dwarfs emit virtually no light at optical wavelengths and are best observed in the infrared. Absolute magnitudes of Y dwarfs have been tentatively measured with $J > 22$ [20] and some spectral features have been identified; in the NIR there is deep absorption of H_2O and CH_4 and potentially NH_3 absorption [20]. The flux peaks in J and H caused by water and methane bands can be used to differentiate Y dwarfs from late T dwarfs as they will be noticeably narrower. The bluer infrared colours seen in T dwarfs (figures (1) and (2)) appears to return to red during the T/Y transition and it is expected that Y dwarfs continue to redden in the NIR.

1.2 Formation & evolution

1.2.1 Stellar & sub-stellar formation

One possible formation mechanism for brown dwarfs (and also giant planets) is disk fragmentation due to gravitational instability in a proto-planetary disk. Attempts to simulate this have both predicted [21][22] and ruled out [23] BD formation through this mechanism; the role of magnetic fields is a critical in proto-planetary disks but is extremely difficult to simulate. As models have improved it has been harder to justify disk fragmentation as an essential mechanism for brown dwarf or giant planet formation, but it has not been ruled out for specific situations [11]. Until simulations improve, the prevalence of this formation mechanism will remain unknown. This theory does, however, provide a mechanism for companions to form around their primary.

Another BD formation mechanism is turbulent fragmentation in forming stellar clusters. Infalling gas from the surrounding molecular cloud creates a structure of filaments that have high gas density. The density of these filaments reduce the Jeans mass, allowing low-mass fragments to form. Strong tidal shocks and high velocity dispersion prevent these fragments from accreting more mass, so the fragments form into brown dwarfs or extremely low-mass stars. In simulations of a turbulent molecular cloud, approximately 10% [24] of objects formed are brown dwarfs. This model implies that UCDs are common in regions with a high density

of stars, but it cannot be the only formation mechanism as UCDs are not exclusively found in these regions.

Tidal shear and high velocity dispersion are not the only obstacles preventing accretion to stellar masses. Low-mass fragments in turbulent filaments can become associated in unstable multiple systems, from which they are ejected before they can accrete more mass. Close companions are the most likely to be ejected, which may account for the apparent lack of close companions in ultracool populations. It has been proposed that accretion can also be halted via photoionisation from nearby OB stars, however it is not thought to be a major mechanism as the brown dwarf mass function is not affected by the presence of nearby O stars [25].

1.2.2 Low-mass stars

Red dwarfs are the most common stars in the universe, making up the majority of the stellar mass in the Milky Way. Found near the end of the main sequence, red dwarfs have less mass and lower effective temperatures than other stars. Dwarfs with masses below $0.5M_{\odot}$ are considered to be low-mass, whilst extremely low-mass stars have masses below $0.1M_{\odot}$. The lower a red dwarf's mass, the lower its effective temperature. Extremely low-mass red dwarfs have temperatures below 2700K, hence they are ultracool dwarfs.

During the accretion phase, extremely low-mass stars have small protoplanetary disks that favour planet formation in the so-called habitable zone; models predict a sizeable population of Earth-mass planets orbiting ultracool dwarfs [26][27]. The TRAPPIST-1 system, an M8V ultracool red dwarf with seven terrestrial planets [28], has demonstrated that UCDs can be lucrative targets for transit surveys.

Stellar UCDs spend the vast majority of their lives on the main sequence. Their interiors are fully convective, so helium generated by P-P chain reactions does not accumulate in the core; this allows hydrogen to reach the core and continue burning until the star is almost completely depleted of hydrogen. As the star ages and the helium fraction increases, less hydrogen reaches the core so the rate of fusion decreases. This causes the core to contract, which generates heat that is transferred to the surface via convection to increase stellar luminosity.

Red dwarfs with lower initial masses have the lowest rates of fusion, giving them the longest lifetimes. Being the least massive stars in the universe, ultra-cool red dwarfs have the longest lifetimes of any stars in the known universe. For example, a $0.1M_{\odot}$ ultracool M7 dwarf with a temperature of 2500K and a radius of $\sim 0.1R_{\odot}$ would have a main-sequence lifetime of 10 trillion years [14] [29]. As ultra-cool dwarf lifetimes are several orders of magnitude greater than the age of the universe, it is not possible for any UCDs to have already evolved off the main sequence. It is thought that M dwarfs will eventually evolve into hypothesised blue dwarfs, and then finally into white dwarfs [27].

M dwarf companions have been shown to have the same metallicity as their primaries [30]. Members of multiple systems are likely to have formed from the same gas cloud, meaning all constituents should have the same metallicity. As metallicity is difficult to measure in the complicated atmospheres of ultracool dwarfs, this relationship can be used to determine a benchmark property in ultracool stars. Figure (6) shows that there is a one-to-one relationship between primary and companion metallicity.

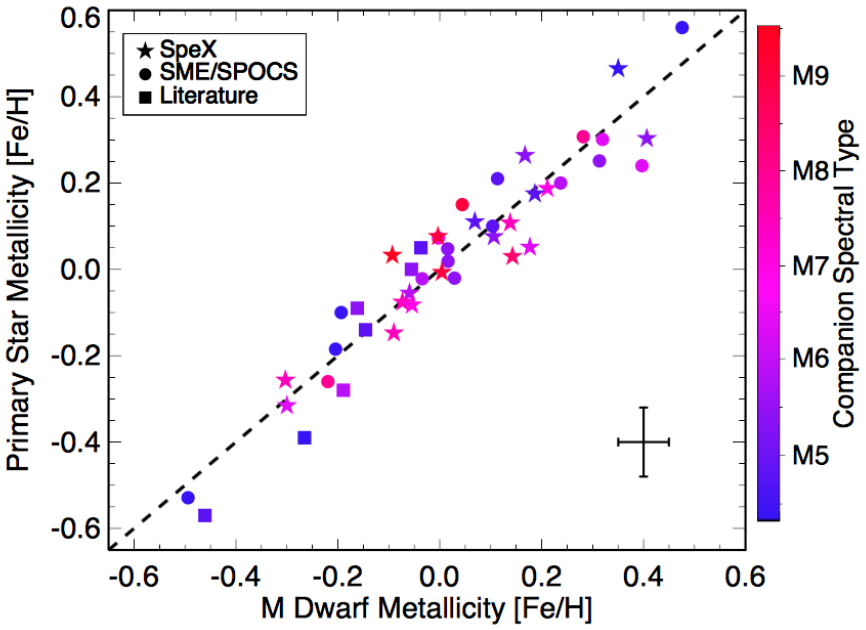

Figure 6: Primary vs companion metallicity for late M dwarfs [30].

1.2.3 Brown dwarfs

Brown dwarfs may form at any mass within the range that defines them; as mass is not being converted to energy in significant quantities they will sustain a near-constant mass throughout their lifetimes. As brown dwarfs age they undergo gravitational contraction, which is the primary source of their luminosity. As they contract they cool down sufficiently for clouds and dust condensates to appear in the atmosphere, leading to new spectral features. As they age, brown dwarfs evolve down the tracks seen in figure (7) to later spectral types.

Luminosity alone cannot be used to determine the age of a brown dwarf; one must first determine its mass before selecting the correct evolutionary track. Because of this, companion brown dwarfs are desirable targets as their masses can be estimated using their orbital motion or the age of the stellar primary.

Before large numbers of brown dwarfs were discovered, it was hypothesised that brown dwarfs could be a candidate for baryonic dark matter. If they were common enough, a hitherto undetected 'dark' population of old brown dwarfs could have

made up the majority of the mass in the galaxy. This has since been disproven; the number of detectable brown dwarfs in the galaxy would have to be orders of magnitude higher than what is observed to account for sufficient numbers of older, undetectable brown dwarfs [31].

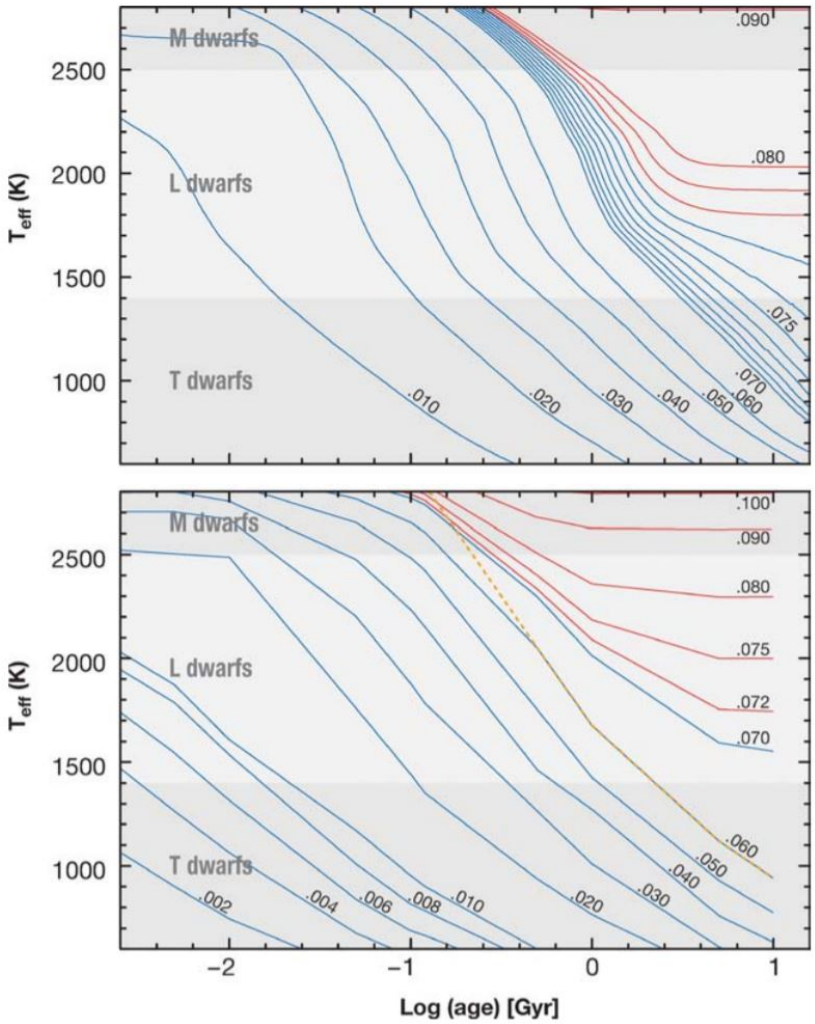

Figure 7: Brown dwarf temperature against age. Top panel from Burrows et al. (1997) [32] and bottom panel from Chabrier (2003) [33] and Baraffe et al. (2003) [34]. Mass is shown along the tracks in solar masses.

1.3 Brown dwarf diversity

Some brown dwarfs exhibit unusual spectral features or colours that are indicative of certain physical properties. These 'peculiar' objects are particularly useful as they can be used to further understanding of brown dwarf composition and evolution. In this section, several well-documented peculiarities will be described along with their causes.

1.3.1 Gravity & youth

The surface gravity g of a brown dwarf - or any other body - is given as $g = \frac{GM}{r^2}$. As brown dwarfs maintain a constant mass through their lifetimes, $g \propto \frac{1}{r^2}$. Given that brown dwarfs undergo significant contraction early in their lives, low surface gravity indicates the object has not yet contracted and it thus an indicator of youth.

A consequence of low surface gravity in brown dwarfs is more atmospheric particulates and thicker clouds. Very low gravity (VLG) brown dwarfs thus have reddened atmospheres through cloud absorption, with their spectra showing weaker CaH, K I, Na I and VO features [36] [37] with the K I reddening the J band significantly [38].

It is of course possible that VLG brown dwarfs could simply be extremely low mass BDs or sub-dwarfs however the r^2 term ensures that gravity is more sensitive to radius than mass, whereas radius does not vary significantly with mass. Low surface gravity objects are thus more likely to be young, large radius objects with a large range of possible masses than old and contracted dwarfs within a very narrow mass range that can produce low-g for small radii.

Identifying young brown dwarfs is especially useful for late-type objects as they likely formed as late-type objects instead of evolving from much earlier types. This is useful for determining the low-mass and sub-stellar IMF and, if formation processes can be inferred from primaries or the neighbouring region, predominant formation processes for low-mass objects may emerge upon comparison with formation processes of more massive UCDs.

1.3.2 Multiple systems

The majority of known UCDs are free-floating, with some companion UCDs known and fewer binary or close companion systems. These systems are difficult to detect as binaries may not be resolvable and close companions may be hidden in the glare from their primary. In order to better understand the formation and evolution of these systems, more systems need to be found.

In some cases, constituents of an unresolved binary will have different spectral types, thus observing their combined emissions as one source will result in peculiar photometry and/or spectral features. In order to resolve UCD binaries, one can model the appearance of various combinations of UCDs for comparison to binary candidates. An example of this is shown in figure (8) from Gagliuffi et al. (2014) [39] where a suspected L4+T4 dwarf is compared to model binaries.

Close companions[3] are unlikely to be detected through direct imaging, instead being more like extrasolar planets in that radial velocity and transit searches are more likely to be successful given their short orbits. Accounting for bias in de-

[3] $<$ 5AU for solar-type stars

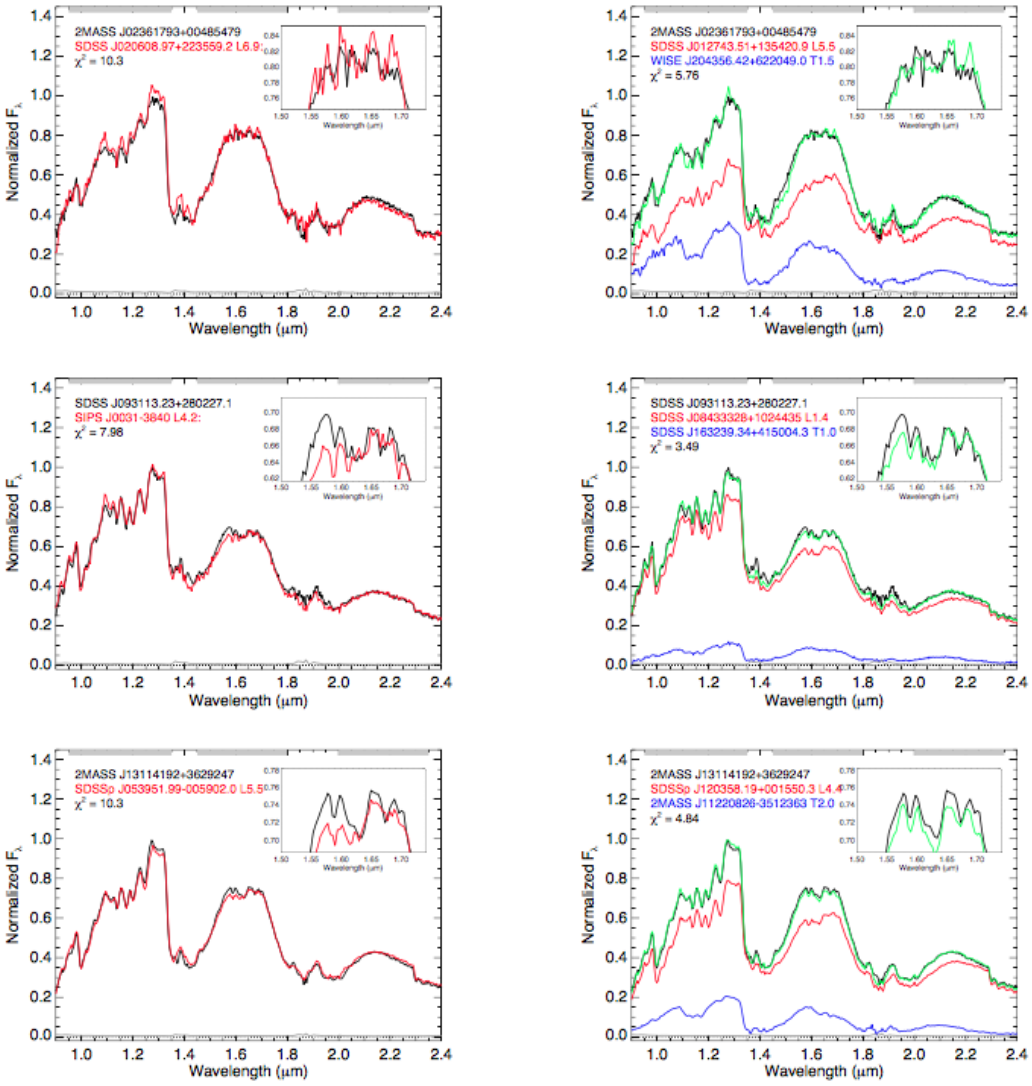

Figure 8: Three candidate binary systems, with observed spectra on the left and their binary fits on the right. On the left, the observed spectra are in black with the best-fit template shown in red. On the right, the best-fit binary template spectra are shown in green, which are the result of combining the primary (red) and secondary (blue) spectra. Taken from Gagliuffi et al. (2014) [39].

tection methods, there still remains an apparent brown dwarf 'desert' where close companions are expected. While there are several confirmed close companions, it is thought that only ∼1% of brown dwarf companions are close companions [40]. To fully explain the brown dwarf desert, formation theories must be improved using future discoveries of close companions.

1.4 Gaia

The European Space Agency's Gaia space observatory, launched in 2013, was designed to catalogue over one billion sources in 3D space. The mission is mostly focused on stars, but also encompasses comets, minor planets, brown dwarfs, extrasolar planets and quasars amongst other celestial bodies. It is thought that Gaia will observe up to 1% of the stars in the Milky Way, vastly outnumbering preceding surveys.

At the time of writing, Gaia is nearing the end of its planned five-year mission, however the spacecraft has sufficient consumables to continue for another four years should its mission be extended. ESA will continue to process and publicly release data for several years beyond the end of the spacecraft's mission.

Gaia was designed to achieve unprecedented astrometric precision, aiming to observe each source 70 times in order to determine not only its position in space but also its motion. Gaia is a successor to the *Hipparcos* survey, which is only $\sim 0.001\%$ the planned size of the final Gaia catalogue and Gaia's positional accuracy is an improvement by a factor of 100 [41].

The first Gaia data release does not include parallax or proper motion data from Gaia itself. The reason for this is that Gaia DR1 is constructed from the first year of observations, which is too short a baseline for accurately measuring motion but sufficient for improving positional certainty for both new and known stars. Gaia DR2 includes a larger number of sources, along with parallax, proper motion and radial velocity measurements using the longer baseline.

The Gaia DR1 release is accomanied by the Tycho-Gaia Astrometric Solution [42]. TGAS matches sources from the Tycho-2 catalogue with Gaia sources to increase the baseline between detections for the determination of parallax and proper motion. Due to the smaller size of Tycho-2 and required baselines for parallax measurements, TGAS is significantly smaller than the full Gaia DR1 release, with just 2.5 million sources. Nevertheless, TGAS is a valuable resource that improves upon its predecessors in both scale and precision.

Figure (9) shows that TGAS parallax uncertainty varies due to requiring overlapping coverage. This is rectified in Gaia DR2, where parallax uncertainty is much more consistent across the sky as well as more accurate, as shown in figure (10).

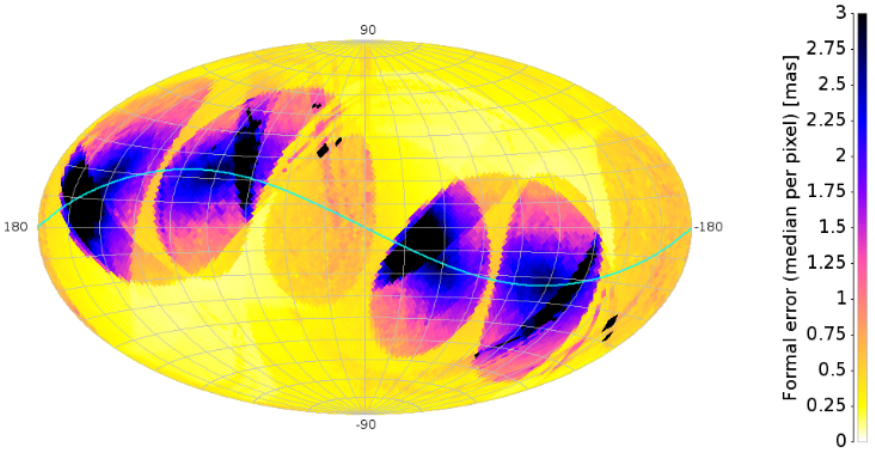

Figure 9: All-sky map of parallax uncertainty for TGAS sources. Taken from Michalik et al. (2015) [42]

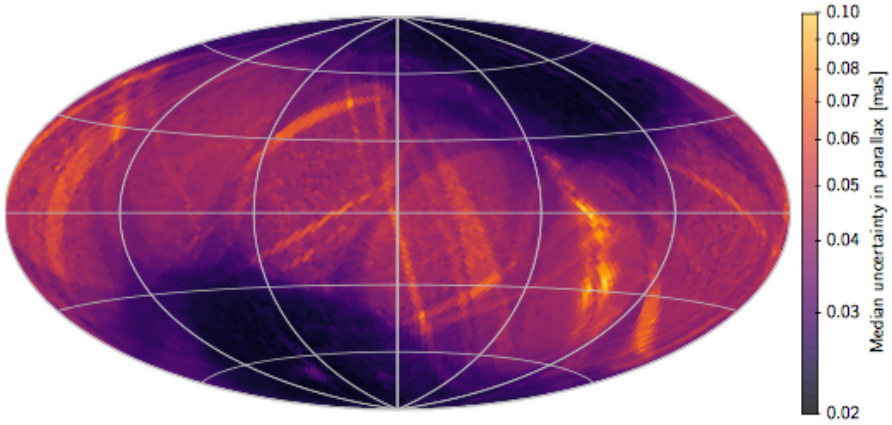

Figure 10: All-sky map of parallax uncertainty for Gaia DR2 sources. Taken from Gaia Collaboration (2018) [43]

1.4.1 Benchmarks

As explained in Pinfield et al. (2006) [44], in order to determine the mass, age and composition of a UCD one must measure T_{eff}, g and metallicity from spectra. In order to do this, one must have accurate theoretical models or a diverse population of UCDs that have had their mass, age and composition determined independently of their spectra. The latter are known as *benchmark* UCDs, as their recorded spectra can be used as calibrators for T_{eff}, g and $[Fe/H]$.

In the case of companions, most stars are brighter and better modelled than UCDs, so their age and composition can be determined and used to constrain properties of companions. For close binaries, dynamical masses can be measured using radial velocity.

The 2MASS All Sky Survey was used to constrain the wide L dwarf companion fraction to $2.7^{+0.7}_{-0.5}$% for 1000-5000 AU, equating to a brown dwarf companion fraction of 34^{+9}_{-6}%. Accounting for limitations in detecting or confirming these companions, only a small number of 2MASS UCDs are thought to be confirmable benchmark companions.

Before the release of the first Gaia catalogues, it had been suggested that ultracool companions to Gaia stars would make excellent benchmark UCDs. Not only does Gaia provide a sizeable catalogue of stars around which one may find companions, but parallax, proper motion and radial velocity measurements can be used to confirm companionship and constrain benchmark properties of their companions.

Marocco et al. (2017) [45] is a comprehensive study of confirmable Gaia benchmarks that simulates the results of a search for benchmark UCDs that are Gaia companions. The study finds ∼24,000 benchmark companions outside the galactic plane and estimates that ∼500 diverse benchmarks could be confirmed with Gaia.

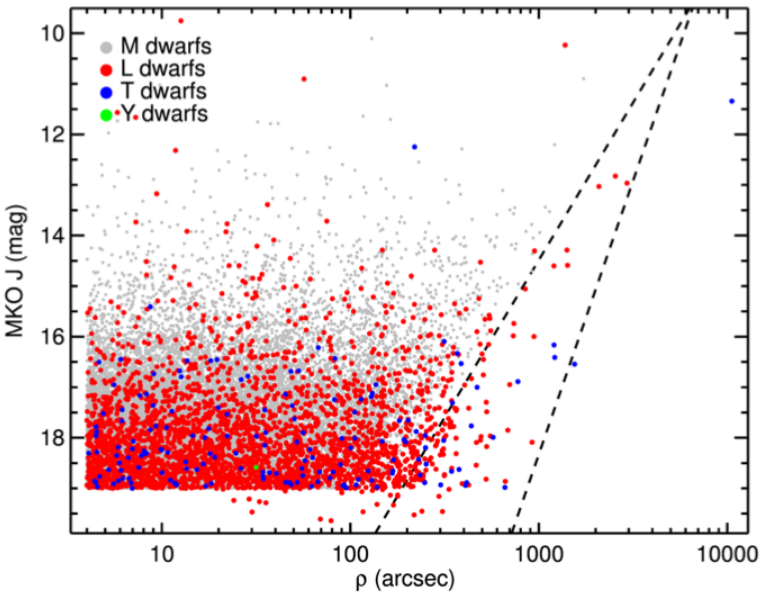

Figure 11: Simulated CGBs separations; the dashed lines represent angular separation cutoffs for M and L systems. Taken from Marocco et al. (2017) [45].

Figure (11) shows the simulated confirmable Gaia benchmark (CGB) population, which truncates at wide separations to minimise the false alarm probability. The mass-age distribution shown in figure (12) shows that one is much more likely to find young companions with ages of 2-3Gyrs.

Marocco conducted a preliminary search for benchmark companions with TGAS, focussing on metal-rich/poor-system, resulting in 13 new benchmarks.

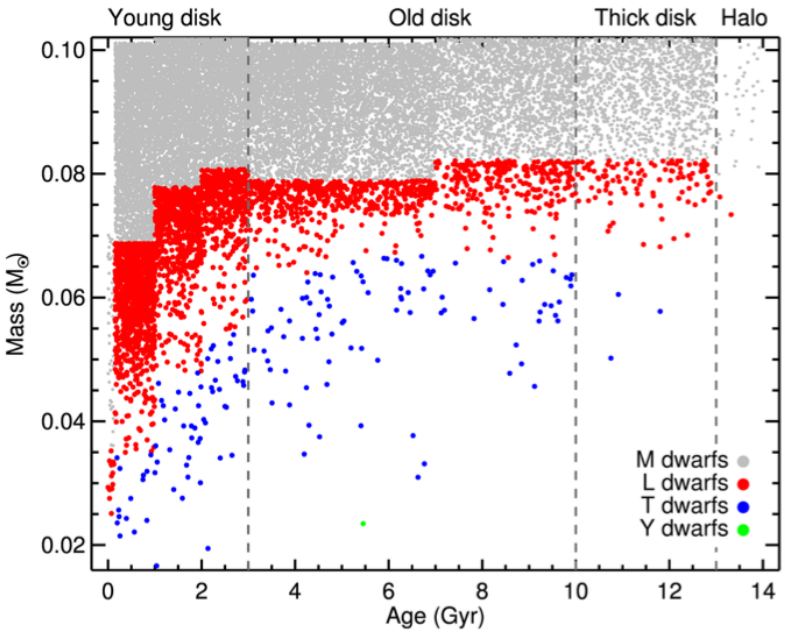

Figure 12: Simulated mass-age distribution of CGBs. Taken from Marocco et al. (2017) [45].

1.4.2 Project motivation

The work of Marocco et al. described in section 1.4.1 shows that a large population of hitherto undiscovered benchmarks exists. This project aims to find these benchmark Gaia companions so that they may further our understanding of UCDs and the physics by which they form and evolve.

A high priority will be given to finding particularly unusual benchmarks that exhibit rare spectral features. Instead of a search using spectra, a photometric method is used to identify catalogue candidates for spectroscopic follow-up. There are few known benchmarks for such objects, making them the least understood UCDs.

In order to select peculiar objects, care is taken to prevent their elimination during bulk selection and a novel photo-typing method is explored in an attempt to quantify peculiarity. Candidate benchmark companions are then put through a variety of tests made possible by Gaia to select the best candidates for follow-up and confirmation of their status as benchmark companions.

The second section of this thesis describes the process of selecting candidates from catalogues and the methods used to identify peculiar objects. The third section describes the results of an observing run whilst the fourth section reviews the final list of candidate benchmark companions. The fifth section analyses the effectiveness of the methods employed for this project and provides recommendations for future work.

2 Selecting candidate ultracool companions

This project's search for ultracool companions can be broken down into several steps

- Identify candidate UCDs from surveys
- Photo-type candidates
- Identify peculiar UCDs
- Cross-match with Gaia catalogues to find primaries
- Remove contamination
- Confirm companionship through common proper motion tests (where possible)
- Conduct follow-up observations with high resolution imaging and spectra

Similar searches have been conducted in the past [46], however this project differs in two major ways. Firstly, a photo-typing routine (see section 2.2) is used to classify a bulk selection of candidates and identify peculiar sources. Secondly, the project does not consider properties of the primary when selecting candidate companions, thus preventing any bias being introduced by prioritising candidate companions to stars with what are thought to be favourable properties.

2.1 Bulk selection

The photo-typing method classifies objects based upon their broad-band photometry. As described in section 2.2, the routine written for this project requires all candidates to have available photometry in the i, z, Y, J, H, K, W1 and W2 filters. In order to get such a wide coverage, it was necessary to select candidates from multiple surveys with overlapping coverage.

For the sake of simplicity, it was decided that multiple surveys should not be used to cover one band (such as using both UKIDSS and VHS for J). Differences in filter construction are difficult to account for, meaning that if source photometry is not perfectly converted to the preferred system there is a risk of introducing systematic uncertainty. Several test selections were made and found that one survey per filter would provide an adequate number of candidates for follow-up, with the option of introducing more surveys remaining open for later searches.

The WISE survey was obviously the only choice for the W1 and W2 filters, however there were several options for the other bands. As Skrzypek (see section 2.2) used UKIDSS and SDSS to define template colours, it was decided that newer data releases of those surveys should be used for the YJHK and iz filters respectively. These surveys were designed for a maximum coverage overlap, which is shown in figure (13).

The UKIDSS Large Area Survey covers an area of 4000 square degrees to a depth of K=18.4 with a mean photometric uncertainty of 0.02mag. As UCDs will be close to the maximum depth of the survey, the mean photometric error for them will be larger. Y dwarfs, along with all but the youngest and closest T dwarfs, are too faint to be detected by this survey and are not expected to be found. M and L dwarfs, on the other hand, should be detected in large numbers.

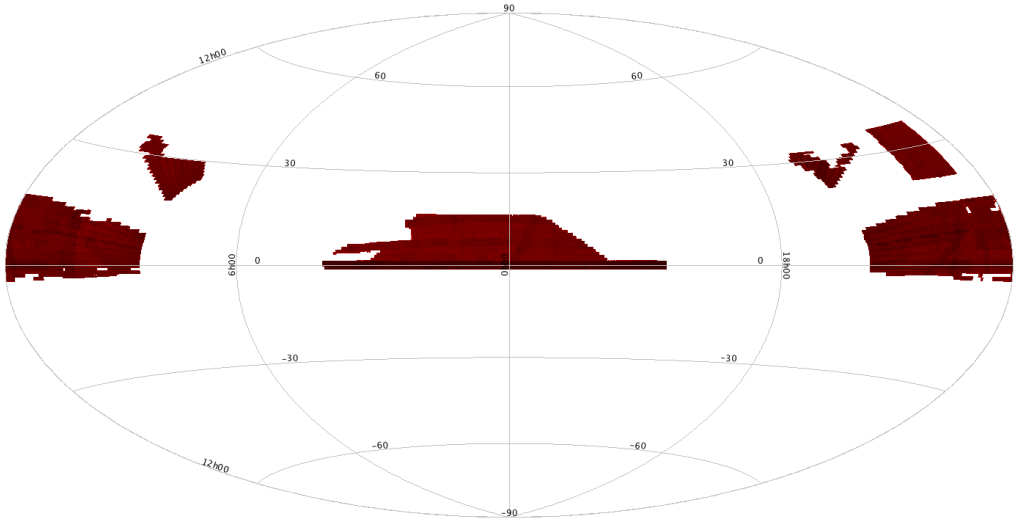

Figure 13: SDSS DR9 & LAS DR9 coverage.

The imaging instrument used for LAS is WFCAM, which has 0.4arcsec pixels. For the most distant detectable UCDs (∼500pc), one can expect a companion to be resolvable if its separation is to the order of 10^3AU. The transmission curves for the survey are designed to be resistant to atmospheric conditions and conversion to and from other photometric systems, such as SDSS bands calibrated on the AB system, is widely documented.

The Sloan Digital Sky Survey was chosen as the source of i and z band photometry as LAS mostly covers areas surveyed by SDSS, meaning that cross-matching the two surveys results in minimal losses. The 9th data release was used for both surveys as they were the newest available on the CDS cross-match service, which was a preferable retrieval source as the large numbers of sources being selected does not suit other retrieval methods. While there are newer data releases for both surveys, they are not significantly larger nor is the data improved in ways that are relevant to the project.

The SDSS i and z bands have a depth of 21.3 and 20.5 respectively and photometric uncertainty below 1%. Optical spectra are available for a small portion of sources, although all but the brighest UCDs would be too faint to have SDSS spectra available. Instead of retrieving spectra for the initial bulk selection, only the

much smaller final candidate list was checked for available SDSS spectra.

As the photo-typer template colours (section 2.2) are all calibrated to Vega, SDSS magnitudes were converted from AB to Vega using generic offsets of 0.37 and 0.54 for i and z respectively [47]. While these conversions are acceptable, it should be noted that more accurate offsets specific to UKIRT filters are available in Hewett et al. (2006) [48]. The difference between the 'generic' offsets and the UKIRT-specific offsets is < 0.01mag so it was not deemed to be worth spending time re-selecting targets with the slightly better conversions.

A decision was made not to cross-match with WISE nor use the W1 or W2 filters in the photo-typing routine. Preliminary tests with a small sample matched with WISE showed that it made little difference to the photo-typing results, especially as this project is more focused on M and L dwarfs than T or Y. Each additional filter increases the time it takes for the photo-typing routine to run, thus only the most useful bands should be used.

The selection process split candidates into candidate M dwarfs[4] and candidate L, T or Y dwarfs. By having two separate candidate lists, file sizes were kept manageable and allowed for testing various IDL routines quickly on the smaller L/T/Y catalogue before running them on the larger M dwarf candidate list. The selection began with a retrieval of all LAS DR9 sources within the Y-J ranges below followed by a 1.5as cross-match with SDSS DR9 and the below i-z cuts. The matching radius is large enough to allow for high proper motion sources to still be matched (up to 10 years at 150mas/yr) whilst minimising the risk of erroneous matches. The colour cuts, which are based upon various published colour-colour diagrams, are deliberately 'generous' by allowing large numbers of contaminatory sources through to ensure that UCDs with even the most extreme peculiarities are not inadvertently removed.

1. M dwarfs
    - $0.6 <$ Y-J < 0.8
    - $1.4 <$ i-z < 2.0
2. L/T/Y dwarfs:
    - $0.8 <$ Y-J
    - $2.0 <$ i-z

There was an additional cut of $P_{noise} < 0.9$ applied to both surveys. While there is a P_{galaxy} parameter offered by SDSS, it was ignored as it is not uncommon for brown dwarfs to be erroneously classified as galaxies by surveys that only consider optical/NIR colours. A $J < 19$ cut was also applied to eliminate sources that have unreliable photometry and would be difficult to follow up observationally. The cuts lead to a sample of 8,932,082 M dwarf candidates and 3,224,326 L/T/Y candidates.

[4] M7-M9

These cuts are deliberately generous to ensure peculiar UCDs aren't eliminated, however this comes at the cost of higher contamination from other sources such as galaxies or earlier M dwarfs.

With the J=19 cut-off, one can expect inherently brighter UCDs to be more frequent as they will be detectable at greater distances. The bulk selection will include M dwarfs that could be beyond 500pc, whereas L dwarfs will only be detectable up to ∼300pc as their absolute magnitudes are fainter. This means the search volume for M dwarfs is ∼5 times larger. T dwarfs may only be detectable within tens of parsecs whilst Y dwarfs may only be detectable within 10pc. Because of these drastically different search volumes, the majority of candidates will be M and L dwarfs with few T dwarfs and very few, if any, Y dwarfs.

2.2 Photo-typing

Determining the spectral type of a candidate companion requires NIR spectra, which is difficult to obtain. While some surveys - such as SDSS - have spectra for some objects, the inherently faint nature of ultracool companions generally restricts spectral type determination to objects that can be observed with precious telescope time. If it were possible to determine spectral type for a large number of candidates without follow-up observations, one could specifically search for benchmark systems with companions from each ultracool sub-type. Furthermore, objects that are atypical and exhibit unusual features would be easier to identify.

In the absence of spectra, it is possible to estimate the spectral type of an ultracool object using broad-band photometry. As demonstrated by Skrzypek et al. (2015) [16], a 'photo-typing' method can be used that compares each candidate to a set of template colours for spectral sub-types and produces a χ^2 statistic that describes how similar a candidate is to the template object. A χ^2 value of zero would indicate a perfect match whilst a very large value would indicate a large difference between the candidate and the template.

Using LAS, SDSS and WISE photometry, Skrzypek identified over 1000 L and T dwarfs using a photo-typing method to classify sources by their best χ^2 match. For this project, the method (described below) was recreated using an IDL routine to read in the initial bulk selection and choose the best matching subtype for each source and record its associated χ^2 value.

For N photometric bands b each source will have measured magnitudes $\hat{m}_b$ with associated uncertainties σ_b. In this case, the bands are Y, J, H, K, i, z, W1 and W2. For each subtype t there is a set of template colours, which are calibrated to a chosen reference band B using the term $c_{b,t}$ (i.e. $c_{B,t} = 0$) which specifies source brightness. The formula for χ^2 is thus:

$$\chi^2(\{\hat{m}_b\}, \{\sigma_b\}, \hat{m}_{B,t}, t) = \sum_{b=1}^{N_b} \left(\frac{\hat{m}_b - \hat{m}_{B,t} - c_{b,t}}{\sigma_b} \right)^2 \quad (1)$$

where

$$\hat{m}_{B,t} = \frac{\sum_{b=1}^{N_b} \frac{\hat{m}_b - c_{b,t}}{\sigma_b^2}}{\sum_{b=1}^{N_b} \frac{1}{\sigma_b^2}}$$

χ^2 is reduced by the number of photometric bands (i.e. divided by 8 if all bands are used). The reference bands describe the subtypes M7-T8, thus the photo-typing method cannot identify Y dwarfs until there are more confirmed examples with which one can construct template subtype colours. An important distinction to note in Skrzypek's method is that it is not based on measured and predicted magnitudes, not colours. The template colours for the method are shown in figure (14).

SpT	$i-z$	$z-Y$	$Y-J$	$J-H$	$H-K$	$K-W1$	$W1-W2$
M5	0.91	0.47	0.55	0.45	0.32	0.11	0.17
M6	1.45	0.60	0.67	0.53	0.39	0.22	0.21
M7	1.77	0.70	0.78	0.56	0.44	0.25	0.24
M8	1.93	0.77	0.87	0.58	0.47	0.26	0.26
M9	1.99	0.82	0.96	0.60	0.51	0.27	0.27
L0	2.01	0.86	1.04	0.63	0.54	0.29	0.27
L1	2.02	0.88	1.11	0.67	0.58	0.33	0.28
L2	2.04	0.90	1.18	0.73	0.63	0.40	0.28
L3	2.10	0.92	1.23	0.79	0.67	0.48	0.29
L4	2.20	0.94	1.27	0.86	0.71	0.56	0.30
L5	2.33	0.97	1.31	0.91	0.74	0.65	0.32
L6	2.51	1.00	1.33	0.96	0.75	0.72	0.36
L7	2.71	1.04	1.35	0.97	0.75	0.77	0.41
L8	2.93	1.09	1.21	0.96	0.71	0.79	0.48
L9	3.15	1.16	1.20	0.90	0.65	0.79	0.57
T0	3.36	1.23	1.19	0.80	0.56	0.76	0.68
T1	3.55	1.33	1.19	0.65	0.45	0.71	0.82
T2	3.70	1.43	1.18	0.46	0.31	0.65	0.99
T3	3.82	1.55	1.18	0.25	0.16	0.59	1.19
T4	3.90	1.68	1.17	0.02	0.01	0.55	1.43
T5	3.95	1.81	1.16	-0.19	-0.11	0.54	1.70
T6	3.98	1.96	1.16	-0.35	-0.19	0.59	2.02
T7	4.01	2.11	1.15	-0.43	-0.20	0.70	2.38
T8	4.08	2.26	1.15	-0.36	-0.09	0.90	2.79

Figure 14: Template colours for M5-T8 UCDs on the Vega system. Taken from Skrzypek (2014) [16].

The M5 and M6 templates were not used, meaning that they would most likely have a best match of M7 but with a high χ^2 that would be easily separated from 'true' M7 dwarfs. In future work, it is recommended that the M5 and M6 template colours are used and included in the photo-typing routine as peculiar mid-M dwarfs may still be of interest to the field and simplify decontamination of the M7 candidates. It is also recommended that the W1 and W2 bands are included as they are useful in identifying T dwarfs and should have complete coverage.

The photo-typing routine was tested by running it on Skrzypek's sample of ∼1300 L and T dwarfs with photo-types and best-match χ^2 values. Some deviation in photo-types and χ^2 was expected due to the removal of the W1 and W2 bands and the usage of later data releases for UKIDSS and SDSS. Figure (15) shows that for the

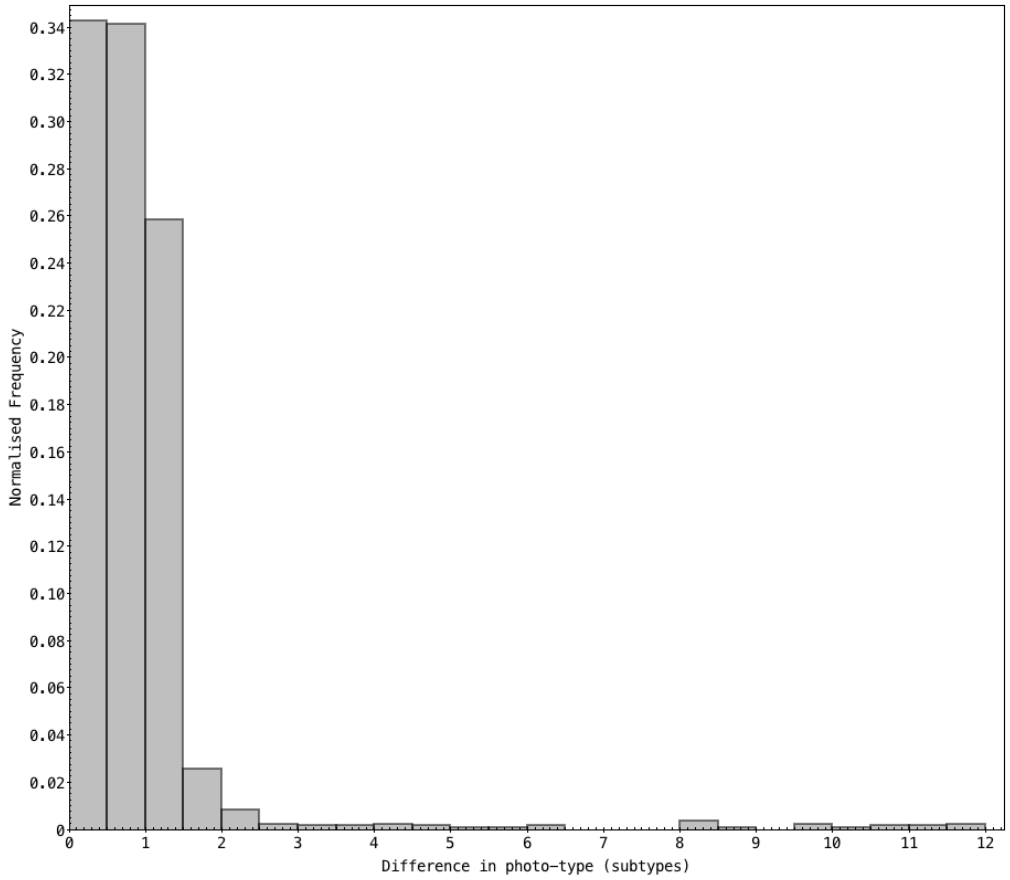

Figure 15: Histogram showing difference in photo-(sub)types between original and re-created photo-typing routine. The normalised frequency represents the fraction of the total sample.

majority of candidates, the recreated photo-typing routine agrees with Skrzypek's routine to within one sub-type. In the recreated sample, the mean subtype is half (0.47) a subtype earlier with a standard deviation of 1.28. Given that photo-typing is not meant to replace spectra and is only meant for estimates, this is an acceptable uncertainty considering Skrzypek's stated 1.5 subtype uncertainty, and that the main purpose of the photo-typing method is to use χ^2 to make peculiar sources stand out.

Figure (16) shows a clear population of L/T transition objects that the recreated routine has mis-typed. Skrzypek's version used WISE colours, which are particularly good at distinguishing objects in this region thus the recreated phototyper performs poorly when photo-typing L/T transition objects. Given that the L/T transition only spans a few faint subtypes, transitionary objects are expected to be relatively uncommon. This is compounded by the limitations of the surveys used in the bulk selection and so the impact of the issues with the recreated photo-typer should be small. The mis-classified L/T transition objects have high χ^2 values thus any L/T transition objects in the bulk selection can still be identified as they will present as peculiar sources.

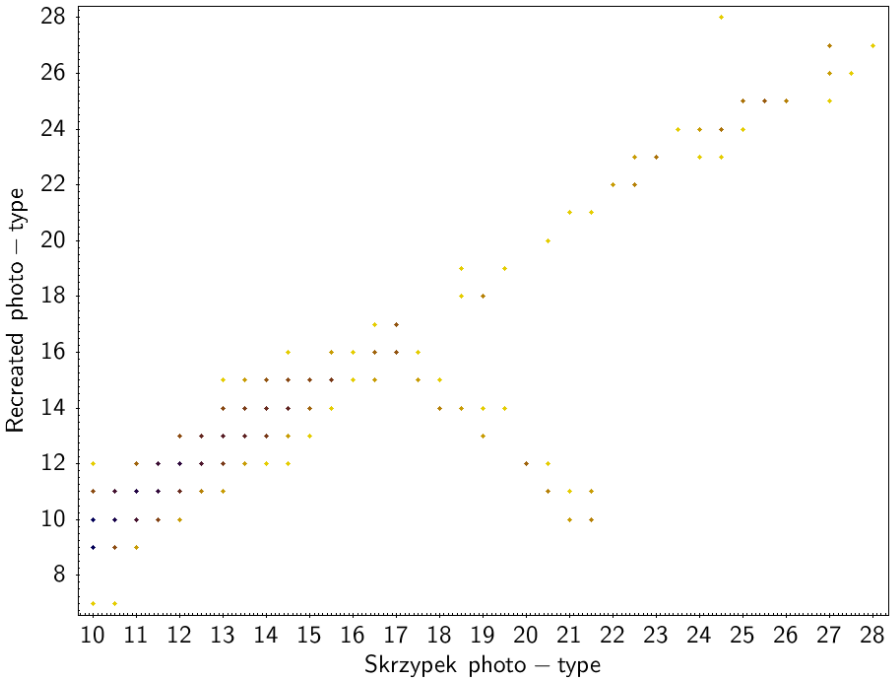

Figure 16: Recreated photo-type against Skrzypek photo-type. 10=L0, 28=T8.

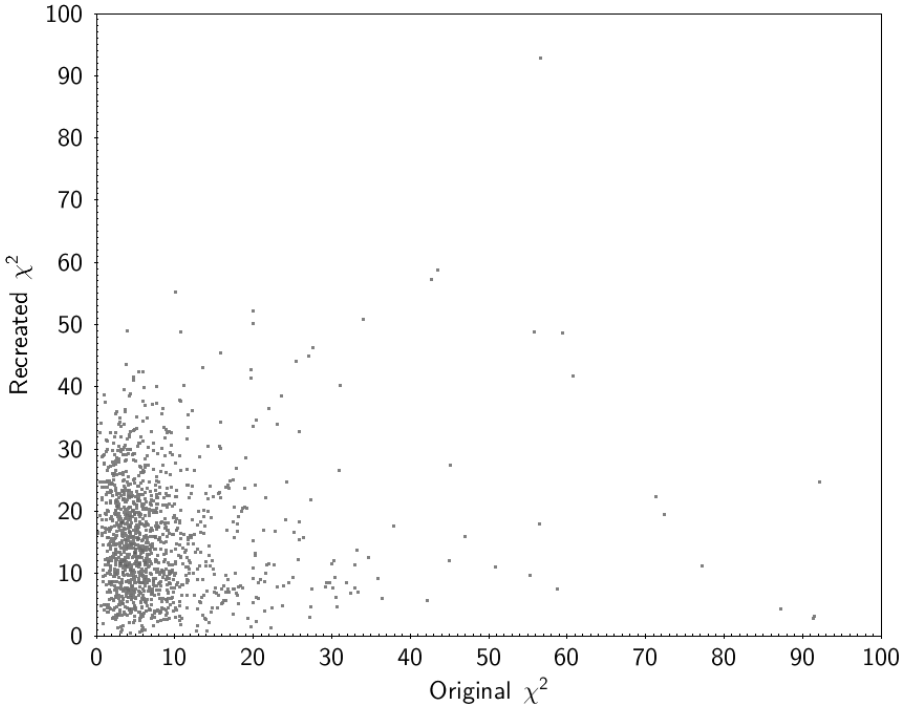

Figure 17: Recreated against original χ^2 (truncated to 100).

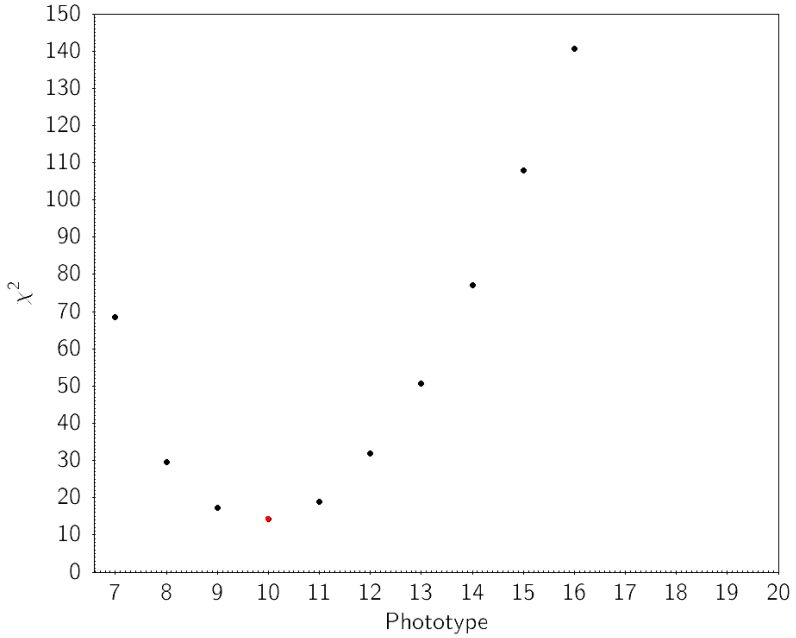

Figure 18: χ^2 per subtype for a randomly selected Skrzypek candidate. The best χ^2 fit (lowest value, marked red) corresponds to L0 thus this object is classified as L0.

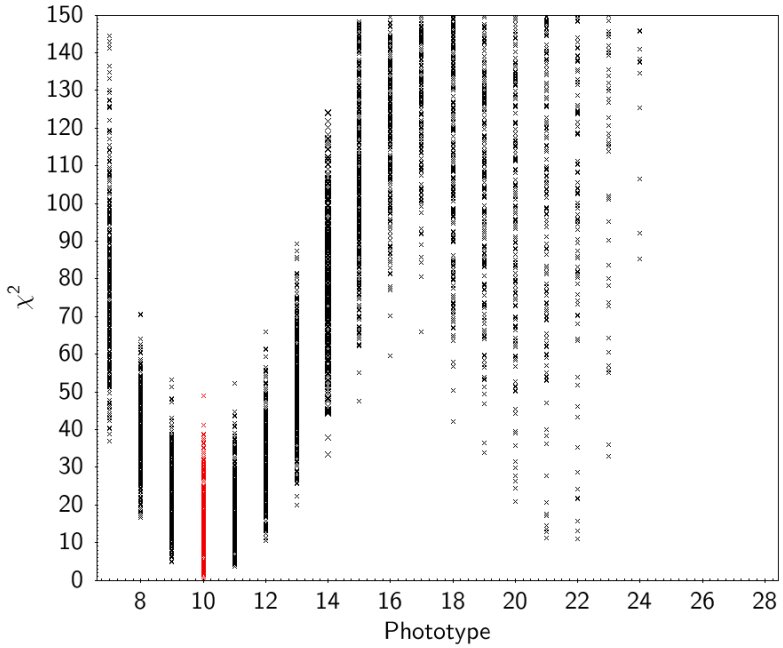

Figure 19: χ^2 per subtype for all Skrzypek candidates that were classified as L0. Note that some L/T transition objects are a good fit to L0; if any are incorrectly classified they can be identified in colour-magnitude diagrams at a later stage.

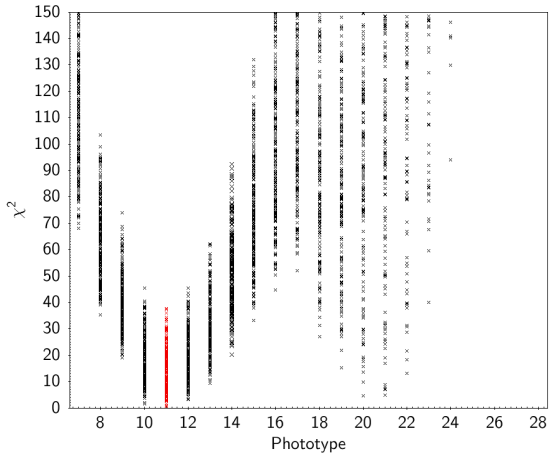

Figure 20: χ^2 per subtype for all Skrzypek candidates that were classified as L1.

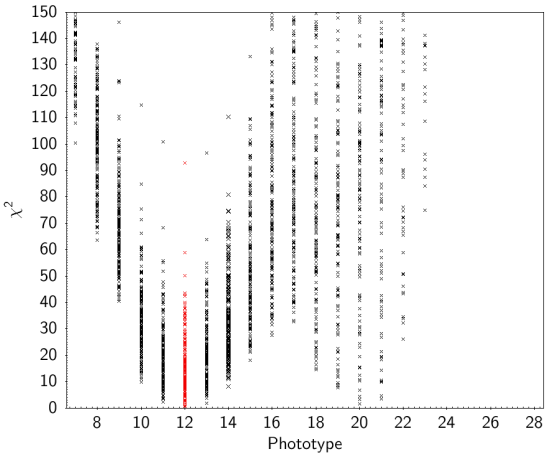

Figure 21: χ^2 per subtype for all Skrzypek candidates that were classified as L2.

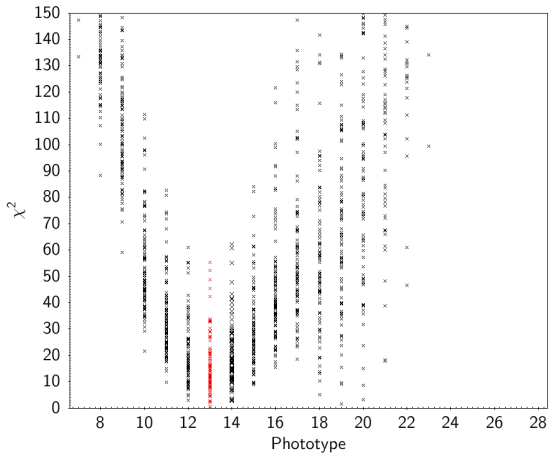

Figure 22: χ^2 per subtype for all Skrzypek candidates that were classified as L3.

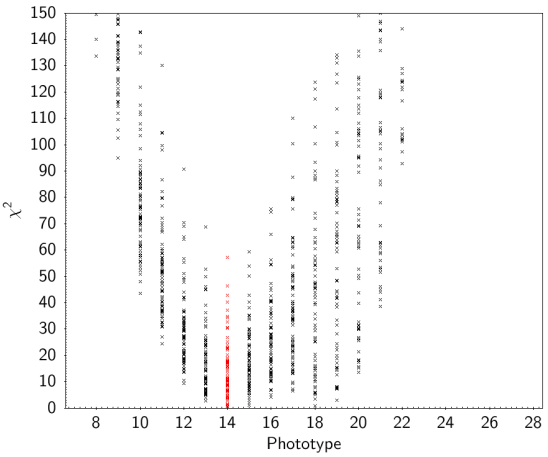

Figure 23: χ^2 per subtype for all Skrzypek candidates that were classified as L4.

The main source of deviation between the χ^2 values from the original and recreated photo-typers is the usage of W1 and W2 filters. Firstly, it should be noted that a reduced χ^2 is being used. As figure (1) shows, W1-W2 remains relatively level from M5 to the L/T transition. As the vast majority of sources tested lie within that range, their W1 and W2 photometry will always be a very good fit for any subtype that the other six bands fit best. This means that the W1 and W2 bands do not significantly increase the χ^2 value before it is reduced. Without those bands, χ^2 is only slightly lower before it is reduced by fewer bands, thus resulting in a higher reduced χ^2.

The χ^2 values themselves are not particularly meaningful; peculiar objects with a worse fit to the template will have a high χ^2 relative to the general population regardless of their absolute χ^2 values. The vast majority of sources were shifted to a higher χ^2, however a small number saw a decrease. The difference in χ^2 between the two photo-typing routines is shown in figure (24). The sources with a large shift are extremely $\chi^2 > 100$ sources that have a lower χ^2 from the recreated photo-typing routine as they are sources with particularly unusual WISE colours.

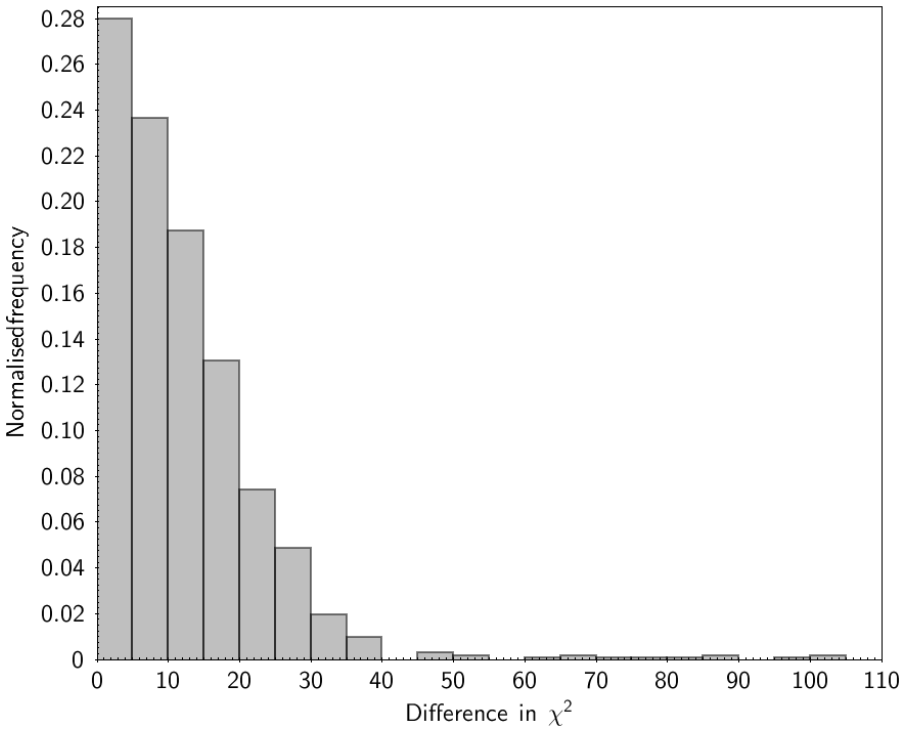

Figure 24: Difference in χ^2 between Skrzypek and recreated photo-typing routines.

Skrzypek defines objects with $\chi^2 < 5$ to be good matches and $\chi^2 > 20$ to be peculiar. These ranges are not applicable to the recreated photo-typing routine, so known UCDs that exhibit peculiar features were photo-typed and compared to the non-contaminated population published by Skrzypek.

The most comprehensive list of peculiar brown dwarfs is compiled by Jonathan

Gagne and combines the popular Dwarf Archives[5] catalogue with the Dupuy parallax database [49]. The three categories that have enough examples are subdwarfs, unresolved binaries and unusually blue UCDs. While these are far from being the only types of peculiarities one can expect to observe - such as unusually red UCDs or close companions - there are too few examples to base an expected χ^2 upon.

As few peculiar objects have full YJHKiz photometry, the i and z bands were dropped to maximise the sample size thus the photo-types are from YJHK photometry alone. The bulk selection has iz photometry, meaning the χ^2 range will differ from this test but the relative distributions of the 'normal' and peculiar samples should give some idea of where these objects will be found in a photo-typed bulk selection.

Figures (25) through (27) show the resulting χ^2 distributions for the three populations of peculiar UCDs. It is immediately obvious that sources flagged with the 'blue' peculiarity do not stand out at all when compared to a standard UCD population, and only a small number of binaries show a higher proportion of high χ^2 sources. It is expected that various binary configurations would produce a wide range of χ^2 values and given that a relatively small sample was used, it is possible that that there could be more deviation with a larger sample. The subdwarf population, which was the largest tested, shows significant deviation from the distribution seen in the Skrzypek population. This shows that the χ^2 statistic can be useful for identifying peculiar sources, as the proportion of sub-dwarfs increases drastically as the population tails off. While subdwarfs are normally most noticeable in optical bands, they are slighly blue in the NIR [50] which is enough to make them stand out in this YJHK test.

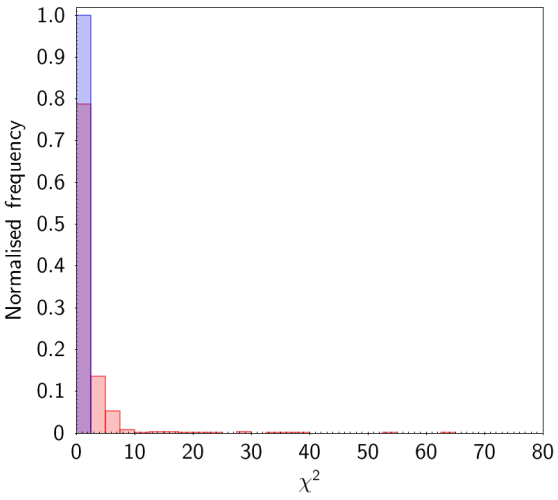

Figure 25: Histogram of χ^2 distribution for a normal population (red) and unusually blue population (blue).

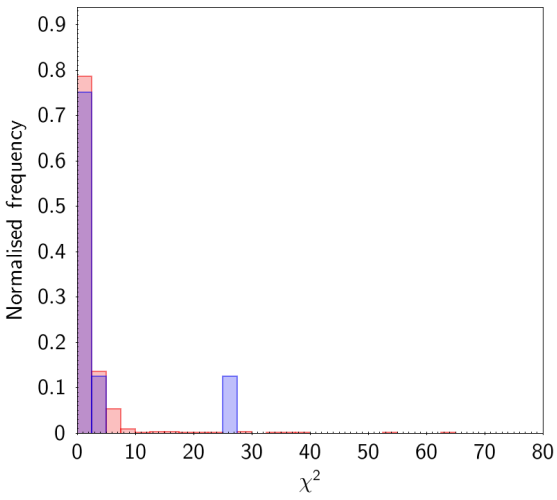

Figure 26: Histogram of χ^2 distribution for a normal population (red) and binary population (blue).

[5]http://dwarfarchives.org

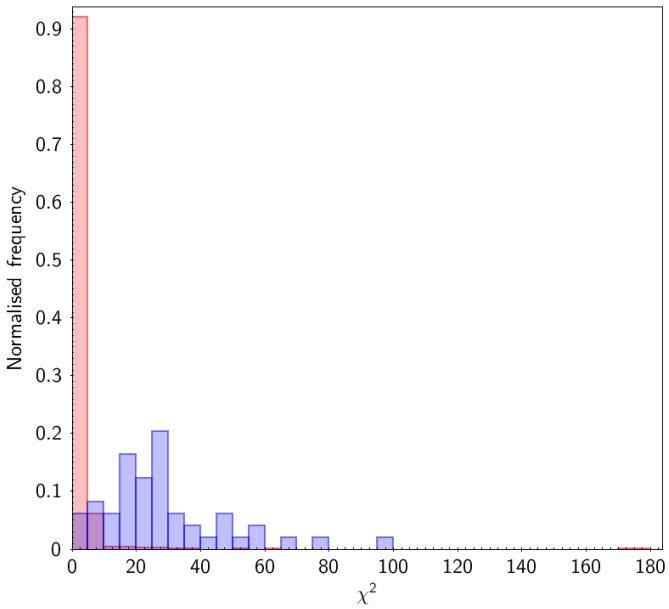

Figure 27: Histogram of χ^2 distribution for a normal population (red) and subdwarf population (blue).

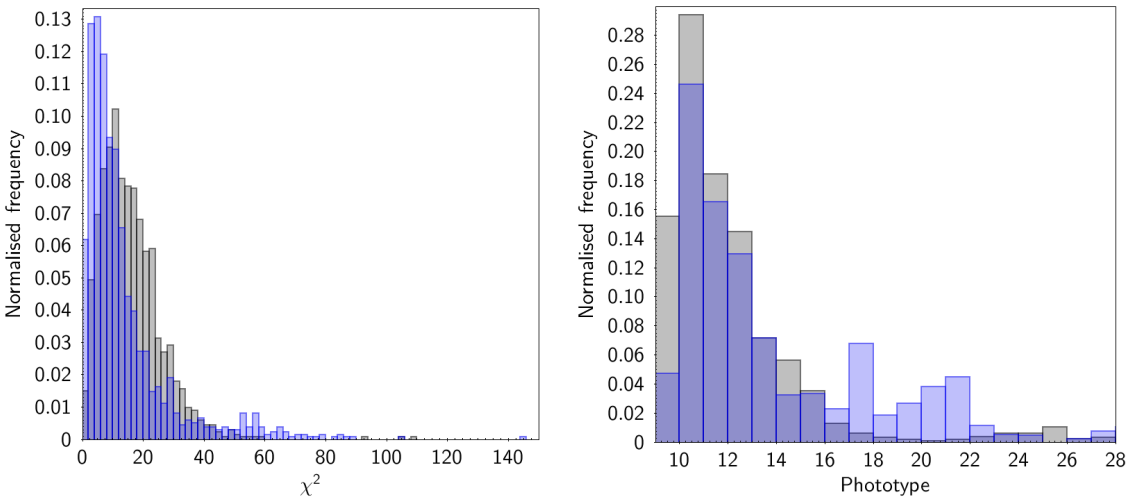

Figure 28: χ^2 (left) and photo-type (right) distributions for a 15 sigma offset in all bands (YJHKiz). The original distribution is shown in grey.

To further explore the sensitivity of the χ^2 statistic, the Skrzypek sample was given various photometric offsets to create 'artificially peculiar' populations that may or may not be identifiable by χ^2 alone. These offsets were added as multiples of the photometric uncertainty of each band, opposed to a fixed change in flux. The resulting distributions are shown in figures (28) through (31).

When all bands are significantly shifted as in figure (28) the mean χ^2 decreases. The reason for this is that the photo-typing routine assigns the sub-type with the lowest χ^2, thus many sources were assigned to a different sub-type after the offset

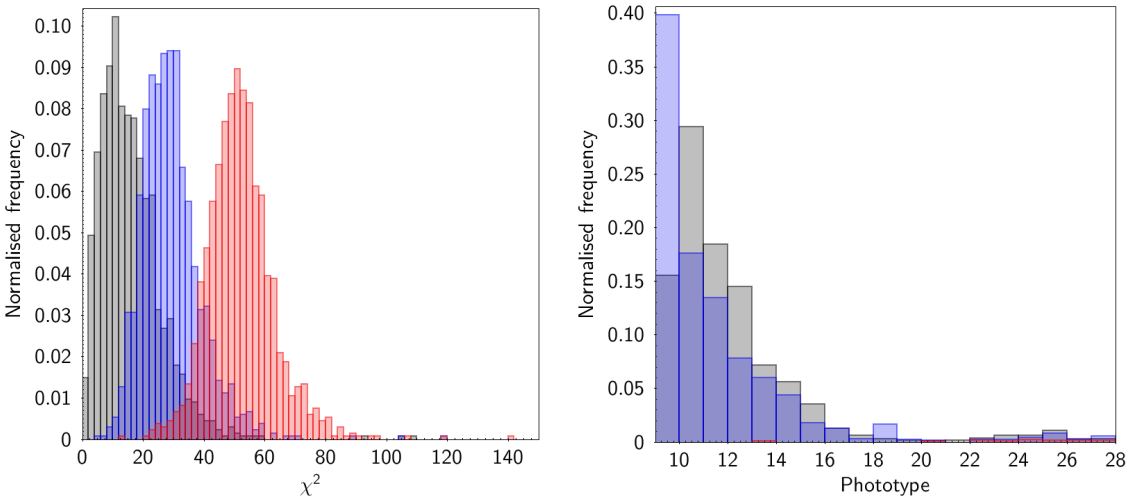

Figure 29: χ^2 (left) and photo-type (right) distributions for 10 (blue) and 15 (red) sigma offsets in J. The original distribution is shown in grey.

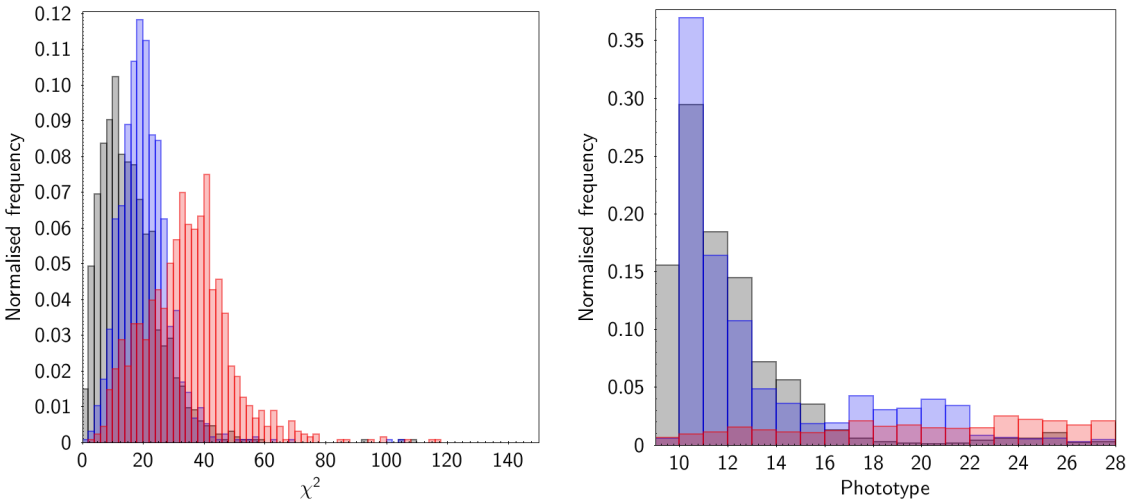

Figure 30: χ^2 (left) and photo-type (right) distributions for 10 (blue) and 15 (red) sigma offsets in i. The original distribution is shown in grey..

was applied. While this is an unrealistic peculiarity for real UCDs, it does highlight a characteristic of the photo-typing method. If a source is sufficiently unusual it may be incorrectly classified as a different sub-type with a relatively low χ^2. Because of this, some extremely unusual sources may go completely unnoticed. For sources that are not mis-classified, there is a noticeable increase in χ^2 that makes them distinctly stand out from the normal population.

When only one band is changed, as seen in figures (29) and (30), χ^2 values increase whilst maintaining the same distribution; this is an ideal result as any type of UCD that is unusual in one band will stand out from the general population. This is, however, something that could be picked up by colour-magnitude diagrams; the most useful application of the photo-typing method is for identifying sources that

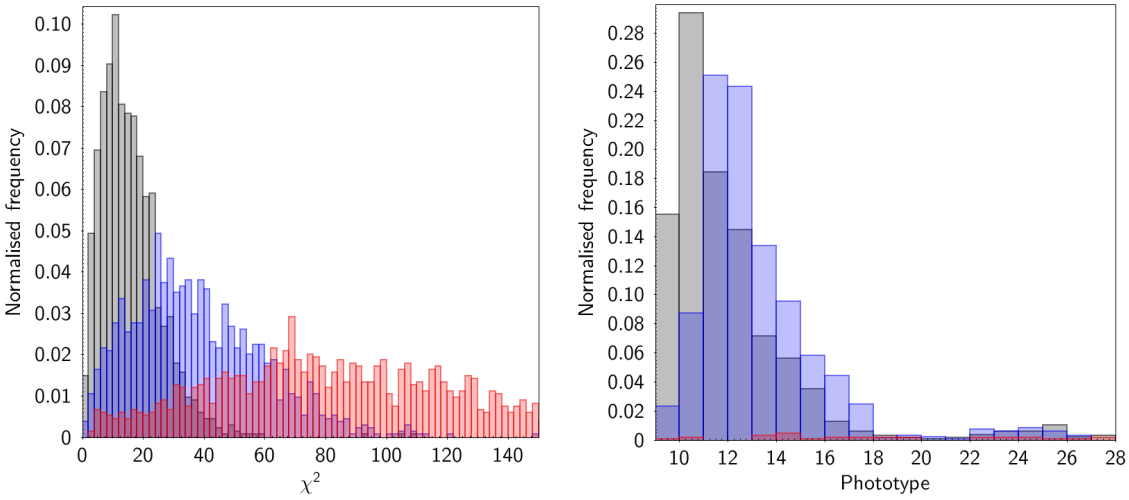

Figure 31: χ^2 (left) and photo-type (right) distributions for 5 (blue) and 10 (red) sigma offsets in both Y and J. The original distribution is shown in grey.

are slightly unusual in several bands but not by enough to stand out through CMDs.

Figure (31) shows that a small peculiarity in just two bands can significantly increase χ^2 and make a UCD stand out from the general population. The distribution resembles that of the subdwarfs (fig 27), which would exhibit a similar photometric deviation from the general population.

It is clear that the χ^2 statistic can identify certain cases of peculiarity, but not all. In some cases, a sufficiently unusual candidate will be mis-classified by the photo-typing routine as a different subtype with a relatively low χ^2. Peculiarities that cause a small deviation across a narrow range of wavelengths (i.e. one band) do not stand out particularly well, but a small deviation in multiple bands will stand out clearly.

Any peculiar UCDs found by looking at χ^2 distributions are subject to a biased selection process and are thus not a representative sample of ultracool populations. In summary:

- Only a small fraction ($\sim$10%) of unresolved binaries stand out, where they either deviate extremely in one band or slightly in several bands.
- Unusually blue UCDs are likely to be misclassified and thus not stand out.
- Subdwarfs stand out very clearly, with $\sim$80% having a χ^2 higher than a normal population.
- Peculiar UCDs are prone to being missed due to the χ^2/photo-type degeneracy, where they are so unusual that they are mis-classified with a low χ^2.
- The greatest benefit over analysing CMDs is that a small deviance across several bands is easily spotted.

2.2.1 Photo-typing results

The M and L/T selections from section 2.1 were photo-typed separately, but the results are combined for presentation in this sub-section. The same photo-typing routine was used for both selections, meaning that some L dwarfs were identified in the M selection and M dwarfs in the L/T selection.

All sources with $\chi^2 > 150$ were deemed to be contaminants and were thus removed, as for all tested UCDs, including peculiar examples, $\chi^2 << 150$. This cut removed 10% of sources in the LT sample and 56% of the M sample. The high level of contamination for the M dwarf photometric stems from the generous colour cuts during the initial bulk selection and it was expected that a χ^2 cut would remove a large portion of the initial selection.

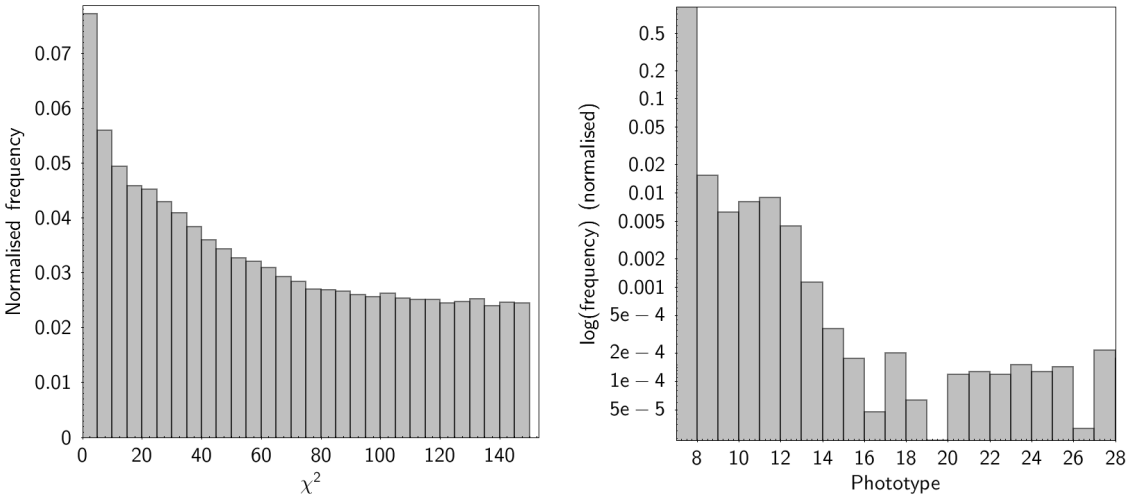

Figure 32: χ^2 (left) and photo-type (right) distributions for the combined results of the M and LT samples after the χ^2 cut.

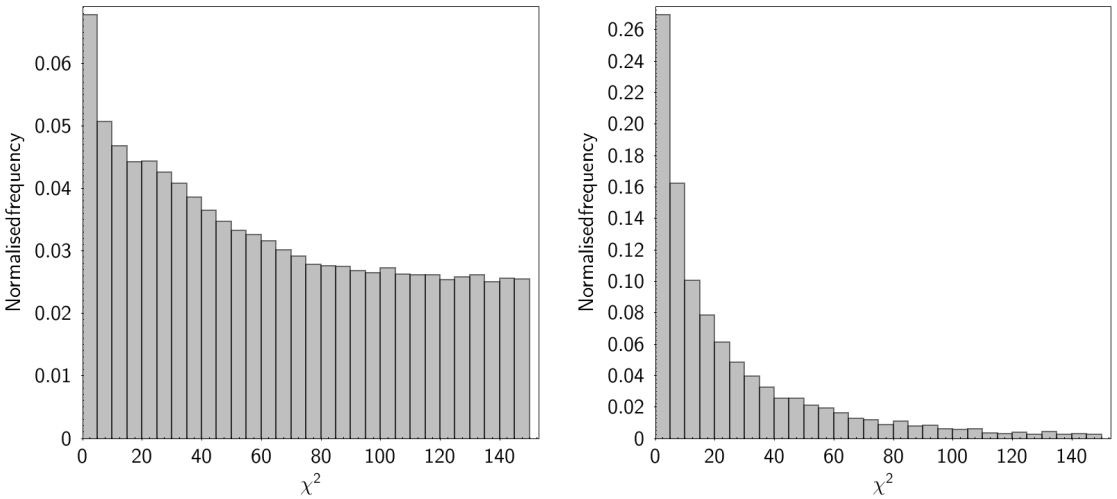

Figure 33: χ^2 distributions for M7 only (left) and M8-T8 (right) after the χ^2 cut.

The results evidently show that contamination is a major issue, with a much higher portion of high-χ^2 sources than samples of confirmed UCDs. In the combined results 98% of sources were photo-typed as M7. These sources are responsible for the majority of contamination as they are likely dwarfs hotter than M7 but close enough to the M7 template colours to survive the χ^2 cutoff.

For the M8-T8 range, the distribution is closer to that of the Skrzypek sample (see figure 31) albeit with a higher portion of low-χ^2 sources. As significant contamination is still present in the sample, the final χ^2 distributions are presented in section 2.5.

It is difficult to determine the level of contamination at this point, but it can be said that it is much higher for earlier sub-types. The majority of remaining candidates at this stage are thought to be contaminants, as comparison to the distribution of χ^2/photo-type in the previously used sample of UCDs shows a disproportionate number of M dwarf UCDs that is not fully explained by selection biases.

2.3 Gaia primaries

The M and LT catalogues were cross-matched with Gaia TGAS [42] with a search radius of 3 arcminutes, with 14.9% of sources matching to a candidate primary. Marocco et al. [46] found 3 arcminutes to be the optimal search radius for UCD companions, as it is large enough to avoid missing companions whilst keeping the false alarm probability acceptably low. When Gaia DR2 was released late in this project, the UCD candidates were cross-matched to it with a 100% match rate. As the majority of this project took place before DR2, the following analysis and results refer to TGAS matches unless stated otherwise (see section 4.2 for full details of the DR2 results).

2.4 Contamination

Assuming candidates are genuine companions, their distances can be determined by inverting the parallax of their primaries and thus the companions' absolute magnitudes can be determined using the distance modulus. For cases of chance alignment, the absolute magnitude of the companion will be false as the assumed distance is incorrect. This can be used to remove some cases of chance alignment as the absolute magnitude will differ from what is expected of an ultracool dwarf. Similarly, with the known limits of the surveys used in this project one can put an upper limit on the distance at which genuine UCDs can be observed.

Typical searches for UCD companions use absolute magnitude to estimate spectral type, however this means that candidates with unusual absolute magnitudes for their spectral type may not be noticed. As candidates have already been photo-typed, it would be unwise to remove anything other than the most extreme cases of unexpected absolute magnitude lest any interesting objects are lost.

The cuts used to decontaminate the candidate list are described below.

M dwarfs:

- Distance < 550pc
- $M_J > 8$

L/T dwarfs:

- Distance < 400pc
- $M_J > 10$

The following cuts were made to both the M and L/T samples:

- Separation $< 30{,}000$ AU
- i < 22
- z < 22
- J < 18.5

The M_J cuts were based on the ultracool parallax catalogue [49], allowing room for slightly hotter sources than the brightest known UCDs. The J, i and z cuts were made to remove candidates with unreliable photometry as they are beyond the quoted depth of the surveys. This also ensures that any candidates are bright enough for low-resolution spectroscopy with 6-8m telescopes.

Galactic reddening was also considered, with line-of-sight reddening estimations for each source retrieved from the NASA/IPAC Infrared Science Archive[6]. A cut of $\mathrm{E}(B-V) < 0.3$ was applied to remove reddened sources.

With the aforementioned cuts, the samples were reduced to 123,146 M dwarf candidates and 3,277 L&T dwarf candidates. Cross-matching these candidates with the SIMBAD database[7] revealed that 33 candidates are known to be galaxies or QSOs, 19 are known to be low-mass stars or brown dwarfs and a further 9 are unclassified IR sources. It should be noted that this was not a comprehensive search of the literature and a more thorough inspection of final candidates one-by-one was carried out at a later stage.

2.5 Proper Motion

As each candidate companion was selected for its proximity in the sky to its potential primary, the majority were expected to be chance alignments and not genuine companions. To test for companionship, candidate systems were subject to a common proper motion check.

[6] http://irsa.ipac.caltech.edu/applications/DUST/
[7] http://simbad.u-strasbg.fr/simbad/

Each candidate companion had already been observed in a minimum of two epochs, allowing for a simple two-point proper motion to be calculated. The uncertainties on two-epoch proper motions with a < 10 year baseline are expectedly large, so this test serves not to prove companionship but instead to remove obvious chance alignments. In the case of wide companions, their long periods make it possible to confirm common proper motion over a relatively short baseline.

The proper motion test described by Deacon et al. (2014) [51] (equation 1) was used, where candidate systems with a proper motion difference more significant than 5σ were rejected.

$$\sigma_{CPM} = \sqrt{\frac{(\mu_{\alpha,1} - \mu_{\alpha,2})^2}{\sigma^2_{\mu_{\alpha,1}} + \sigma^2_{\mu_{\alpha,2}}} + \frac{(\mu_{\delta,1} - \mu_{\delta,2})^2}{\sigma^2_{\mu_{\delta,1}} + \sigma^2_{\mu_{\delta,2}}}}$$

α is R.A.
δ is Dec.
μ is proper motion (mas/yr)
σ is the proper motion uncertainty (mas/yr)
1 is the primary and 2 is the candidate companion

As many UKIDSS sources were missing positional uncertainties, a maximum possible error was determined. Figure (34) shows that for LAS sources brighter than J=19 (i.e. all UCD candidates) the positional uncertainty remains below 55mas.

J=19 was used instead of J=18.5 (from previous cuts) to allow for objects that may be bright in J compared to other bands and thus have larger astrometric uncertainty larger than a typical J=18.5 object. The positional uncertainty is overestimated - especially for brighter objects - which is preferable to underestimated uncertainties as they could lead to false positives. While a curve-fitting routine could have been used to estimate UKIDSS uncertainties, the risk of underestimated errors was deemed too large.
Applying the $\sigma_{CPM} < 5$ test yielded 96,140 common proper motion candidates. The majority of these candidate systems pass only because of extremely large uncertainties in proper motion caused by short baselines. Objects outside of the parameters below were removed to reduce the sample to systems with good confidence of common proper motion:

- $\sigma_\alpha <| 300 mas/yr |$
- $\sigma_\delta <| 300 mas/yr |$
- $PM/dPM > 2$

Where PM/dPM is a significance parameter giving the proper motion in units of uncertainty:

$$PM/dPM = \sqrt{(\frac{\mu_\alpha}{\sigma_{\mu_\alpha}})^2 + (\frac{\mu_\delta}{\sigma_{\mu_\delta}})^2}$$

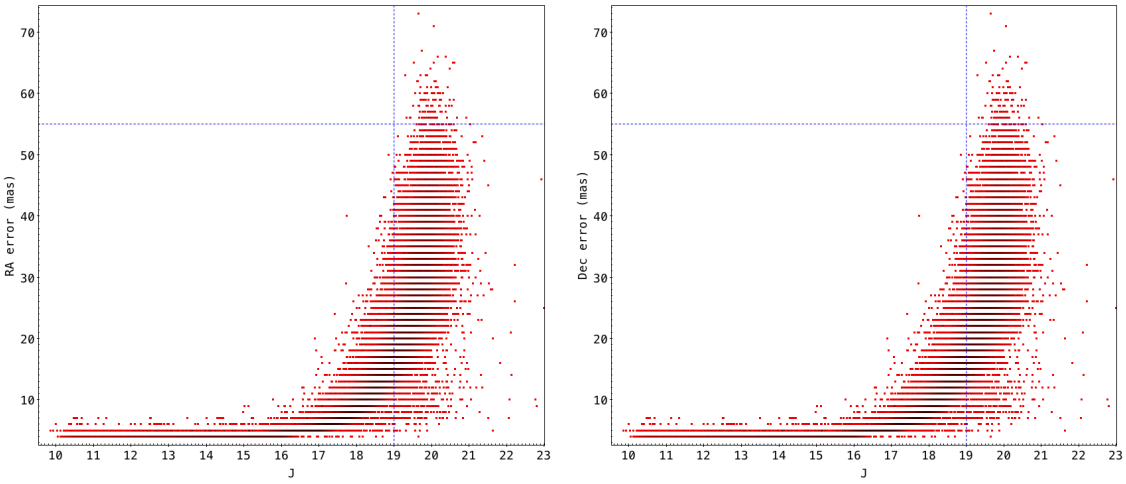

Figure 34: RA (left) and dec (right) uncertainty against J for all UKIDSS LAS sources. All candidate UCDs lie within the lower left area enclosed by dashed blue lines.

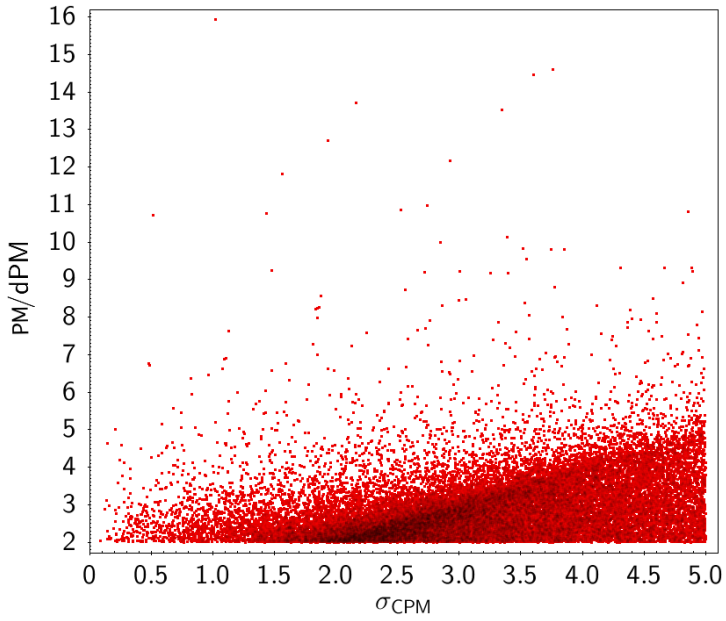

Figure 35: Proper motion quality against common proper motion confidence for candidate systems. Ideal systems would be in the upper left, with the lower right region being the least likely to be common proper motion systems.

With the above cuts, the number of candidate systems was reduced to 27,487. An ideal candidate system would have $\sigma_{CPM} \to 0$ and $PM/dPM \to \infty$, however the quality of two-epoch proper motions means that very few candidate systems have both high PM/dPM and low σ_{CPM}, as shown in figure (35). Two-epoch proper motions taken from catalogue positions are not good enough to confirm that a candidate companion is indeed co-moving with the Gaia source, thus an effort was made to find a third epoch for the candidate companions with which to calculate better constrained proper motions.

Two surveys were used for a third epoch: Pan-STARRS and the SuperCOSMOS Sky Survey. Pan-STARRS normally provides averaged positions and epoch from multiple observations, so individual J band positions and epochs were instead retrieved. The SuperCOSMOS Sky Survey provides extremely long baselines, in some cases several decades, however it has limited depth and only a small portion of sources were detected by the survey.

Between Pan-STARRS and SuperCOSMOS, the vast majority of candidate companions had positions from a minimum of three epochs. A simple IDL curve-fitting routine was used to determine proper motion for these candidates and the σ_{CPM} and PM/dPM cuts were applied. With three-point proper motions, a total of 9695 candidates were found to have common proper motion with their Gaia primary.

2.6 Filtering candidates

The 9,695 candidates selected represent only $\sim 0.08\%$ of the initial combined selection of 12,156,408 sources. For the benefit of any future work, the fraction of candidates removed at each stage is broken down below. The percentage remaining from the original bulk selection is given; note that changing initial cuts or the order in which these filters are applied will change the percentage removed at each stage.

Bulk selection
100% remaining
⇓
Photo-typing (removing $\chi^2 > 150$)
93% of those removed were in M dwarf selection
54% remaining
⇓
Matching to TGAS primaries (3arcmin radius)
With DR2, none were lost
7% remaining
⇓
Cuts - M_J, distance, separation, observability (mag limit), reddening
1% remaining
⇓
Common proper motion test (three-epoch)
0.08% remaining

3 Observing candidate systems

Observing time was acquired to follow-up strong candidate systems with the FIRE infrared spectrometer on the 6.5m Magellan telescopes at Las Campanas Observatory. The original plan was to obtain spectra for candidate companions so they could be spectroscopically confirmed to be ultracool dwarfs and any unusual features that contribute to the high χ^2 of candidates could be characterised.

Unfortunately, the FIRE spectrometer experienced a cooling pump failure shortly before the observing run. Because of this, the candidates were instead imaged with the FourStar infrared camera to obtain accurate astrometry for the improvement of proper motions. A list of approximately two dozen targets was created, however they were not all observed due to unfavourable weather.

This section describes how a small number of candidates were selected from the best common proper motion candidates from the 9,695 sources identified in section 2.5, and the results of the observations that took place on 2017-11-06 and 2017-11-07.

3.1 Viewing Limits

The approximate viewing limits of the Magellan telescopes in November are between right ascensions of 16h30m and 5h30m and declinations below 30°. A total of 4,044 candidates fall within these limits; one major disadvantage of using facilities in the southern hemisphere is that all candidates in this project belong in more northern skies covered by UKIDSS.

Target altitude and moon avoidance are important considerations when planning observations, so several star tracks were generated using the ING Object Visibilty service[8] to visualise which regions should be avoided, as shown in figure (36). These tracks show the altitude and lunar separation for a range of sky regions that include all of the candidates.

When one must select ∼30 candidates out of 4,044, a simple cut based upon lunar separation and altitude is a tempting prospect. This would, however, be unwise. Instead, the aforementioned observability parameters were taken into consideration amongst several other factors to judge targets on an individual basis in later iterations of the target list. Star tracks were made for each candidate submitted for observation to aid in planning.

[8] http://catserver.ing.iac.es/staralt/

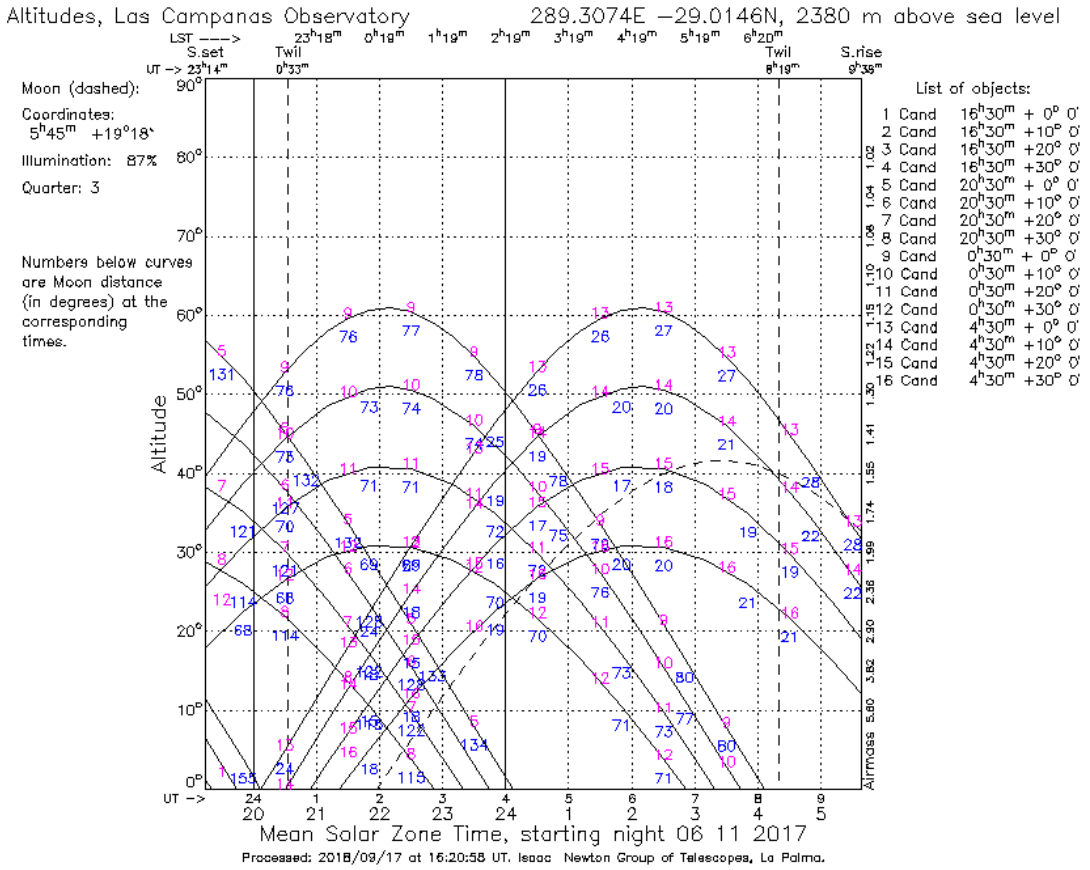

Figure 36: A range of possible star tracks on the night of observations, courtesy of the ING Staralt service. The moon is shown as a dashed line and angular distance to the moon is shown in blue.

3.2 Colour-magnitude diagrams for chance alignment

The three-epoch proper motions in section 2.5 were an improvement over the two-epoch proper motions, however a large number chance-aligned pairs passed the proper motion test. This is because sources measured to have a very high proper motion with a large uncertainty can pass both the σ_{CPM} and PM/dPM tests regardless of if they are truly co-moving with the Gaia star.

A large number of these chance-aligned systems were removed by analysing colour-magnitude diagrams. As described in section 2.4, the Gaia parallaxes can be used to determine the distance to a companion and determine its absolute magnitude. If a source detected by UKIDSS/SDSS is *not* a companion to its nearest Gaia star, the assumed distance to the source, hence also its absolute magnitude, may be incorrect.

To identify candidate UCDs with wrongly assumed distances, colour-magnitude diagrams were plotted showing both the candidates and confirmed UCDs from the Dupuy ultracool parallax catalogue [49].

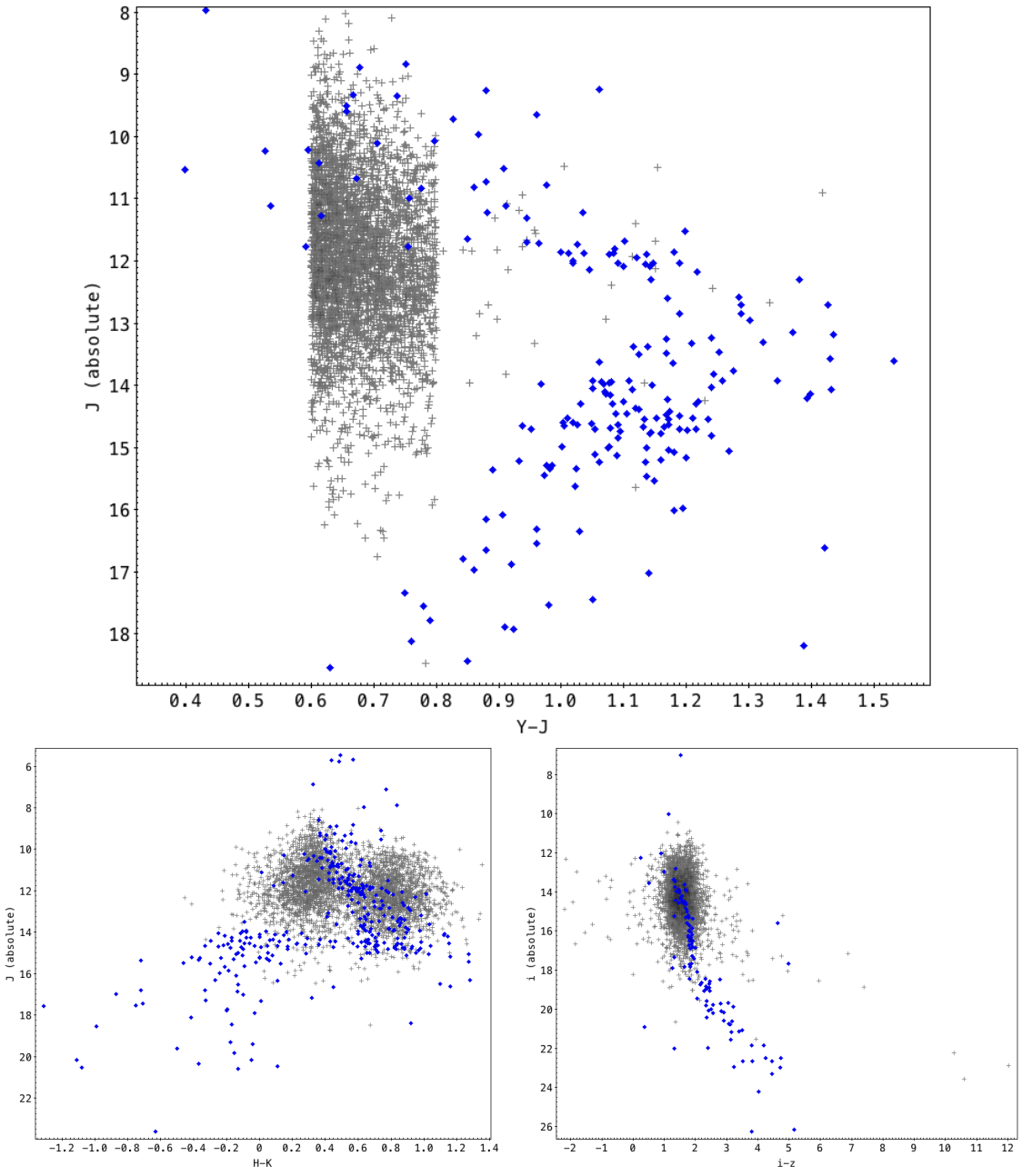

Figure 37: Colour-magnitude diagrams showing candidate companions (grey) and the Dupuy ultracool parallax sample (blue). Note that the Dupuy sample covers a full range of UCDs whilst the candidates are mostly M and early L dwarfs, so the candidates do not cover the full populations shown.

The majority of candidates are late M dwarfs, which comes as no surprise given their prevalence and brightness relative to later types. The Y-J colour varies significantly with absolute M_J, making chance-aligned candidates stand out as being too faint for Y-J<0.8. As all filters are affected equally, only one cut based upon an absolute magnitude is required. Colours such as i-z do not vary significantly with individual magnitudes, so they cannot be used to identify chance-aligned can-

didates without potentially eliminating genuine companions with unusual colours. Removing all objects where $Y - J < 0.8$ *and* $M_J > 12.5$ reduces the number of candidates to 1,275.

3.3 Visual Inspection

With 1,275 candidates observable, visual inspection becomes a viable option. Images from UKIDSS and SDSS were retrieved along with, when available, DECaLS and Pan-STARRS images. At the time of writing, the DECaLS survey does not ha ve a public data release with positional and epoch data easily accessible, however the images are easily accessed.

A simple system was used to classify candidates based upon their appearance. All LAS bands were inspected individually whilst colour images were used for the other surveys. All images were considered when classifying an object, however the UKIDSS and SDSS images were the most important as candidates were initially chosen using the photometry from said images.

Approximately 20% of candidates could be confidently rejected; these were sources that were clearly galaxies, image artefacts, diffraction spikes or other spurious sources. Some examples of said sources are shown in figures (38) through (40).

Point-source candidates were separated into two categories: high confidence and low confidence. High confidence candidates were selected for being point sources that are in no way elongated, not blended with other sources in the sky (such as oversaturation from the primary) and have a high SNR. A low-confidence classification means the source failed to meet the high-confidence criteria but could not be rejected, for example slightly elongated sources that were not obvious galaxies (i.e. several other sources in the image are similarly elongated). Another example of a low-confidence source would be one that is buried in noise or glare from a nearby star, or a source that appears to be a galaxy cluster member but could be a foreground UCD. An example of a low-confidence candidate is shown in figure (41). Where possible, low-confidence sources were given flags (e.g. possible galaxy) to help differentiate between cases that couldn't be confidently eliminated and those that only just fell short of being high-confidence.

Candidates ranked as high confidence are clear, bright point sources and are not affected by the aforementioned undesirable features. Young, bright UCDs with a large angular separation were thus more likely to be selected. An example of a high-confidence source is shown in figure (42).

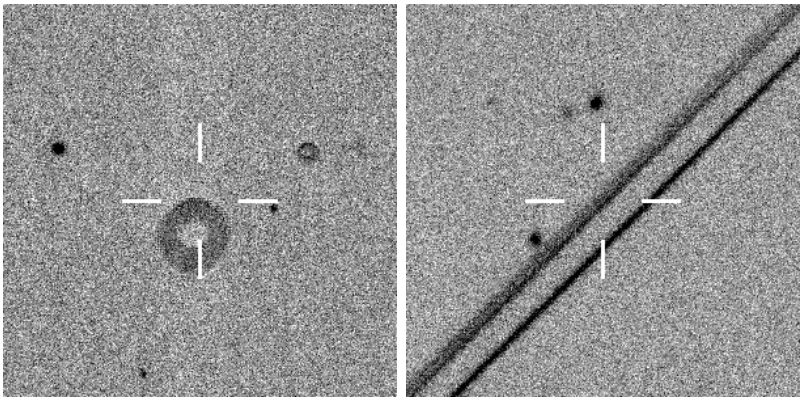

Figure 38: Common image artefacts seen in UKIDSS Y.

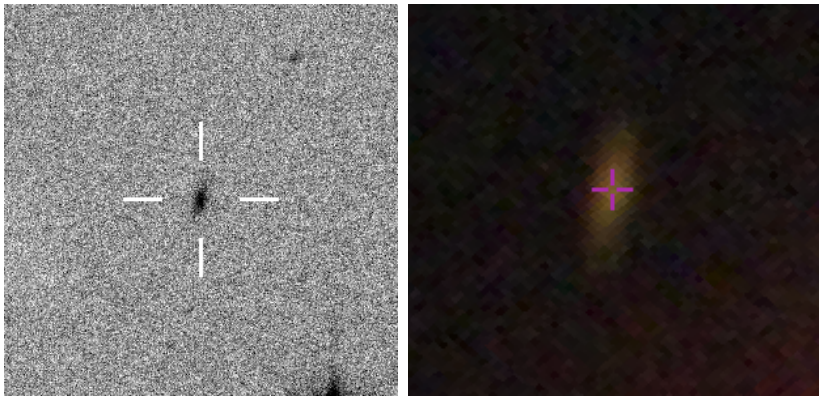

Figure 39: Suspected galaxy seen in UKIDSS Y (left) and SDSS colour (right).

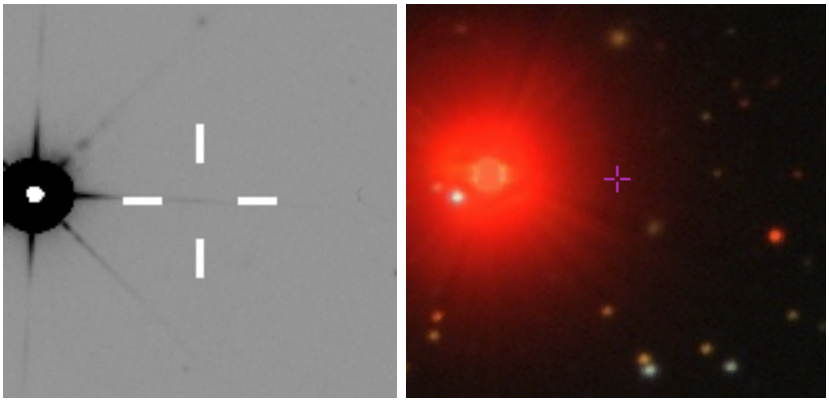

Figure 40: Diffraction spike in UKIDSS images, shown in UKIDSS K (left) and SDSS colour (right) where there is no discernible point source.

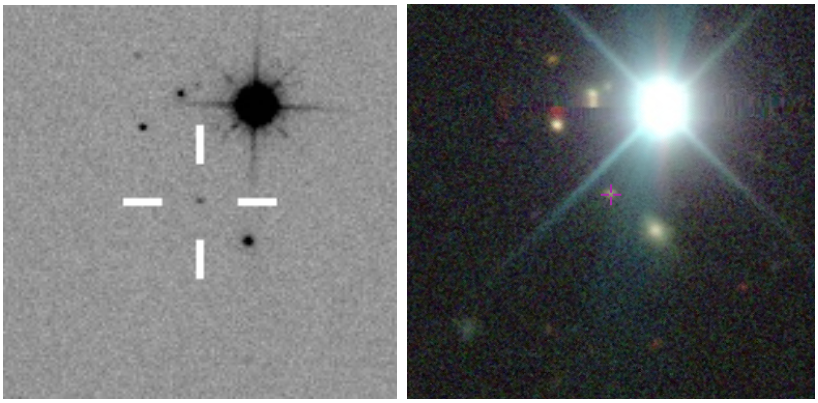

Figure 41: A faint low-confidence candidate seen in UKISS K (left) and SDSS colour (right). The source was not visible in UKIDSS J or Y and the SDSS image photometry may be contaminated by the bright nearby primary. UKIDSS images also show some elongation.

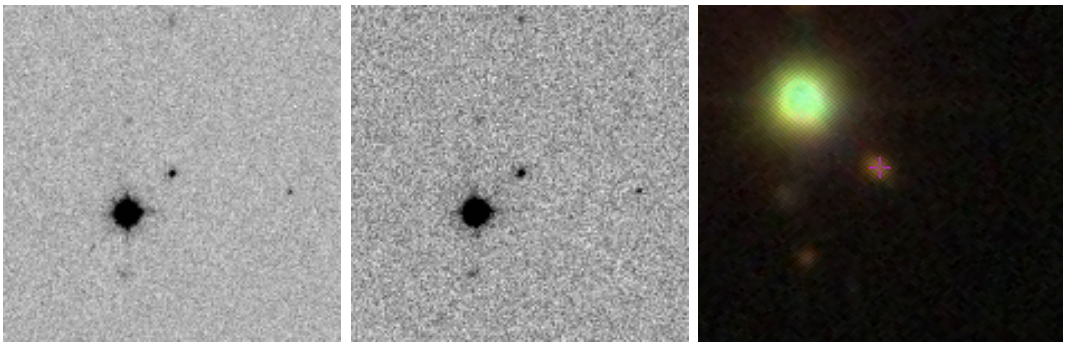

Figure 42: Images of a high-confidence candidate in UKIDSS J (left), UKIDSS H (centre) and SDSS colour (right). The source is distinct and bright across UKIDSS filters and is as well defined in SDSS images as all neighbouring sources. The candidate is at the centre of each image.

High-confidence candidates, along with borderline low-confidence candidates, were double-checked to minimise human error. The majority of candidates were ranked as low-confidence, with ∼40 high-confidence candidates remaining. Approximately 200 sources were rejected with the rest being marked as low-confidence.

3.4 Selecting priority targets

As only a small portion of the high-confidence candidates could be observed, priority was given to peculiar objects. So far, peculiarity has only been measured using the χ^2 statistic which does not characterise the way in which the candidate deviates from template colours.

The first step was to estimate each candidate's spectral type based upon M_J for comparison to their photo-types. The template M_J for each subtype was taken from the weighted averages provided by the Dupuy ultracool parallax catalogue

[49]. As figure (43) shows, the remaining candidates were all photo-typed to be objects earlier than L3. This is a result of the visual inspection process, as the criteria for high-confidence candidates during visual inspection favour brighter sources. For many candidates, M_J does not agree with the template for their photo-type, suggesting that i) they are not companions (see section 3.2), ii) they were incorrectly photo-typed, iii) they are genuinely peculiar in J. An M_J-determined spectral type was given to each candidate and the difference between photo-type and estimated spectral-type was recorded.

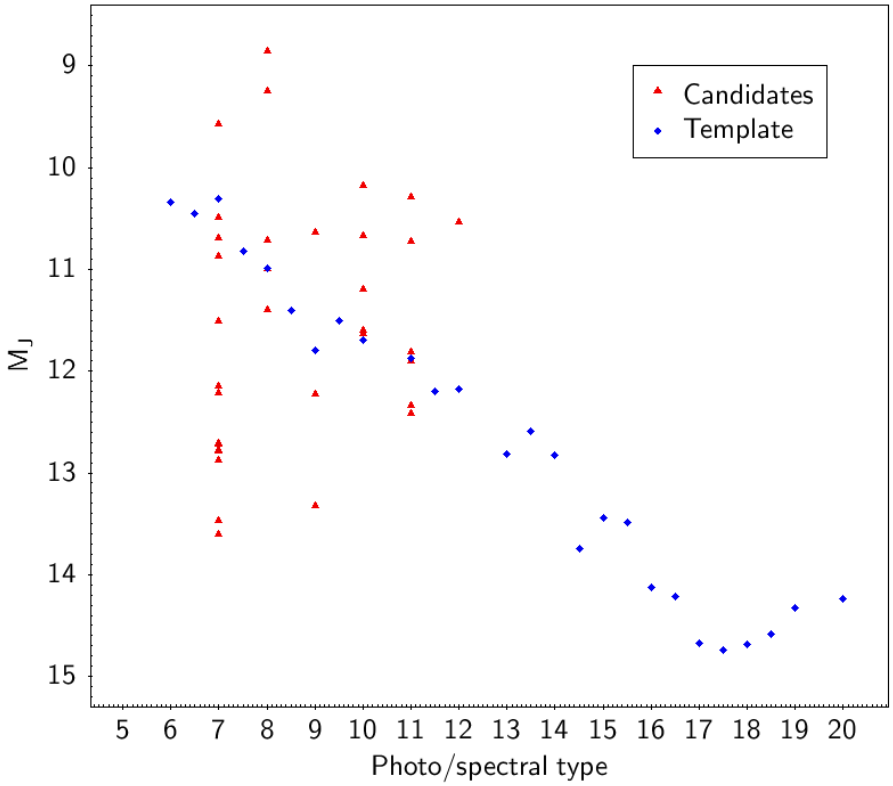

Figure 43: A comparison of candidates with measured magnitudes & photo-types and the template magnitudes for each spectral sub-type. Candidates (plotted against photo-type) are shown in red and the subtype templates (against spectral type) are shown in blue. The subtype templates are weighted averages from from Dupuy et al. (2012) [49]. 05=M5, 20=T0.

To identify which of the aforementioned causes for disagreement in classification had occurred, colour magnitude diagrams using M_J and M_Y were compared. As shown in figure (44), there is very little difference between the M_J and M_Y plots, suggesting that no candidates strongly deviate from the templates in one band only. This means that the candidates must be falsely aligned or both Y and J are unusual, leading to an incorrect classifications from either the photo-typing routine and/or the M_J estimates. The Y-J CMDs show a small group of objects that do not fit with the Dupuy population; these candidates were flagged as they must either be falsely aligned or peculiar in Y-J.

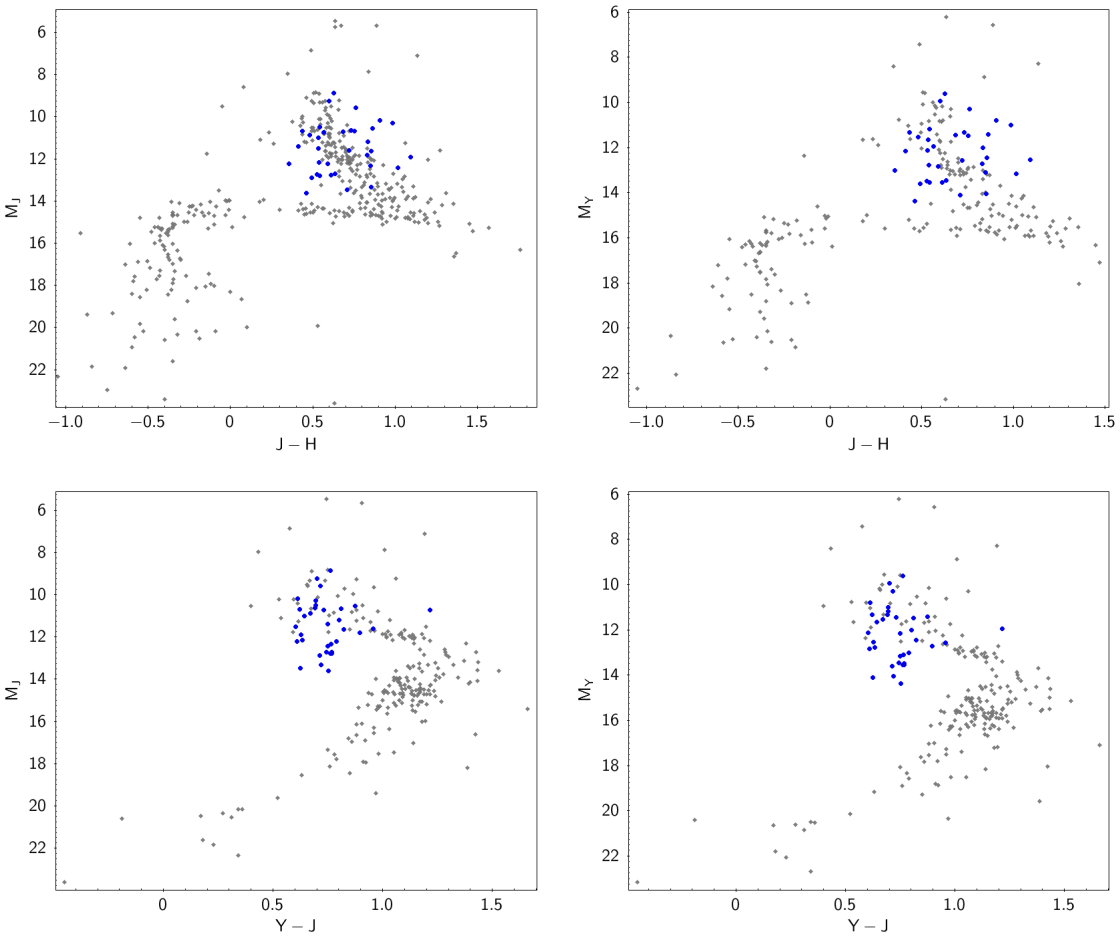

Figure 44: CMDs with M_J (left) against M_Y (right) against J-H (top) and Y-J (bottom). Candidates are shown in blue and UCDs from the Ultracool Parallax Catalogue [49] in grey.

To further explore the photometry of the candidates, candidates were plotted on colour-colour diagrams for comparison with known UCDs. As parallax was not required, the larger confirmed UCD compilation by Jonathan Gagne[9] was used.

In the first three colour-colour diagrams shown in figure (45), four unusually red candidates stand out immediately. Regardless of if they have been phototyped correctly, they are unusually red at optical and near-IR wavelengths for a UCD of any type. While they may well be peculiar UCD companions, they could also be dust-obscured sources or background galaxies/QSOs.

With the selection narrowed down to 33 candidates, it was decided that all of them should be submitted to the observer with the expectation that a dozen would be observed. Each candidate was given a priority level to aid the observer in planning the observations.

[9]https://jgagneastro.wordpress.com/list-of-ultracool-dwarfs/

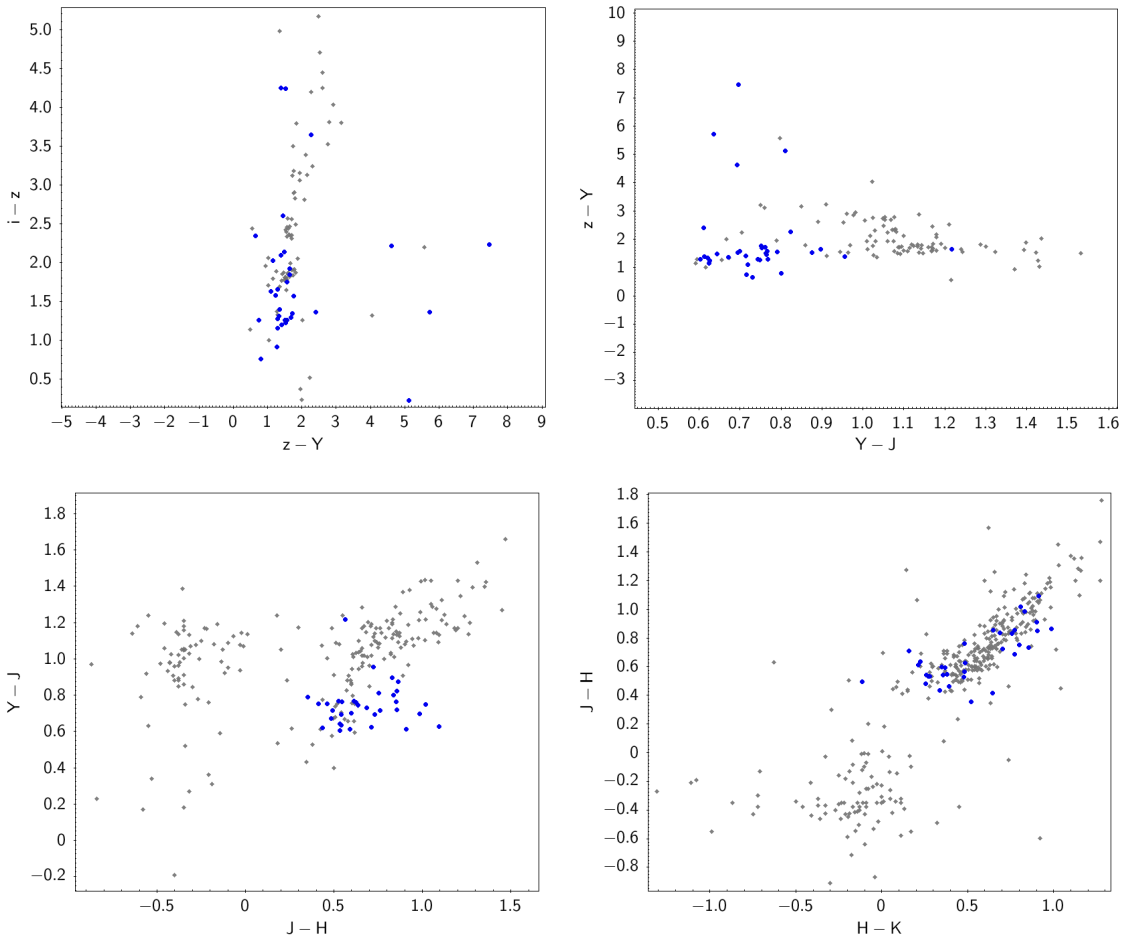

Figure 45: Colour-colour diagrams for candidates (blue) compared to the Gagne UCD compilation (grey).

Priorities were chosen based upon common proper motion confidence and peculiarity. To do this, candidates were ranked with a metric of $\sigma_{CPM} + \frac{1}{PM/dPM}$, with lower values being best. The original plan was to obtain spectra using the FIRE spectrograph, however a technical fault meant that the FourStar instrument had to be used instead. As other members of the research group had a strong need for narrowband observations, they were given higher priority whilst this project was only given time for a few targets to be observed in J.

The observations were carried out by Dr. Radostin Kurtev[10] on 2017-11-06 and 2017-11-07. Four targets were observed; the final target list is shown in table (1) with the observed candidates highlighted.

[10]radostin.kurtev@uv.cl

Name	Priority	Photo-type	χ^2	M_J type	σ_{CPM}	PM/dPM	Distance (pc)	Separation (AU)	μ_α (mas/yr)	μ_σ (mas/yr)	σ_{μ_α}	σ_{μ_δ}	Notes
J020530.76+035701.7	TOP	M8	70.14	M8	2.12	2.76	244.4	12083	24.38	-21.64	11.96	11.58	Slightly red
J001737.06+120245.4	TOP	M7	2.52	L3.5	0.7	3.23	127.5	5296	43.59	-16.32	14.45	13.82	Slightly blue
J014149.22+010631.0	TOP	L1	118.21	M7.5	4.52	5.77	416.6	22509	24.09	37.91	7.88	7.73	Red
J021016.01+125625.9	TOP	L0	5.28	M8	3.2	3.73	297.6	5479	30.89	-19.06	9.78	9.55	Red
J220957.64+021051.7	HIGH	M8	34.56	M8	4.78	10.13	147.2	18270	-119.22	-48.65	12.65	13.03	
J222754.95+013653.5	HIGH	M7	4.17	M9.5	2.5	5.99	128.5	22191	-42.74	-61.53	-11.79	-12.87	
J005200.24+132101.3	HIGH	L1	13.09	L2.5	3.04	2	159.7	4093	-29.69	4.43	14.97	14.96	
J225411.99+060155.3	HIGH	M8	0.96	<M5	3.86	6.65	476.1	19753	-21.59	-50.12	-7.77	-8.28	
J230539.34+111234.9	HIGH	M9	36.54	L2	4.06	2.81	85.1	14996	12.02	-41	-14.16	-15.29	
J230026.86+125733.8	HIGH	M7	13.92	L0	1.1	2.83	138.6	23603	34.37	12.45	12.84	13.16	NGP
J234923.40+010225.7	HIGH	M7	2.34	L0.5	4.34	4.39	93.1	13242	34.43	-17.95	8.8	8.97	Red, NGP (M5)
J015038.72+051122.1	MID	M7	3.33	M8.5	4.97	3.21	140.2	21794	63.52	-44.6	-21.8	-32.57	
J014435.22+145344.0	MID	L3	11.01	M6.5	2.12	2.01	324.6	6000	-227.23	-80.68	119.76	118.72	Slightly red
J235831.64+033735.1	MID	M7	2.04	M8.5	0.39	4.77	138.5	15922	-49.22	-29.43	-11.71	-12.96	
J000520.00+160956.2	MID	L0	24.42	M5	1.85	4.32	347.2	14962	-41.23	-60.54	16.92	16.92	
J001607.64+042932.7	MID	M8	1.41	M8	1.86	2.63	250	16967	-24.43	-38.61	-10.97	-27.41	
J035417.77-000955.3	MID	L0	8.63	L0	4.81	2.97	187.2	20599	-18.74	33.36	13.61	12.67	
J233422.71+052554.2	MID	M7	14.31	L2	4.93	2.46	81.2	11731	-18.47	2.97	-7.56	-9.06	
J230942.59+102824.1	MID	L1	1.19	M5	4.25	3.15	325.7	21458	-11.18	-47.4	-8.06	-16.7	
J002338.60+093851.2	MID	M7	1.92	M9.5	2.96	3.37	100.6	15359	-4.11	-63.09	-17.19	-18.74	
J033712.71+040051.8	MID	L1	55.78	L1	3.43	3.03	151	5661	6.23	45.87	14.92	15.24	Slightly blue
J005248.58+103626.2	MID	M7	4.86	M5	4.63	3.08	284.9	5026	29.91	-46.5	-16.36	-18.7	
J022656.98+071855.5	MID	M8	7.46	M5	3.29	4.63	273.9	8009	38.98	-42.77	12.85	12.2	
J001239.77+045909.9	MID	M7	4.06	L2	4.86	4.2	56	4874	48.05	-76.24	-21.29	-21.46	
J035122.21+005343.1	MID	M9	9.42	M8.5	4.89	5.44	324.6	5655	53.73	-68.5	16.82	15.51	Red
J020425.84+040818.0	MID	L0	4.69	L0	0.83	3.47	283.2	3812	57.1	-24.11	17.76	18.27	
J015357.99+134715.4	MID	M8	37.29	L4	1.37	2.19	88.4	12013	129.29	-157.03	92.01	93.43	NGP
J211236.98+005328.0	LOW	L1	12.16	L3.5	4.21	3.98	162.3	4699	-27.14	-120.28	32.2	30.85	
J024028.12+015331.5	LOW	L0	14.39	L0.5	2.54	2.09	202.8	25128	-1.11	54.23	26.78	25.94	
J220712.38+012537.2	LOW	L1	3.31	L1	0.79	3.09	215.5	7944	27.47	26.84	12.37	12.48	
J223240.78+012808.0	LOW	M7	0.57	M7	3.26	3.25	366.3	28999	112.46	1345.53	432.27	414.3	Binary primary
J022251.73-003517.2	LOW	M7	5.12	M7.5	1.84	2.49	240.3	3284	231.24	-72.1	97.23	96.67	
J022053.62+024000.1	LOW	M7	49.8	M6.5	2.77	2.67	416.6	5367	324.63	214.22	145.82	143.82	

Table 1: Target list for the observing run. Targets in bold were observed in the J band; those not in bold were not observed. NGP = (potential) non-Gaia primary; these are candidates that have small angular separation to a star in SIMBAD that could be an alternative candidate for its primary.

3.5 Follow-up observations & measurements

The observing run was part of a joint follow-up campaign using Magellan, with two collaborators also imaging candidate ultracool companions to Gaia stars. Six targets were observed for Dr. Federico Marocco (FM) that are thought to be companions to subgiants, whilst twenty-four targets were observed for Matthew Rickard (MR) which are candidate companions to young stars.

As part of the collaborative effort, imaging data was reduced by MR whilst I (LD) determined proper motions. While the original plan was to have FIRE spectra and classify candidates spectroscopically, having high-resolution images in a new epoch presented the opportunity to significantly improve upon previous proper motion measurements.

This sub-section describes the process used to measure proper motion from the FourStar images and presents the results. At the time of writing, the FM and MR results are being used to advance their respective projects.

The most accurate method to measure proper motion is to transform catalogue images so that movement of the target object can be measured between the catalogue and FourStar images in pixel co-ordinates. This method effectively measures proper motions relative to background stars, instead of relying upon sky co-ordinates from telescopes that have an associated positional uncertainty.

The first step is to identify a suitable reference (catalogue) image. The image should be in the same filter as the FourStar image, so the majority of reference images were in J. The only exceptions were where J-band catalogue images were not suitable and there was a FourStar image in another waveband. Images were retrieved from both UKIDSS LAS and VISTA VHS.

For each pair of images, 15-20 bright (but not oversaturated) reference stars were manually selected then centroided in ds9. Care was taken to ensure reference stars were selected in all areas of the field and did not include the target or the primary. Using the pixel co-ordinates of the reference stars, the IRAF geomap package was used to compute the transform with a polynomial fit to the third order. The geomap GUI was used to check the fit; if residuals were greater than 2 pixels or the root-mean-square errors were greater than 0.5 pixels, the transform was recomputed with different reference stars.

With the transform complete, the co-ordinates of the target in the reference image were converted to the co-ordinate system of the FourStar image in the geoxytran IRAF package. As the x and y axes were already aligned to R.A. and dec, the movement along each axis in arcseconds was easily calculable using the pixel scale of FourStar, along with the rms errors for positional uncertainty.

Sixteen images could not be used due to a lack of useable reference stars (shown as N/A in table 2). The remaining eighteen objects had their proper motions mea-

R.A.	Dec	Observer	σ_{CPM}	PM/dPM	μ_α	σ_{μ_α}	μ_δ	σ_{μ_δ}	Primary source	Reference image
25.1695	3.7636	FM	10.87	8.32	-121.28	18.33	-118.69	23.46	DR2	LAS J
26.7649	5.3702	FM	0.82	1.22	-8.56	21.16	-21.7	18.76	DR2	LAS J
31.1323	**2.9772**	**FM**	**3.04**	**3.66**	42.01	11.48	-5.46	23.66	DR2	LAS J
46.4911	12.048	FM	N/A	N/A	N/A	N/A	N/A	N/A		
56.4199	17.7652	FM	N/A	N/A	N/A	N/A	N/A	N/A		
60.5803	18.0391	FM	N/A	N/A	N/A	N/A	N/A	N/A		LAS K
31.3781	**3.9504**	**LD**	**2.53**	**2.21**	10.05	13.22	47.7	22.92	DR2	LAS J
35.2234	2.6667	LD	N/A	N/A	N/A	N/A	N/A	N/A		LAS J
57.8425	0.8953	LD	5.03	3.66	-37.82	11.51	25.17	15.54	DR2	LAS J
58.574	**-0.1653**	**LD**	**2.02**	**7.72**	-11.46	6.35	-37.36	4.97	DR2	LAS J
2.3442	0.6321	MR	11.02	18.95	302.33	16.66	-58.7	10.69	DR2	LAS J
5.1155	0.5202	MR	N/A	N/A	N/A	N/A	N/A	N/A		VHS H
31.5268	-10.2406	MR	N/A	N/A	N/A	N/A	N/A	N/A		
77.1133	-2.3591	MR	92.22	1.61	-0.9	0.59	-0.21	0.4	DR1 (BAD DR2 MATCH)	LAS H
83.2991	-2.1752	MR	N/A	N/A	N/A	N/A	N/A	N/A		
113.6871	-7.5321	MR	N/A	N/A	N/A	N/A	N/A	N/A		LAS J
117.3932	-8.036	MR	6.88	7.95	0.61	0.52	-2.83	0.36	DR2 (NEW PRIMARY)	VHS J
307.0578	-13.815	MR	N/A	N/A	N/A	N/A	N/A	N/A		VHS J
325.3743	**-2.773**	**MR**	**4.48**	**8.36**	-106.03	13.23	-42.5	17.61	DR1 (BAD DR2 MATCH)	VHS J
329.2704	0.6094	MR	11.08	4.79	-13.33	6.97	54.27	12.32	DR2	LAS J
331.0344	2.5687	MR	11.61	4.61	-66.19	18.37	83.65	28.92	DR1	LAS J
331.0587	2.5955	MR	9.56	4.55	-67.46	22.33	47.47	13.94	DR1	LAS J
332.5661	-1.4103	MR	N/A	N/A	-4719.78	8.71	16546.88	16.25		VHS J
332.5786	-1.446	MR	N/A	N/A	-13533.67	8.71	26907.68	16.25		VHS J
334.7317	**-1.143**	**MR**	**4.44**	**8.89**	111.64	18.34	-82.9	12.77	DR2	LAS J
335.7249	-2.0235	MR	8.46	6.6	1.75	0.59	2.47	0.41	DR2 (NEW PRIMARY)	VHS J
336.7247	-4.5545	MR	N/A	N/A	N/A	N/A	N/A	N/A		VHS J
339.0752	0.1728	MR	8.81	3.7	3.89	13.96	-41.98	11.35	DR1	LAS J
347.3824	-2.466	MR	3.22	0.89	-6.36	12.68	14.42	19.62	DR2 (NEW PRIMARY)	VHS J
353.0856	**-12.2866**	**MR**	**3.11**	**2.94**	49.76	19.37	33.49	23.29	DR2 (NEW PRIMARY)	VHS J
120.7049	-8.2243	MR	N/A	N/A	N/A	N/A	N/A	N/A	N/A	VHS J
128.7641	-16.1472	MR	N/A	N/A	N/A	N/A	N/A	N/A	N/A	VHS J
307.9683	-13.7948	MR	N/A	N/A	N/A	N/A	N/A	N/A	N/A	VHS J
307.0811	-13.7797	MR	N/A	N/A	N/A	N/A	N/A	N/A	N/A	VHS J

Table 2: Observed targets and their proper motions calculated using FourStar images with geomap & geoxytran.

sured to a comparable or higher accuracy than previous three-epoch measurements, partly due to the longer baseline afforded by the new FourStar images along with the improved method.

As Gaia DR2 has since become available, a new search for companions using Gaia DR2 was made for calculating σ_{CPM} and PM/dPM with its slightly improved proper motions. For several objects, matching candidates to DR2 results in a different primary than a match to DR1. In cases where this happened, σ_{CPM} was calculated for both primaries and the one that yielded the highest confidence was selected as the primary. The results of the proper motion measurements are presented in table (2).

The new proper motions make the majority of candidates fail the common proper motion test[11], however six of them pass. Of those six, the one with the highest common proper motion confidence was selected by this project. The two candidates selected by this project that pass the common proper motion test are discussed below.

[11] $PM/dPM > 2$ and $\sigma_{CPM} < 5$

ULAS J035417.77-000955.3 (σ_{CPM}=2.02, PM/dPM=7.72)
This candidate has the highest common proper motion confidence of all targets from the observing run and is a promising candidate. The primary is HD 24538, an F5/6V variable star with no previously known companions. The companion is unusually red in optical and NIR bands, however its L0 photo-type is consistent with absolute magnitude estimates and χ^2=8.63. This target is a priority for follow-up as it is a wide companion with potential benchmark features. It is recommended that spectra are obtained for this object to determine its spectral type and identify any features that would cause reddening.

ULAS J020530.76+035701.7 (σ_{CPM}=2.53, PM/dPM=2.21)
This candidate M8 companion has χ^2=70.14, making it an extremely unusual source. This candidate is blue in optical wavelengths and slightly red in the NIR, with M_J being consistent with a late M dwarf. There is a chance this is a misclassified object belonging to an earlier subtype, as it is not extremely peculiar in one band but slightly in several. Nevertheless, this source is worth investigating as it (barely) passes the common proper motion test and could be an ultracool companion.

4 Overview of candidate companions

Only 42% (4,044) of the 9,645 three-epoch proper motion candidates were considered in section 3 due to viewing limits, with 1,020 (∼11%) passing further tests and visual inspection. Only 33 of those candidates could be selected, however the remaining sources are nevertheless candidate companions. Of the four candidates that were observed for this project, two had their common proper motion confidence improved while one got worse[12] and another could not be measured. Four observed candidates is too few to estimate what portion of all 'good' candidates are genuine companions, however it does show that the selection process is successful in finding ultracool companions.

Applying the colour-magnitude cuts from section 3 to the non-observable candidates[13] yields 2,896 candidates. An appreciable fraction of these candidates would be rejected during visual inspection, however alternate methods to reduce the number of candidates should be employed before undergoing inspection of such a large number of candidates.

In total, there are 6,890 candidate companions to TGAS stars. It is likely that a large portion of these are not candidate companions, however they cannot be removed without also removing genuine ultracool companions. That being said, χ^2 and σ_{CPM} can be used to select a small number of the most promising candidates for follow-up should the opportunity arise. Several notable candidates have been identified, and are discussed in section 4.1.

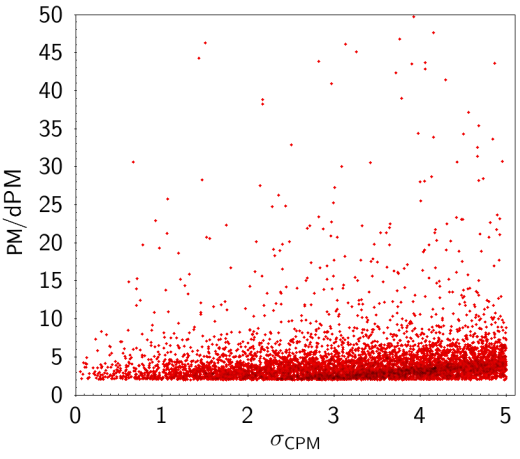

Figure 46: Common proper motion confidence for final TGAS candidates (PM/dPM truncated to 50).

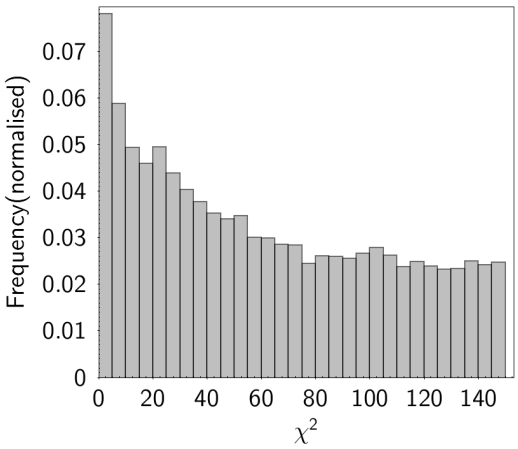

Figure 47: χ^2 distribution for final TGAS candidates.

[12]The proper motion measurement was improved
[13]excluding visual inspection

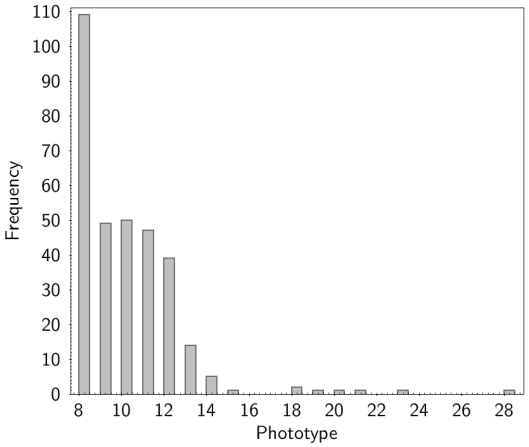

Figure 48: Photo-type distribution for M8 to T8 for final TGAS candidates. 95% of candidates are M7 (not shown). 07=M7, 28=T8.

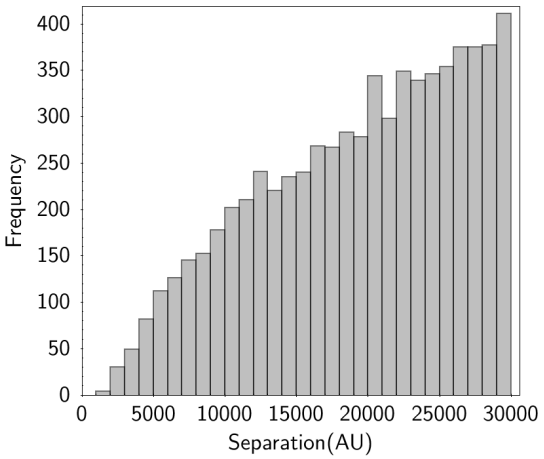

Figure 49: Separation distribution for final TGAS candidates.

4.1 Notable Candidates

A 2.0as cross-match with SIMBAD reveals that 29 of the candidates are known. None of the candidates appear in the Dupuy or Gange catalogues, however neither catalogue has been updated in several years so this is not surprising. Amongst the 29 known candidates are two confirmed brown dwarfs, three candidate UCDs, three mid-M dwarfs and one low-mass star. Additionally, there are fourteen objects that are classified as galaxies in literature (i.e. not automatically by SDSS or similar surveys). There are considerably fewer known UCDs than the earlier SIMBAD match in section 2.4, the reason likely being that they failed the common proper motion tests due to high uncertainty or not being companions.

Objects within SIMBAD are not the only notable candidates; objects with high common proper motion confidence or other interesting properties are explored in this section.

4.1.1 Possible companions to previously confirmed UCDs

The five candidates that are confirmed or candidate UCDs in SIMBAD were not previously thought to be companion systems. All five of them appear in Skrzypek's catalogue [52] and have hence been previously photo-typed. Properties of each candidate are shown in figures (50) through (54).

BRLT 144

This candidate is listed as an L5 dwarf in SIMBAD, however Marocco et al. (2015) [53] used spectra to determine that it is likely an L2+T3 binary. The primary, HD 101512, is an F5 star with low proper motion (∼14mas/yr). As the spectrum has already been measured, any further observations should aim to constrain the candidate's proper motion over a long baseline.

Photo-type (LD)	L3
Photo-type (Skzrypek)	L2.5
χ^2 (LD)	5.08
χ^2 (Skzrypek)	6.09
M_J	10.39
σ_{CPM}	3.81
PM/dPM	4.18
Separation (AU)	17143
Separation (arcsec)	68.74
Distance (pc)	249.4

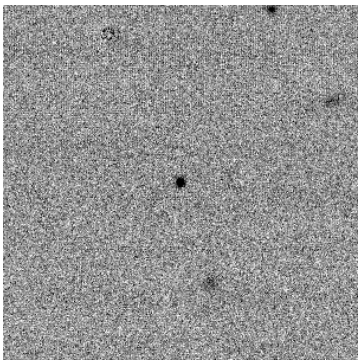

Figure 50: BRLT 144 properties and a 1' UKIDSS J cutout.

BRLT 142

Similarly to BRLT 144, this candidate had its spectrum measured by Marocco et al. and was classified as an L2.5 brown dwarf. As with BRLT 144 any further observations should focus on proper motion. The primary, TYC 4930-522-1, is a variable star. The candidate is not thought to be a binary or exhibit any peculiarities.

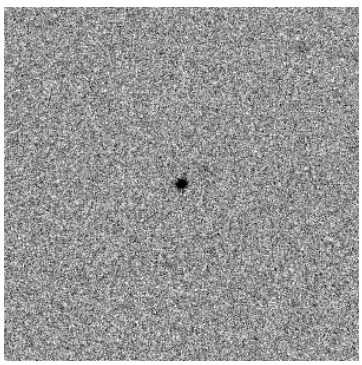

Photo-type (LD)	L5
Photo-type (Skzrypek)	L4.5
χ^2 (LD)	1.43
χ^2 (Skzrypek)	1.53
M_J	10.69
σ_{CPM}	4.64
PM/dPM	4.93
Separation (AU)	28418
Separation (arcsec)	168.25
Distance (pc)	168.9

Figure 51: BRLT 142 properties and a 1' UKIDSS J cutout.

ULAS J155902.28+260619.3
This candidate was identified as a candidate UCD by Skzrypek [52] and has no yet had its spectrum measured. Its primary, HD 143352, is an F2 RV Tau variable. Both spectra and proper motion should be obtained in any future observation.

Photo-type (LD)	L1
Photo-type (Skzrypek)	L1.5
χ^2 (LD)	2.56
χ^2 (Skzrypek)	8.07
M_J	10.72
σ_{CPM}	3.81
PM/dPM	4.60
Separation (AU)	21909
Separation (arcsec)	118.30
Distance (pc)	185.2

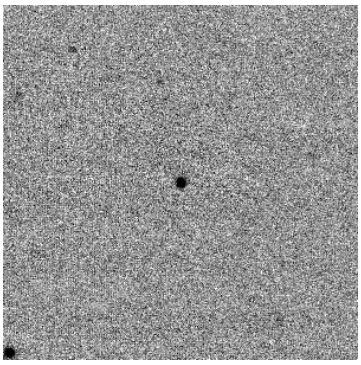

Figure 52: ULAS J155902.28+260619.3 properties and a 1' UKIDSS J cutout.

ULAS J124922.71+031025.6
Similarly to ULAS J155902.28+260619.3, this is a candidate brown dwarf that has not had its spectrum measured. The primary, HD 111485, is an F8V high proper motion star. The high proper motion of the primary makes this a good target for further proper motion measurements to verify companionship. **ULAS**

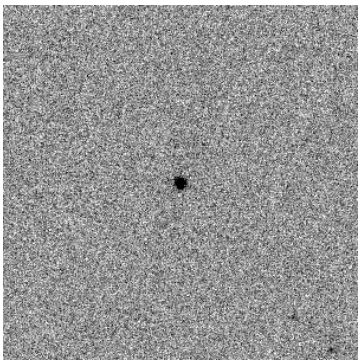

Photo-type (LD)	L3
Photo-type (Skzrypek)	L4
χ^2 (LD)	2.79
χ^2 (Skzrypek)	5.51
M_J	11.27
σ_{CPM}	3.14
PM/dPM	4.72
Separation (AU)	14820
Separation (arcsec)	154.70
Distance (pc)	95.8

Figure 53: ULAS J124922.71+031025.6 properties and a 1' UKIDSS J cutout.

J115105.79+111920.7
Another candidate brown dwarf with no available spectra. The primary is BD+12 2385, a G5 star.

Photo-type (LD)	L0
Photo-type (Skzrypek)	L1
χ^2 (LD)	0.30
χ^2 (Skzrypek)	8.13
M_J	10.92
σ_{CPM}	4.06
PM/dPM	5.13
Separation (AU)	11596
Separation (arcsec)	56.70
Distance (pc)	204.5

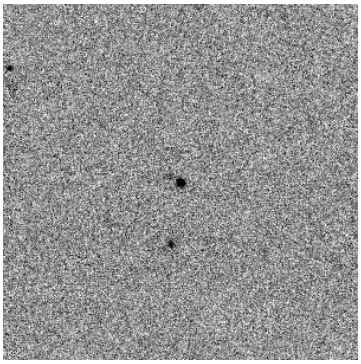

Figure 54: J115105.79+111920.7 properties and a 1' UKIDSS J cutout.

4.1.2 New ultracool companions: the strongest candidates

As mentioned in section 4.1, properties such as χ^2 and σ_{CPM} can be used to select the strongest candidates. In this subsection, a select few candidates that are the strongest candidate companions will be presented.

There are 755 candidates that have $\sigma_{CPM} < 3$ and $PM/dPM > 4$, meaning they have a very high common proper motion confidence and are thus less likely to be chance aligned or contaminant objects. 734 of these candidates are ranked as M7, so the less contaminated and rarer objects that are later than M7 are shown in table (3). If these companions can be spectroscopically confirmed, they are likely to be useful benchmarks.

R.A.	Dec	Photo-type	χ^2	M_J	σ_{CPM}	PM/dPM	Sep (AU)	Dist (pc)
07h 43m 44s	+29° 00m 27s	M8	2.33	9.41	2.66	4.91	10115	546.4
07h 59m 57s	+18° 54m 05s	L1	84.55	12.13	1.07	4.00	24405	223.2
08h 26m 45s	+02° 25m 39s	M8	21.64	11.35	2.24	79.62	4577	169.2
08h 43m 09s	+04° 15m 57s	M9	14.60	9.62	1.79	4.61	15644	531.9
08h 43m 29s	−01° 03m 34s	L0	5.54	10.47	1.55	4.97	6419	306.7
08h 46m 04s	+07° 40m 33s	L3	8.10	12.36	2.48	6.59	13615	133.5
08h 53m 18s	+09° 37m 55s	M8	33.93	9.42	1.77	4.30	19748	381.6
09h 03m 09s	+01° 40m 38s	M8	4.79	10.68	2.43	5.66	18591	404.8
09h 37m 31s	+30° 56m 54s	L0	15.26	11.20	2.26	8.24	17971	263.8
09h 55m 34s	+07° 40m 03s	M9	19.89	10.33	2.26	4.09	10828	242.1
10h 03m 33s	+07° 49m 43s	L0	6.33	11.09	1.45	12.09	14852	371.7
10h 45m 38s	+13° 08m 17s	L1	23.73	10.50	2.14	27.48	12514	392.1
11h 11m 58s	+08° 22m 48s	M8	0.33	11.93	2.73	4.38	23821	163.1
12h 22m 31s	+03° 53m 32s	M8	1.49	9.14	2.96	4.49	5906	301.2
12h 40m 48s	+22° 50m 32s	M9	4.12	10.54	2.70	4.10	5156	328.9
13h 51m 02s	+03° 34m 27s	M8	1.11	12.38	2.02	5.32	27457	197.6
14h 09m 46s	+08° 06m 30s	M9	3.79	10.59	1.30	4.07	18344	458.7
15h 45m 32s	+04° 02m 30s	L1	99.88	13.61	2.63	8.16	5293	99.3
16h 14m 19s	+30° 13m 47s	M8	1.04	10.23	2.36	5.02	21819	353.3
20h 57m 44s	+00° 23m 38s	L3	35.65	12.06	2.32	4.17	14971	225.2
23h 00m 22s	+12° 55m 39s	L2	60.38	12.70	2.03	5.67	6005	138.6

Table 3: The strongest TGAS common proper motion candidates.

4.1.3 Multiplicity

In many cases, several candidate companions matched to the same star. Many of these apparent systems - particularly the larger ones - are likely a result of duplicate candidates. The nine-candidate system in table 4, for example, is three sources that have nine UKIDSS entries between them. Eliminating duplicate systems is not straightforward, as duplicates can have an angular separation close to that of two different candidates. The safest way to identify these sources is visual inspection, however this is left for future work.

Candidates in system	1	2	3	4	5	6	7	8	9
Frequency	4625	775	168	31	9	4	1	1	1

Table 4: TGAS systems with multiple companions

4.2 DR2 bulk selection

After Gaia DR2 was released, a new search for primaries was conducted using the same photo-typed selection as in section 2.3, with the only difference being that SDSS DR9 data was replaced with SDSS DR12 data. For TGAS, the search for potential primaries was a simple cross-match to find the closest star to the UCD candidate. For the DR2 search, however, a different process was used.

Using LAS and SDSS, a two-epoch proper motion using catalogue positions was calculated for each candidate. Using those proper motions, the candidates were then matched to Gaia DR2 by calculating σ_{CPM} for every DR2 source within 3 arcminutes. The source that produced the lowest σ_{CPM} was selected as the primary.

There was a DR2 primary found for 100% of the UCD candidates. All of the decontamination cuts applied to the TGAS sample were applied to the DR2 sample, with the only difference being that a slightly smaller 25,000 AU separation cut was used to reduce contamination. The cuts applied to the TGAS sample in section 3 were not applied to the DR2 selection.

The final number of candidates was 7,402. Several multi-candidate systems were found as indicated in table 5.

Candidates in system	1	2	3	4	5	6
Frequency	7018	360	19	4	0	1

Table 5: DR2 systems with multiple companions

There are only 161 candidates from the DR2 selection that appear in the final TGAS companion selection. This, along with only having 7,402 candidates despite DR2 being significantly bigger than TGAS, can be explained by only using two-point proper motions for the DR2 selection. These poor quality proper motions lead to a high PM/dPM, causing most to be rejected. Attempting to match to

SuperCOSMOS or Pan-STARRS for a third epoch was deemed to be beyond the scope of this project due to time constraints.

227 candidates have $\sigma_{CPM} < 3$ and $PM/dPM > 4$, 141 of which are later than M7. This is a significant expansion upon analysis with TGAS primaries. These candidates are shown below.

R.A.	Dec	Photo-type	χ^2	M_J	σ_{CPM}	PM/dPM	Sep (AU)	Dist (pc)
00h 01m 12s	+15° 35m 34s	L5	18.1	12.96	2.62	11.04	52	31.6
00h 01m 12s	+15° 35m 34s	L5	20.68	12.95	2.72	11.42	53	31.6
00h 02m 26s	+08° 42m 29s	L2	31.02	11.69	2.78	4.1	19205	283.4
00h 22m 44s	+14° 27m 28s	L0	2.59	12.35	2.44	4.06	9445	205
00h 28m 45s	+11° 31m 55s	L0	3.2	11.57	0.9	4.11	141	71.6
00h 32m 05s	+02° 18m 59s	L2	3.6	12.28	2.17	7.93	124	24.3
00h 41m 04s	+09° 23m 20s	L1	3.06	14.72	1.66	4.16	5740	33.5
01h 04m 24s	+13° 39m 50s	L6	19.65	14.4	1.19	13.05	10427	64.1
01h 04m 59s	+14° 23m 44s	M8	5.47	12.27	2.06	6.27	12879	144.4
01h 09m 08s	+06° 25m 59s	L1	0.41	11.97	2.84	13.84	94	31.9
01h 33m 01s	+00° 06m 50s	L3	12.55	12.15	1.72	5.18	12332	141
01h 44m 27s	+15° 34m 08s	M8	36.6	15.08	1.12	4.29	2335	51.9
01h 53m 54s	+14° 04m 52s	L0	3.54	11.68	1.29	4.68	36	48.3
02h 07m 36s	+13° 55m 55s	L3	4.78	12.46	2.05	6.23	2679	38.1
03h 23m 36s	+06° 28m 02s	L1	26.73	13.81	2.94	4.78	12959	96
03h 30m 35s	−00° 25m 37s	L4	3.52	12.96	1.91	5.24	93	28.2
07h 47m 52s	+26° 58m 48s	L0	0.68	11.65	0.61	5.18	35	65
07h 59m 10s	+24° 27m 11s	L0	0.79	11.58	1	7.87	125	67.3
08h 06m 48s	+22° 15m 44s	L5	7.56	13.29	1.01	8.22	443	49.3
08h 19m 02s	+26° 09m 23s	L0	3.83	11.57	2.3	6.92	75	83.6
08h 20m 05s	+02° 45m 09s	M8	11.33	12.31	2.68	4.39	16813	113.6
08h 23m 48s	+24° 28m 58s	L4	5.99	12.97	1.4	8.61	37	25.3
08h 35m 58s	+05° 48m 31s	L2	1.22	11.55	0.7	5.72	29	38.8
08h 37m 14s	+07° 27m 19s	L0	9.64	15.31	2.85	4.21	1060	43.9
08h 39m 30s	+04° 26m 50s	M8	4.59	12.48	1.14	4.23	20893	154.6
08h 43m 33s	+10° 24m 43s	L2	1.28	12.33	1.98	8.53	132	30.7
08h 52m 58s	+25° 53m 27s	M9	11.77	14.35	2.82	5.34	6150	58.4
09h 03m 04s	+31° 00m 26s	M8	9.67	11.79	2.98	6.77	14075	143.1
09h 06m 19s	+28° 45m 19s	L1	0.52	12.36	0.56	4.19	23940	137.3
09h 15m 34s	+04° 22m 05s	L6	6.18	13.21	2.93	10.82	21	18.2
09h 17m 31s	+09° 22m 04s	L0	18.49	12.78	2.15	4	5495	165.2
09h 36m 30s	−00° 53m 06s	L0	0.94	11.59	1.55	5.65	38	51.7
09h 39m 06s	+34° 12m 57s	L0	0.83	11.55	2.49	7.3	59	61.5
09h 40m 36s	+33° 10m 59s	L1	28.95	13.68	1.42	4.69	16078	109.4
09h 53m 24s	+05° 26m 59s	L1	1.81	11.92	1.44	10.1	227	57.7
09h 54m 44s	+04° 26m 46s	L4	2.8	12.85	0.85	4.8	4054	124.7
09h 58m 33s	+07° 03m 48s	M8	2.56	13.06	1.77	4.42	15227	95.2

Table 6 continued from previous page

R.A.	Dec	Photo-type	χ^2	M_J	σ_{CPM}	PM/dPM	Sep (AU)	Dist (pc)
09h 58m 34s	+03° 48m 22s	M9	2.62	13.51	1.31	4	11646	106.8
10h 00m 45s	−01° 39m 19s	L0	7.09	11.65	2.06	5.21	28	47.2
10h 11m 59s	+05° 08m 59s	M8	3.02	12.84	1.76	4.85	8021	113.1
10h 13m 08s	+07° 46m 27s	L1	51.96	14.01	2.47	5.7	14227	96.7
10h 17m 08s	+13° 08m 39s	L2	1.29	11.71	0.3	10.5	33	28.9
10h 17m 08s	+13° 08m 39s	L2	0.68	11.74	2.35	13.57	38	28.9
10h 19m 02s	+05° 00m 51s	M8	3.45	11.66	1.92	4.58	4095	165.3
10h 31m 31s	+12° 37m 36s	L4	1.54	11.92	1.77	5.29	4184	97.8
10h 32m 08s	+05° 12m 06s	M9	47.98	12.89	0.53	4.39	21581	131.4
10h 33m 09s	+12° 16m 25s	L0	2.78	11.74	2.21	29.17	128	46.7
10h 35m 29s	+09° 59m 27s	L1	12.46	12.05	2.65	4.14	16597	233.9
10h 36m 22s	+13° 08m 55s	M9	2	12.87	2.44	4.64	9947	131.4
10h 36m 42s	+06° 45m 53s	L2	35.21	12.03	2.62	4.61	23550	231.4
10h 43m 05s	+10° 04m 54s	M8	1.55	12.39	2.87	4.57	8192	144.8
10h 43m 41s	+04° 38m 22s	M8	1.96	11.5	1.64	6.98	117	99.1
10h 51m 37s	+13° 18m 09s	L0	3.95	13.4	2	4.79	11197	124
10h 51m 37s	+13° 18m 09s	L0	1.63	13.18	2.22	4.86	11206	124
11h 05m 04s	+02° 28m 32s	L0	5.23	11.68	1.26	8.44	689	117.6
11h 10m 36s	+11° 25m 12s	T4	3.96	11.82	1.15	4.86	10034	221
11h 20m 21s	+12° 53m 37s	M8	1.18	12.12	0.36	5.51	20889	134.7
11h 25m 05s	+05° 56m 43s	L0	0.35	11.67	1.54	12.41	85	60.5
11h 25m 49s	+08° 57m 23s	M8	6.28	12.43	2.91	8.22	6317	86.1
11h 28m 07s	−01° 52m 01s	L0	3.4	11.72	2.04	4.12	33	66
11h 38m 44s	+07° 48m 20s	L0	3.48	11.65	2.71	17.39	150	60.9
11h 40m 58s	+04° 37m 41s	M8	1.22	11.86	1.53	5.12	10517	142.2
11h 58m 25s	+13° 54m 48s	L0	9.59	11.58	1.14	19.3	56	28
11h 58m 31s	−00° 08m 50s	L0	1.85	11.5	2.65	4.36	79	79.6
11h 58m 31s	−00° 08m 50s	L0	1.73	11.5	1.63	6.4	102	79.6
12h 09m 37s	+11° 15m 16s	L7	10.51	14.53	2.69	5.32	10809	70.2
12h 11m 30s	+04° 06m 08s	L4	2.84	12.84	0.67	14.02	60	34.2
12h 12m 34s	+02° 06m 27s	L2	12.92	12.06	1.37	7.35	63	55.3
12h 14m 03s	−00° 38m 21s	L5	7.29	13.42	2.3	7.87	3033	94.6
12h 14m 15s	+10° 41m 45s	L0	1.55	11.51	1.96	11.18	65	46.7
12h 14m 34s	+08° 46m 55s	T8	17.62	14.14	2.42	4.07	6336	51.2
12h 15m 18s	+00° 42m 57s	L2	1.05	12.3	1.86	5.21	30	45.6
12h 21m 28s	+02° 57m 20s	L0	1.09	11.73	2.27	21.74	26	18.5
12h 24m 30s	+11° 11m 05s	M9	10.56	11.87	1.76	4.03	22571	138.6
12h 28m 12s	+11° 01m 13s	L0	2.48	11.78	1.35	5.46	38	52.8
12h 32m 11s	+15° 35m 21s	L7	14.16	11.94	1.82	4.66	23690	188.8
12h 50m 14s	+24° 09m 21s	M8	4.81	15	1.33	5.93	3895	25.7
12h 52m 38s	+03° 47m 35s	L0	0.64	11.7	2.24	18.9	140	70.5
12h 57m 55s	+34° 15m 54s	L0	1.94	12.03	2.17	4.43	12523	185.4
12h 59m 35s	+06° 11m 17s	L0	1.25	12.76	2.51	4.15	23803	161.1
12h 59m 42s	+10° 01m 38s	L7	41.59	13.7	0.89	10.13	403	45.7

Table 6 continued from previous page

R.A.	Dec	Photo-type	χ^2	M_J	σ_{CPM}	PM/dPM	Sep (AU)	Dist (pc)
13h 04m 33s	+09° 07m 07s	L1	1.23	11.57	2.5	4.59	44	55
13h 07m 25s	−01° 41m 37s	M8	1.6	11.86	2.4	5.05	15622	128.9
13h 08m 31s	+08° 18m 53s	L2	1.42	11.78	1.5	20.08	121	47.2
13h 08m 31s	+08° 18m 53s	L2	0.93	11.82	0.77	9.67	78	47.2
13h 10m 05s	+22° 22m 35s	L0	2.89	13.25	2.72	4.03	22409	137.7
13h 11m 25s	+26° 04m 50s	L0	12.69	11.97	2.47	4.86	1599	181.3
13h 12m 22s	+29° 09m 34s	L0	4.7	11.87	0.89	11.32	123	49.1
13h 12m 22s	+29° 09m 34s	L0	1.78	11.94	1.38	12.09	127	49.1
13h 13m 55s	+22° 30m 06s	L3	1.1	13.64	1.83	6.48	1807	67.2
13h 14m 06s	+04° 52m 20s	L0	2.28	11.66	0.93	14.24	140	79.4
13h 15m 34s	+22° 30m 10s	L2	0.45	11.6	1.48	4.51	2624	87.3
13h 15m 46s	+24° 54m 07s	L0	2.81	11.69	1.62	4.64	36	56.6
13h 19m 18s	+26° 31m 17s	M9	1.85	11.99	0.77	6.97	23942	134.6
13h 25m 11s	+05° 17m 03s	L1	3.4	12.2	2.87	8.85	31	37.9
13h 25m 11s	+05° 17m 03s	L1	3.65	12.25	1.54	9.8	34	37.9
13h 25m 11s	+05° 17m 03s	L3	50.54	12.29	2.4	9.75	33	37.9
13h 27m 15s	+07° 59m 38s	L3	1.18	11.87	0.88	4.47	64	34.8
13h 30m 57s	+24° 27m 21s	L0	17.93	12.91	2.85	5.22	1276	109.7
13h 35m 29s	+30° 10m 52s	T1	2.73	14.35	1.49	6.07	6641	38.8
13h 36m 25s	+25° 40m 37s	L4	1.56	12.44	2.22	10.84	9289	79.1
13h 37m 30s	+28° 11m 51s	M8	1.95	12.16	0.54	4.48	65	87.1
13h 38m 36s	+35° 20m 59s	M8	3.72	11.55	1.43	4.84	5290	151
13h 44m 58s	+26° 19m 08s	M8	1.72	11.53	1.81	5.07	62	93
13h 46m 07s	+08° 42m 34s	L3	1.69	12.16	1.15	15.09	121	46.2
13h 46m 07s	+08° 42m 34s	L3	1.29	12.19	2.13	7.43	77	46.2
13h 46m 41s	+11° 25m 25s	L1	5.58	11.57	1.84	4.01	24417	199.8
13h 48m 05s	+02° 01m 18s	L3	1.53	12.82	0.98	4.29	23329	139.8
13h 48m 44s	+26° 17m 06s	M8	4.48	11.86	1.27	4.49	66	91.8
13h 49m 31s	+29° 45m 54s	L4	1.89	12.47	1.33	6.43	33	43.2
13h 51m 32s	+12° 03m 18s	L1	7.9	12.31	2.38	4.51	10499	213.1
13h 55m 35s	−01° 08m 02s	M8	1.53	13.21	0.83	4.02	10417	109.6
13h 57m 50s	+10° 50m 58s	M8	10.6	11.55	1.4	5.35	73	99
14h 00m 36s	+07° 47m 20s	L0	4.99	11.6	0.98	9.59	84	58.5
14h 02m 32s	+01° 48m 30s	L1	1.9	12.24	2.06	6.49	104	42.6
14h 03m 12s	+04° 13m 31s	L7	16.48	13.13	1.64	4.21	5011	92.8
14h 07m 24s	+06° 24m 38s	M8	2.29	12.25	2.64	5.95	13057	135.5
14h 08m 06s	+02° 00m 38s	L0	3.9	13.17	2.19	4.21	2601	139.1
14h 16m 24s	+13° 48m 27s	L8	67.7	13.15	2.37	13.74	13	9.2
14h 17m 45s	+07° 59m 07s	L0	1.85	12.91	2.55	4.17	14682	96.9
14h 20m 11s	+03° 29m 33s	M8	5.12	11.76	1.87	5.38	8634	152.8
14h 21m 12s	+01° 43m 31s	L2	2.29	13.04	2.45	11.44	6766	73.4
14h 22m 57s	+08° 27m 50s	L2	5.73	12.45	1.78	19.1	126	32.4
14h 23m 08s	+00° 31m 34s	M8	3.18	13	1.9	4.22	19705	125.8
14h 24m 39s	+09° 17m 09s	L5	2.81	13.04	0.62	12.15	177	33.4

Table 6 continued from previous page

R.A.	Dec	Photo-type	χ^2	M_J	σ_{CPM}	PM/dPM	Sep (AU)	Dist (pc)
14h 24m 39s	+09° 17m 09s	L5	1.14	13.04	0.64	11.38	175	33.4
14h 29m 52s	+12° 08m 27s	M8	32.22	12.06	2.9	4.59	22119	221.2
14h 31m 37s	+08° 49m 23s	M8	0.93	12.25	2.95	4.17	23681	184.5
14h 31m 45s	+00° 45m 06s	M8	8.36	14.43	2.75	8.13	7919	47.1
14h 33m 51s	−02° 34m 42s	M8	1.73	11.67	0.99	4.61	19932	158.4
14h 48m 26s	+10° 31m 58s	L6	2.77	13.68	2.45	12.08	26	14
14h 52m 01s	+09° 31m 36s	L0	4.66	12.01	1.25	11.42	73	46.2
15h 02m 12s	+05° 55m 13s	M8	4.2	11.69	2.74	4.33	12033	124.9
15h 04m 15s	−00° 16m 17s	L4	1.16	12.46	2.77	5.38	3405	160
15h 04m 23s	+31° 02m 32s	M9	5.53	13.41	0.67	5.62	10828	66.8
15h 17m 22s	+30° 23m 50s	M8	40.22	11.51	2.7	4.43	2514	193.1
15h 18m 34s	−00° 36m 20s	M8	2.6	12.77	2.45	6.34	4887	137.9
15h 40m 51s	+02° 42m 42s	L0	3.08	12.44	1.79	4.83	14705	136.8
22h 50m 16s	+08° 08m 22s	L0	8.99	12.31	1.82	5.86	125	43.3
23h 31m 29s	+15° 52m 22s	L1	0.91	11.98	2.68	5.71	47	39.7
23h 46m 39s	+15° 19m 41s	M8	2.49	12.89	2.79	5.35	20175	148.8

5 Conclusions & future work

In this section, there is a summary of the project followed by a review of its various components and proposed future work.

5.1 Summary

This project has established methods to identify and classify ultracool companions to Gaia stars, including photometric outliers, using catalogue data. Methods to prioritise candidates for follow-up were explored and successfully identified several candidate companions that are recommended for follow-up.

The observing run resulted in six potential companions being identified through common proper motion, two of which were found by this project. The search for ultracool companions with TGAS data resulted in five previously detected UCDs (confirmed or candidate) being identified as potential companions to Gaia stars. A further 755 new candidate UCDs were identified with a high common proper motion confidence; a large portion of these are thought to be contaminant objects that could be analysed in future work. Of those 755 new candidate companions, the most promising 21 sources were identified with 10 of them being high-χ^2 (i.e. peculiar) sources. A repeated search using Gaia DR2 was conducted, identifying 227 candidates. Further reduction of this candidate list with improved (three-epoch) proper motions is left for future work, with a likely result of a few dozen high-confidence candidate ultracool companions.

It is recommended that the 32 TGAS candidates companions[14] are followed up with an observing run whilst the 227 DR2 companions should be further reduced to a few dozen candidates - through improved proper motions - before following up on an observing run.

5.2 Bulk selection

Sky coverage was a major limitation for this project, prohibiting full exploitation of Gaia's vast catalogue. The project was effectively limited to northern skies and would have benefited greatly by using VISTA VHS alongside UKIDSS LAS to expand coverage. Other surveys that would be useful for finding ultracool dwarfs are Pan-STARRS and WISE. Pan-STARRS covers much of the SDSS footprint, however it offers deeper coverage with more precise astrometry while WISE would be beneficial for colour cuts and photo-typing.

The initial colour cuts applied to the surveys only used the bands used for photo-typing, despite more bands being available from said surveys. While too many cuts can cause problems, an exploration of more colours may have revealed some useful cuts for decontamination.

[14] 6 new & observed with Fourstar, 21 new with three-epoch proper motions and 5 previously detected

5.3 Photo-typing and χ^2 analyis

The photo-typing proved to be a useful tool for classifying candidates with reasonable accuracy, whilst also having some - albeit limited - use for identifying peculiarities. Additionally, the upper χ^2 limited helped to remove contamination. With some improvement, however, the photo-typing routine could become a much more powerful tool.

The IDL routines used for photo-typing in this project were inflexible; sources would only be considered if full photometry was available. It is planned that in the near future a new photo-typing code will be written, with one major change being that it can accept any combination of bands instead of rejecting all sources with missing photometry.

It is also planned that the new photo-typer will go beyond simply selecting the best-match χ^2. In some cases, the difference in χ^2 between possible types for a candidate can be as small as 0.01. Candidates that closely match several template colours for multiple spectral types should be marked, for example being classified as an L1-L3 instead of an L2. This would help to identify peculiar candidates and give some idea of how accurate each classification is.

Yet another planned improvement to the photo-typing method is that it will differentiate between sources that have a high χ^2 for deviating in all bands and sources that only deviate in one or two bands, as certain peculiarities could be picked up by this (e.g. low-gravity BDs).

5.4 Companionship

The process of cross-matching used in section 4.2, where the primary with the best-match σ is selected was a vast improvement over the TGAS match that only selected the closest star. As well having a 3 arc-minute maximum angular separation, a minimum separation should also be considered. Furthermore, this minimum separation should be a function of the primaries' apparent magnitude to remove systems where the UCDs' photometry is spoiled by glare from the primary.

Measuring common proper motion was decidedly the most challenging aspect of the project, as measuring the motion of faint UCDs is extremely difficult. There is no easy solution for measuring UCD proper motions that does not rely on waiting for more surveys or improvements in technology. Other methods of testing for companionship should be considered, such as using photo-types to predict absolute magnitudes and thus expected apparent magnitudes.

Appendix A: Potential transient

While attempting to measure the proper motion of J022053.62+024000.1 with a FourStar image, it was noticed that the UKIDSS reference image contains a source close to the candidate that does not appear in the deeper FourStar image. Two UKIDSS images from December 2010 - shown in figure (55) - have two sources with extremely small angular separation. The FourStar image in figure (56) only shows one source in this location. It is unlikely that almost identical anomalies would appear in two different UKIDSS images, however this was not ruled out immediately.

Measuring the surface brightness of the source(s) in the three images shows a double peak in UKIDSS Y and a skewed peak in J, whilst the FourStar J image has a single unskewed peak. This shows that the two sources seen in UKIDSS are indeed separate, and not one elongated source. Furthermore, the two sources have very different colours: the candidate's Y-J is 0.716 whilst the second source's Y-J is -0.354.

UKIDSS images in H and K are also available, however they were taken one month earlier (11/2010). In these images, the sources are less distinct and look similar to one extremely elongated source. Unforunately, the two sources could not be resolved to obtain photometry. Nevertheless, the evidence suggests that between 11/2010 and 12/2010 there were two closely aligned sources that were not visible in 2017. The likelihood of repeated, but not identical, artefacts over a month is extremely unlikely and any terrestrial or solar system object would have changed position. This leads to the conclusion that the transient source is a background object undergoing a period of increased luminosity.

Images from SDSS, Pan-STARRS and SuperCOSMOS were retrieved and all show only one source - the candidate UCD - with photometry that is consistent in all epochs. The duration of this event has been contrained to a minimum of one month and a maximum of five years by using the aforementioned catalogue images.

Unfortunately, little can be done to determine the nature of this transient source. The only known observations are from the two nights of UKIDSS in 2010 and the candidate companion does not have photometry that would suggest a background object is contributing to its measured flux. Had this been noticed during the transient event, high-resolution images (i.e. with AO) to fully resolve the two sources would have been extremely useful. Based upon the blue colour of the transient, it is speculated that the phenomenon could have been an extragalactic nova. The Fourstar image - which corresponds to only one of the UKIDSS sources - was not used to measure an improved proper motion due to the lack of suitable reference images (the UKIDSS image would have been ideal were it not for the second source).

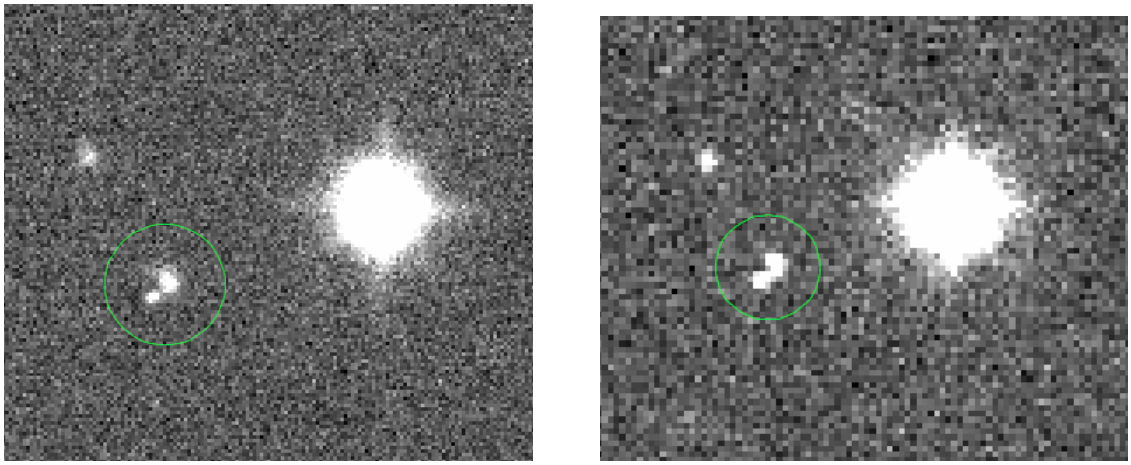

Figure 55: LAS J (left) and Y (right) images from 12/2010 showing two sources in the circled region.

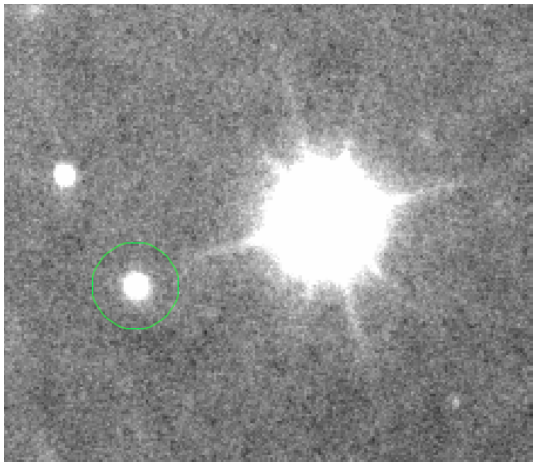

Figure 56: FourStar J image from 11/2017 of the same target (circled) with only one source visible.

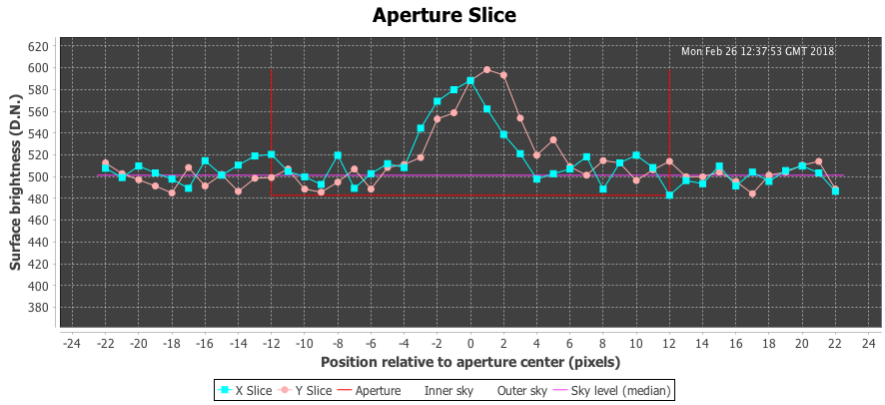

Figure 57: Surface brightness in an aperture covering the two sources in the UKIDSS J image.

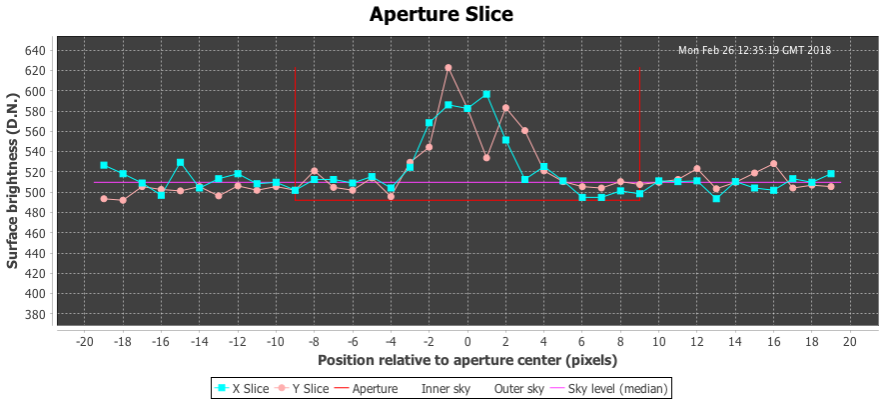

Figure 58: Surface brightness in an aperture covering the two sources in the UKIDSS Y image.

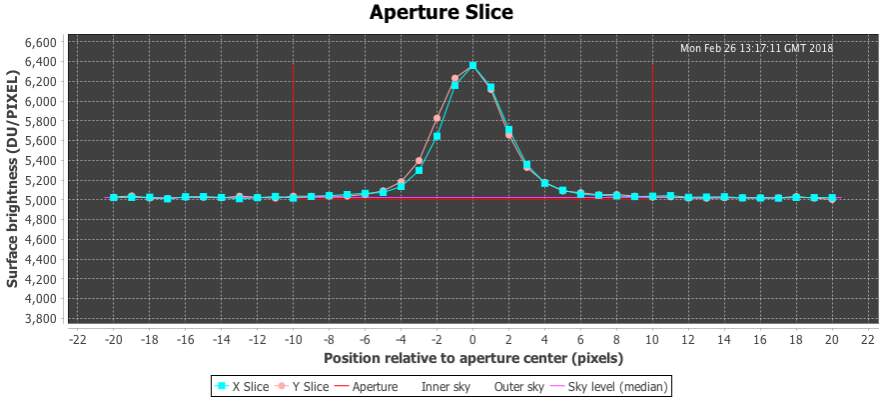

Figure 59: Surface brightness in an aperture covering the two sources in the FourStar J image. The slight offset between X and Y matched that of a reference star, implying it is a detector bias.

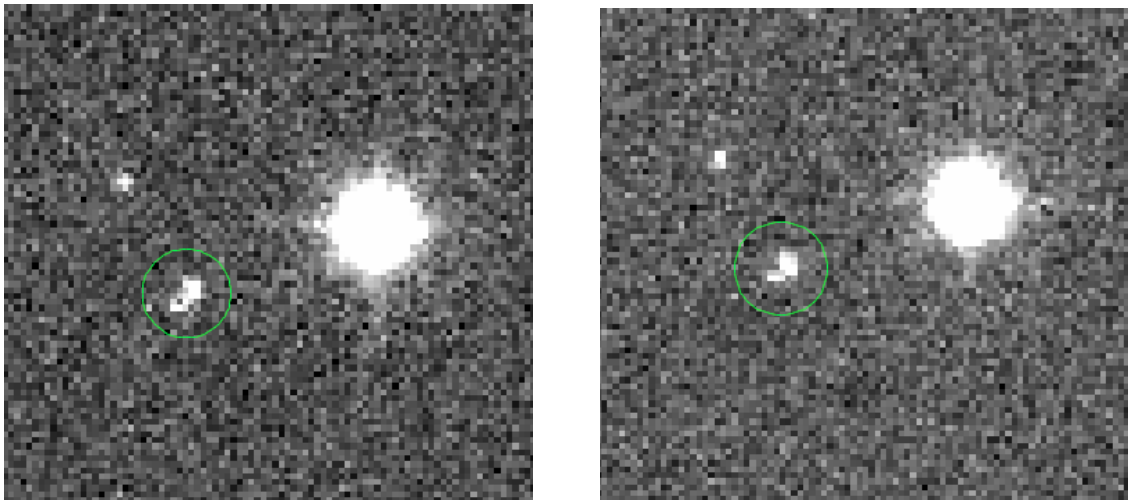

Figure 60: LAS H (left) and K (right) images from 11/2010 showing either one elongated or two distinct sources (circled).

References

[1]J. Davy Kirkpatrick, T. J. Henry, D. A. Simons, "The Solar Neighborhood 2: The first list of dwarfs with spectral types of M7 and cooler", The Astronomical Journal (1995) 10.1086/117323.

[2]J. Davy Kirkpatrick, T.J. Henry, M.J. Irwin, "Ultra-Cool M Dwarfs Discovered by QSO Surveys.I: The APM Objects", Astronomical Journal (1997) 10.1086/118357.

[3]J. R. Cantrell, T. J. Henry, R. J. White, "The Solar Neighborhood XXIX: The habitable real estate of our nearest stellar neighbors", The Astronomical Journal (2013) 10.1088/0004-6256/146/4/99.

[4]S. S. Kumar, "Study of Degeneracy in Very Light Stars", The Astronomical Journal (1962) 10.1086/108658.

[5]J. Tarter, "The interaction of gas and galaxies within galaxy clusters", P.h.D. Thesis (University of California, 1975).

[6]T. Nakajima, B.R. Oppenheimer, S.R. Kulkarni, D.A. Golimowski, K. Matthews, S.T. Durrance, "Discovery of a cool brown dwarf", Nature (1995) 10.1038/378463a0.

[7]R. Rebolo, M.R. Zapatero Osorio, E. L. Martín, "Discovery of a brown dwarf in the Pleiades star cluster", Nature (1995) 10.1038/377129a0.

[8]S.B. Dieterich et al., "THE SOLAR NEIGHBORHOOD. XXXII. THE HYDROGEN BURNING LIMIT", The Astronomical Journal (2014) 10.1088/0004-6256/147/5/94.

[9]A.P. Boss et al., "Working Group on Extrasolar Planets", IAU Transactions (2003) 10.1017/S1743921306004509.

[10]Q.M. Konopacky et al., "Discovery of a Substellar Companion to the Nearby Debris Disk Host HR 2562", The Astrophysical Journal (2016) 10.3847/2041-8205/829/1/L4.

[11]G. Chabrier, A. Johansen, M. Janson, R. Rafikov, "Giant planet and brown dwarf formation", in *Protostars and Planets VI* (2014).

[12]J. Davy Kirkpatrick, T.J. Henry, D.W. McCarthy, W. Donald Jr., "A standard stellar spectral sequence in the red/near-infrared - Classes K5 to M9", The Astrophysical Journal Supplement Series (1991) 10.1086/191611.

[13]E. L. Martín, G. Basri, and M. R. Zapatero Osorio, "The Lithium Test in Young Brown Dwarf Candidates", The Astronomical Journal (1999) 10.1086/300983/.

[14]L. Kaltenegger, W.A. Traub, "Transits of Earth-like Planets", The Astrophysical Journal (2009) 10.1088/0004-637X/698/1/519.

[15]J. Davy Kirkpatrick et al., "Dwarfs Cooler than "M": The Definition of Spectral Type "L" Using Discoveries from the 2 Micron All-Sky Survey (2MASS)", The Astrophysical Journal (1999) 10.1086/307414.

[16]N. Skrzypek et al., "Photometric brown-dwarf classification. 1. A method to identify and accurately classify large samples of brown dwarfs without spectroscopy", Astronomy & Astrophysics (2015) 10.1051/0004-6361/201424570.

[17]A. J. Burgasser et al., "The Classification of T Dwarfs", Proceedings of IAU Symposium 211 (2003).

[18]A. Burrows, D. Sudarsky, J. Lunine, "Beyond the T Dwarfs: Theoretical Spectra, Colors, and Detectability of the Coolest Brown Dwarfs", The Astrophysical Journal (2003) 10.1086/377709.

[19]K.L. Luhman et al., "Confirmation of One of the Coldest Known Brown Dwarfs", The Astrophysical Journal (2012) 10.1088/0004-637X/744/2/135.

[20]M. C. Cushing et al., "The Discovery of Y Dwarfs Using Data from the Wide-field Infrared Survey Explorer (WISE)", The Astrophysical Journal (2011) 10.1088/0004-637X/743/1/50.

[21]D. Stamatellos et al., "Radiative transfer and the energy equation in SPH simulations of star formation", Astronomy & Astrophysics (2007) 10.1051/0004-6361:20077373.

[22]E.I. Vorobyov, S. Basu, "The Burst Mode of Protostellar Accretion", The Astrophysical Journal (2006) 10.1086/507320.

[23]P. Hennebelle, R. Teyssier, "Magnetic processes in a collapsing dense core II. Fragmentation. Is there a fragmentation crisis?", Astronomy & Astrophysics (2008) 10.1051/0004-6361:20078310.

[24]I. A. Bonnell, P. C. Clark, M. R. Bate, "Gravitational fragmentation and the formation of brown dwarfs in stellar clusters", MNRAS (2008) 10.1111/j.1365-2966.2008.13679.x.

[25]A.P. Whitworth, H. Zinnecker, "The formation of free-floating brown dwarves and planetary-mass objects by photo-erosion of prestellar cores", Astronomy & Astrophysics (2004) 10.1051/0004-6361:20041131.

[26]M. J. Payne, G. Lodato, "The potential for Earth-mass planet formation around brown dwarfs", MNRAS (2007) 10.1111/j.1365-2966.2007.12362.x.

[27]F.C. Adams, P. Bodenheimer, G. Laughlin, "M dwarfs: planet formation and long term evolution", Astronomische Nachrichten (2005) 10.1002/asna.200510440.

[28]M. Gillon et al., "Temperate Earth-sized planets transiting a nearby ultracool dwarf star", Nature (2016) 10.1038/nature17448.

[29]F.C. Adams, G. Laughlin, "A Dying Universe: The Long Term Fate and Evolution of Astrophysical Objects", Reviews of Modern Physics (1997) 10.1103/RevModPhys.69.337.

[30]A. W. Mann et al., "Prospecting in Ultracool Dwarfs: Measuring the Metallicities of Mid- and Late-M Dwarfs", Astronomical Journal (2014) 10.1088/0004-6256/147/6/160.

[31]C.G. Tinney, "The Dark Matter Implications of Brown Dwarfs", The Third Stromlo Symposium: The Galactic Halo (1999) 1999ASPC..165..419T.

[32]A. Burrows et al., "A Nongray Theory of Extrasolar Giant Planets and Brown Dwarfs", The Astrophysical Journal (1997) 10.1086/305002.

[33]G. Chabrier, "Galactic Stellar and Substellar Initial Mass Function", Publications of the Astronomical Society of the Pacific (2003) 10.1086/376392.

[34]I. Baraffe et al, "Evolutionary models for cool brown dwarfs and extrasolar giant planets. The case of HD 209458", Astronomy & Astrophysics (2003) 10.1051/0004-6361:20030252.

[35]J. Davy Kirkpatrick et al., "Discoveries from a near-infrared proper motion survey using multi-epoch two micron all-sky survey data", The Astrophysical Journal (2010) 10.1088/0067-0049/190/1/100.

[36]E.L. Martín, R. Rebolo, M.R. Zapatero Osorio, "Spectroscopy of New Substellar Candidates in the Pleiades: Towards a Spectral Sequence for Young Brown Dwarfs", The Astrophysical Journal (1996) 10.1086/177817.

[37]K.L. Luhman, Jame Liebert, G.H. Rieke, "Spectroscopy of a Young Brown Dwarf in the rho Ophiuchi Cluster 1", The Astrophysical Journal (1997) 10.1086/316784.

[38]N.I. Gorlova, M.R. Meyer, G.H. Rieke, J. Liebert, "Gravity Indicators in the Near-Infrared Spectra of Brown Dwarfs", The Astrophysical Journal (2003) 10.1086/376730.

[39]D.C.B. Gagliuffi et al., "SpeX Spectroscopy of unresolved very low mass binaryies. II. Identification of 14 candidate binaries with late-M/early-L and T dwarf components", The Astrophysical Journal (2014) 10.1088/0004-637X/794/2/143.

[40]A. L. Kraus, M. J. Ireland, F. Martinache, J. P. Lloyd, "Mapping the Shores of the Brown Dwarf Desert I.: Upper Scorpius", The Astrophysical Journal (2008) 10.1086/587435.

[41]L. Eyer, P. Dubath, S. Saesen, D.W. Evans, L. Wyrzykowski, S. Hodgkin, N. Mowlavi, "From Hipparcos to Gaia", New Horizons in Time Domain Astronomy Proceedings IAU Symposium No. 285, 2012 (2012) 10.1017/S1743921312000506.

[42]D. Michalik, L. Lindegren, D. Hobbs, "The Tycho-Gaia astrometric solution. How to get 2.5 million parallaxes with less than one year of Gaia data", Astronomy & Astrophysics (2015) 10.1051/0004-6361/201425310.

[43]Gaia Collaboration, "Gaia Data Release 2: The astrometric solution", Astronomy & Astrophysics (2018) 10.1051/0004-6361/201832727.

[44]D. J. Pinfield, H. R. A. Jones, P. W. Lucas, T. R. Kendall, S. L. Folkes, "Finding benchmark brown dwarfs to probe the sub-stellar IMF as a function of time.", MNRAS (2006) 10.1111/j.1365-2966.2006.10213.x.

[45]F. Marocco, D.J. Pinfield et. al, "Ultracool dwarf benchmarks with Gaia primaries", MNRAS (2017) 10.1093/mnras/stx1500.

[46]F. Marocco, D.J. Pinfield et al., "Outlier Benchmark Systems With Gaia Primaries", MNRAS (2016) 10.5281/zenodo.59238.

[47]M. R. Blanton, S. Roweis, "K-Corrections and Filter Transformations in the Ultraviolet, Optical, and Near-Infrared", Astronomical Journal (2007) 10.1086/510127.

[48]P. C. Hewett, S. J. Warren, S. K. Leggett, S. T. Hodgkin, "The UKIRT Infrared Deep Sky Survey ZY JHK Photometric System: Passbands and Synthetic Colours", MNRAS (2006) 10.1111/j.1365-2966.2005.09969.x.

[49]T.J. Dupuy, M.C. Liu, "The Hawaii Infrared Parallax Program. 1. Ultracool Binaries and the L/T Transition", The Astrophysical Journal (2012) 10.1088/0067-0049/201/2/19.

[50]A. J. Burgasser et al., "The First Substellar Subdwarf? Discovery of a Metal-poor L Dwarf with Halo Kinematics", The Astrophysical Journal (2003) 10.1086/375813.

[51]N. Deacon et al., "Wide, Cool and Ultracool Companions to Nearby Stars from Pan-STARRS1", The Astrophysical Journal (2014) 10.1088/0004-637X/792/2/119.

[52]N. Skrzypek, S. J. Warren, J. K. Faherty, "Photometric brown-dwarf classification II. A homogeneous sample of 1361 L and T dwarfs brighter than J = 17.5 with accurate spectral types", Astronomy & Astrophysics (2016) 10.1051/0004-6361/201527359.

[53]F. Marocco, H.R.A. Jones et al., "A large spectroscopic sample of L and T dwarfs from UKIDSS LAS: peculiar objects, binaries, and space density", MNRAS (2015) 10.1093/mnras/stv530.